NTNU

Norwegian University of
Science and Technology

A gas to liquid Fischer-Tropsch process integrated with Solar Thermal Water Split

Techno-Economical Feasibility

Morten Thomas Emhjellen

Chemical Engineering and Biotechnology
Submission date: June 2016
Supervisor: Magne Hillestad, IKP
Co-supervisor: Erling Rytter, IKP

Norwegian University of Science and Technology
Department of Chemical Engineering

SUMMARY / ABSTRACT

Hydrocarbons are used in many products, and are the primary energy source for current civilizations, mainly as combustible fuel. There is a rapidly growing demand for environmentally friendly and renewable energy sources due to the depletion in fossil energy reserves and the need to reduce greenhouse gas emissions.

The purpose of this work was to further study, optimize and integrate promising process designs for environmentally friendly production of Fischer Tropsch (FT) products, hydrocarbons with a widespread of carbon numbers. Syngas, a mixture of H_2 and CO, is the feed for the FT synthesis, and this syngas is derived by using pressure-swing solar thermal water splitting, also known as the pressure swing hercynite cycle. The processes of syngas production from solar thermal water split and the FT synthesis from this syngas are individually studied recently at NTNU.

The primary focus in this thesis was on the process development. Key elements were to explore different design alternatives and optimizing independent variables for the conceptual design and for the heat exchanger network. The conceptual design was developed in Aspen HYSYS®. Different conceptual design choices was explored and investigated. Three different conceptual design configurations were optimized in order to be compared and to decide upon a best case. Three different design configurations of heat exchanger networks (HENs) for the best case conceptual design were proposed. Simulations in Aspen Energy Analyzer® (AEA) were used for developing 60 near optimum HENs for all configurations and to decide upon the best HEN configuration.

The best case utilizes external methane together with the oxygen produced from the solar thermal water splitting to produce additional syngas. 8716kg/h heavy FT product with mass fraction 0.945 of a lump with average carbon number 60 is produced, about 3.25 times higher flowrate than when no external methane is utilized. The overall energy efficiency and carbon efficiency of the final best case is 71.07% and 99.95%, respectively. Finally, a project evaluation was performed and the economic lifetime of the plant was set to 20years, operating 334days a year, 8 hours a day, in South Africa.

The fixed capital investment for the entire plants is MM US$ 269.12, and with the total annual manufacturing cost of MM US$ 31.1, the average sale price of the total FT

product has to be US$ 1.89/kg, in order to break even. This sale price is in between the average sale price for FT wax and the sale price of the most valuable FT wax. Several factors, such as the incentives for environmentally friendly production, have not been accounted for when arriving at this number. The debate about green house gas emissions is creating continuously increasing incentives for environmentally friendly production, which indicates a potentially bright future for the plant proposed in this thesis.

PREFACE

The work with this Master Thesis has been carried out in the Department of Chemical Engineering at the Norwegian University of Science and Technology during the spring of 2016.

I would like to thank my supervisor Professor Magne Hillestad and co supervisor Professor Erling Rytter for support and guidance throughout the course of this project and for making this Master thesis possible. They showed interest for the project and held weekly meetings. I would also like to thank PhD-Student Mohammad Ostadi for guidance and information about implementing a Fischer Tropsch reactor model from Aspen Custom Modeller in Aspen HYSYS.

I hereby declare that this is an independent work according to the exam regulations of the Norwegian University of Science and Technology.

Trondheim, 2016-06-20

Morten Thomas Emhjellen,

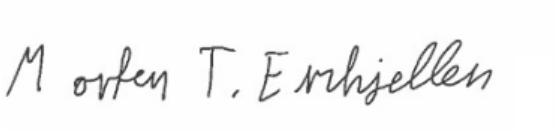

CONTENTS

LIST OF TABLES

LIST OF FIGURES

LIST OF ABBRIVATIONS

AACE	Association for Advancement of Cost Engineering
ACM	Aspen Custom Modeler
AEA	Aspen Energy Analyzer
ATR	Autothermal Reformer
FT	Fischer Tropsch
HC	Hydrocarbon
HEN	Heat Exchanger Network
ISBL	Inside Battery Limit
LHV	Lower Heating Value
LPG	Liquefied Petroleum Gas
O&M	Operation and Maintenance
RWGS	Reverse Water Gas Shift
VF	Vapor Fraction
WGS	Water Gas Shift
WHB	Waste Heat Boiler

NOMENCLATURE

α	Propagation Probability in Fischer Tropsch Reaction	-
e_{helio}	Energy Provided by Heliostats	kW/m^2
ΔH_{rx}	Reaction Enthalpi	kJ/mol
$\Delta Tmin$	Minimum Pinch Temperature for Heat Exchangers	°C
f_{er}	Installation Cost Factor for Equipment Erection	-
f_p	Installation Cost Factor for Piping	-
f_i	Installation Cost Factor for Instrumentation and Control	-
f_{el}	Installation Cost Factor for Electrical	-
f_c	Installation Cost Factor for Civil	-
f_s	Installation Cost Factor for Structures and Buildings	-
f_l	Installation Cost Factor for Lagging and Paint	-
f_m	Installation Cost Factor for Material	-
OS	Fixed Capital Cost Factor for Offsites	-
D&E	Fixed Capital Cost Factor for Design and Engineering	-
X	Fixed Capital Cost Factor for Contingency	
S	Allowable stress in material	ksi
T_{max}	Maximum Temperature corresponding to allowable stress	°C

1 INTRODUCTION

Hydrocarbons are used in many products depending on its chemical origin, and are the primary energy source for current civilizations. The dominating usage of hydrocarbons is as a combustible fuel source for energy output. There is a rapidly growing demand for environmentally friendly and renewable energy sources due to the depletion in fossil energy reserves and the need to reduce greenhouse gas emissions. Solar energy is a renewable energy source, of which may play a vital role for the future [1].

Using solar thermal energy, it is possible to split water into O_2 and H_2. Further, having the resulting hydrogen react with CO_2 yields synthesis gas, a mixture of H_2 and CO, which then can be converted into Fischer Tropsch (FT) products. FT products consists of hydrocarbons with a wide range of carbon numbers which can be processed by means of hydrocracking, into a variety of petroleum products, including naphtha, jet fuel, kerosene, lubricant oil, liquefied petroleum gas (LPG), diesel and wax [2, 3]. One of the main concerns for the solar thermal energy derived syngas production is the economic uncertainty. It is desired to investigate its viability when the syngas production is integrated with a FT synthesis loop.

The goal of this work is to further study, optimize and integrate promising process designs for syngas production by solar thermal water splitting and the process of converting this syngas to FT product, both individually studied recently at NTNU [4, 5, 6]. There are three main focus areas in this study, as listed below.

1. To explore different design alternatives and optimize independent variables in order to optimize the production of FT product and the energy efficiency for the entire plant, while implementing correct reaction kinetics for the FT reactor.
2. To ensure realistic and efficient heat integration for the entire system which has a high influence on the profitability of this process.
3. To perform a cost and value analysis and derive a techno-economical feasibility.

2 LITERATURE REVIEW

A literature search has been conducted with main focus on three areas:

- Syngas production processes for FT Synthesis
- FT Synthesis
- Solar thermal energy derived syngas.

The work presented in this thesis is based upon recent studies at NTNU, whereas Erevik [4] and Souskova et al. [5] are assessments of the design and optimization of solar thermal energy derived syngas and Erevik [4] is a further development of Souskova et al. [5]. An assessment of the design and optimization of FT synthesis from the solar thermal energy derived syngas in Souskova et al. [5], is performed in Emhjellen [6]. The integration between the syngas production and the FT synthesis is conducted in a close cooperation between Erevik [4] and Emhjellen [6] in the respective assessments. The primary focus in Erevik[4] and Souskova et al. [5] is to optimize the temperature of the feed to the solar reactor by heat exchanging with process streams, in order to reduce the energy required from the heliostats while maintaining the desired product of syngas. The primary focus in Emhjellen [6] is to optimize the design and conditions in the FT synthesis loop in order to maximize the production of heavy FT product from the syngas derived by solar thermal energy in Souskova et al. [4].

Processes in oil refinery, such as catalytic cracking, reforming, hydroforming, and diesel production, are described in Moulijn et al. [7]. This book gives insight in potential applications for FT product. In addition, this book covers production of light

alkenes and production of synthesis gas in detail, as well as Fischer Tropsch general concepts, reactors, catalysts and conditions.

In Aasberg-Petersen et al. [8], synthesis gas production for FT synthesis, including gas preparation and purification is discussed. The Fischer Tropsch synthesis benefits from having a low concentration of inert components, such as CH_4, N_2 and a high CO/CO_2 ratio in the makeup synthesis gas feed, which is explained in Aasberg-Petersen et al. [8].

Various methods of converting natural gas into synthesis gas for multiple usages is discussed in Rice & Mann [9], *whereas s*ynthesis gas and autothermal reformer (ATR) technical basics, as well as ATR technical issues is described. While this literature does not describe the usage of syngas in FT synthesis directly, it describes how it is evident that recycling of CO_2 to the ATR is required for achieving a desirable syngas composition while maximizing syngas production, and Moulijn et al. [7] agrees. In addition, Rice & Mann [9] describes how a pre reformer is used to convert heavy hydrocarbons to methane and lighter components, accommodate swings in natural gas composition and to debottleneck the existing primary reformer.

Technologies for large scale conversion of gas, including conversion of natural gas to synthesis gas by ATR then to liquid fuel by FT synthesis is described in Aasberg-Petersen et al. [10].While this literature is discussing a flow scheme with syngas produced only from natural gas in an ATR with water, CO_2 and O_2, but not using solar thermal water splitting to produce H_2 and O_2, this process differs in some ways to the one proposed in this thesis. However, the composition of synthesis gas into the FT reactor and the usage of a pre reformer will be the same, since the parts of the plant in question are almost identical. In addition, this literature's conclusion that the cost of the manufacturing of synthesis gas is a key parameter for making the conversion of natural gas into liquid FT product is supporting the research in this thesis using solar thermal energy derived synthesis gas, as an alternative to this literatures concluded cheapest solution of natural gas conversion in an ATR.

The nature of coke formation and its definition is described in Appleby et al. [11]. This literature discusses coke formation in catalytic cracking and how it can be dealt with by flushing with inert gas. However, coke formation is usually suppressed at high steam/carbon ratios and high oxygen/carbon ratios [12].

A techno-economic analysis is performed on a FT synthesis from natural gas in Rafiee & Hillestad [13]. The design, optimization and the location for placement of a CO_2 removal unit is discussed in this literature.

Upgrading of Fischer Tropsch product to produce diesel is described with graphs and numbers for different configurations of FT synthesis in Sasol Technology Research and Development [2]. In Collins et al. [3], the research history of upgrading FT product is presented and it is revealed that the BP exploration America Inc. - FT process was producing FT product with an average carbon number of 39.3.

How to model the Fischer Tropsch product distribution and reaction kinetics is described in detail in Hillestad [14]. This literature is describing the propagation probability, α, how it depends on the H_2/CO molar ratio, and its correspondence to the product distribution and reaction rate. Modeling and optimization of a slurry bubble column reactor for producing FT liquid hydrocarbons are presented in Sehabiague et al. [15] as well. This literature discusses the optimal conditions for the FT synthesis at different design basis parameters.

Solar thermal splitting of water for production of hydrogen is discussed in Munich et al. [16]. Solar thermal water splitting by an isobar temperature swing reduction-oxidation cycle is described, and it is discussed how solar thermal water splitting by an isothermal pressure swing reduction-oxidation cycle is beneficial for the production of hydrogen.

A technical and economical analysis on how to reduce the cost of solar heliostats and the solar plant is performed in Kolb et al. [17] and Sargent & Lundy LLC consulting group [18], respectively. Both of the reports have detailed calculations of investment costs and operating costs. However, the operating costs are estimated individually for each case, by approximations such as replacement rates and by percent of total equipment cost. The investment cost of the solar heliostats is estimated to US$ 127/m^2 in 2015 in Kolb et al. [17] and the energy provided by the heliostats per m^2, e_{helio} is found to be 0.58kW in Stine et al. [19] and it is found to be 0.60kW in Practical Solar [20]. The value from Stine et al. [19] is used in this thesis in order to be conservative in the plant evaluation. A method for estimating the annual cost of cleaning the heliostat field is discussed in Kolb et al. [17] and it is suggested that there is a need for similar methods to calculate other operating costs for solar plants. The annual cost of cleaning the heliostats is calculated by this method to be US$ 0.35/m^2, assumed constant across heliostat size variations [17].

An initial selection process for evaluating the processes for solar thermochemical cycles for hydrogen production that are most likely to be feasible is performed in Perret [21]. Out of more than 350 possible cycles 9 cycles made it past the initial selection process and participated in the evaluation. Summaries of the technical status of the processes evaluated are provided and the cycles have been studied in the range from less than one year to over 30 years. The response time and conversion efficiency of the hercynite cycle was stable over multiple cycles and this cycle was amongst the cycles that were recommended to continue investigating and it is described that it has the potential for initiating reduction at lower temperatures than other cycles of the same reaction class. In addition, it is described how a lot of research remains, such as establishing its stability under repetitive cycling, its behavior and costs associated with its active material.

In International Renewable Energy Agency [22], a cost analysis is performed for concentrating solar power systems and a robust estimate of the operating and maintenance cost for a solar thermal energy plant, including insurance and all other miscellaneous costs is estimated to be in the range of US$ 0.02/kWh to US$ 0.03/kWh.

3 GENERAL CONCEPT AND THEORY

In general, syngas, or synthesis gas, a mixture of H_2 and CO, is produced in a solar reactor with metal oxide catalysts at temperatures between 1200 and 1500°C, which is reached by using concentrated solar energy. Solar radiation is reflected by heliostats, focusing concentrated solar radiation on a receiver, usually fixed on the top of a tower. A real image of the solar power tower plant of Abengoa Solar in Seville, Spain, using solar thermal energy to produce steam for generating electricity in a steam turbine, is provided in the figure below.

Figure 1: Solar Power Tower plant in Seville, Spain, using solar thermal energy to produce steam for generating electricity in steam turbines [23].

The image in figure 1 is showing a solar power tower where the solar thermal energy is concentrating radiation on the receiver producing steam for generation of electricity in a steam turbine. Instead of using solar thermal energy for producing steam, the concentrated solar radiation provides solar thermal energy to an integrated thermal receiver, which is the solar reactor in this thesis.

The solar reactor, also known as the hercynite cycle, is a two step thermodynamic cyclic system using a metal oxide for reduction and oxidation of the feed stream being either H_2O, forming ½ O_2 and H_2, or CO_2, forming ½ O_2 and CO. The oxidation and reduction reactions occur in the same reactor and are controlled by either a temperature swing, which means changing the temperature with isobaric conditions in the reactor, or a pressure swing, changing the pressure with isothermal conditions in the reactor [16]. During the reduction step, oxygen is produced and leaves the reactor in a separate stream than the H_2 and CO which is produced in the oxidizing step. While the oxygen produced is considered a valuable product, the produced H_2 and CO (syngas), is used as feed for various processes, such as methanol synthesis or Fischer Tropsch (FT) synthesis. The usage of syngas depends on the H_2/CO molar ratio, of which may be

manipulated to its optimal ratio for the intended process, by adjusting the flowrate of the CO_2 feed.

The optimal H_2/CO ratio for FT synthesis depends on the type of reactor, catalyst and temperature. Catalysts currently used for FT synthesis are based upon cobalt or iron. Iron based catalysts promote the water gas shift (WGS) reaction, which results in an increased H_2/CO ratio inside the reactor. Therefore it requires a low H_2/CO ratio in the syngas makeup feed compared to the cobalt based catalyst, of which does not promote the WGS reaction. The water gas shift reaction is presented in the equation below.

$$\boldsymbol{H_2O + CO \rightarrow H_2 + CO_2} \quad \textbf{(3.1)}$$

Normally, the feedstock for FT synthesis consists of significant amounts of inert components, such CO_2, N_2 and H_2S that needs to be removed from the feed stream; however, this may not be the case when the syngas is derived from a solar reactor [7].

The most valuable products from the FT synthesis are a widespread of lighter and heavier hydrocarbons in their liquid state, which are removed from the gas stream by separation, as FT raw product. The liquid FT raw product is sent for upgrading to synthetic crude by hydrocracking followed by separation into the end products, yielding products such as liquefied petroleum gas (LPG), naphtha, jet fuel, kerosene, lubricant oil, diesel and wax [2, 3]. The remaining gas phase contains unconverted syngas, water, components that are inert in the FT reactor, such as CO_2, and light hydrocarbons, which is referred to as tail gas. The tail gas can be sent through additional FT reactors after readjusting the H_2/CO molar ratio, or be recycled back to the FT reactor in order to achieve more efficient production. The recycling may be done by processes such as introducing a partial purge and directly recycling the remaining tail gas, or by removal of inert components and recycling through an autothermal reformer (ATR), which converts lighter hydrocarbons into syngas [7].

3.1 Base case of the particular process

This thesis is based upon recent studies at NTNU whereas the syngas is produced by solar thermal water split and is intended for FT synthesis [4, 5, 6]. The FT synthesis uses a cobalt based catalyst in a slurry bubble column and the tail gas is purified of CO_2 in an amine plant before being recycled through an ATR.

3.1.1 Solar thermal water split

The pressure swing reduction-oxidation cycle has a better potential with respect to hydrogen production than the temperature swing reduction-oxidation cycle, and is therefore to be preferred [16]. The figure below illustrates a simplified sketch of the oxidation-reduction cycle for solar thermal water splitting.

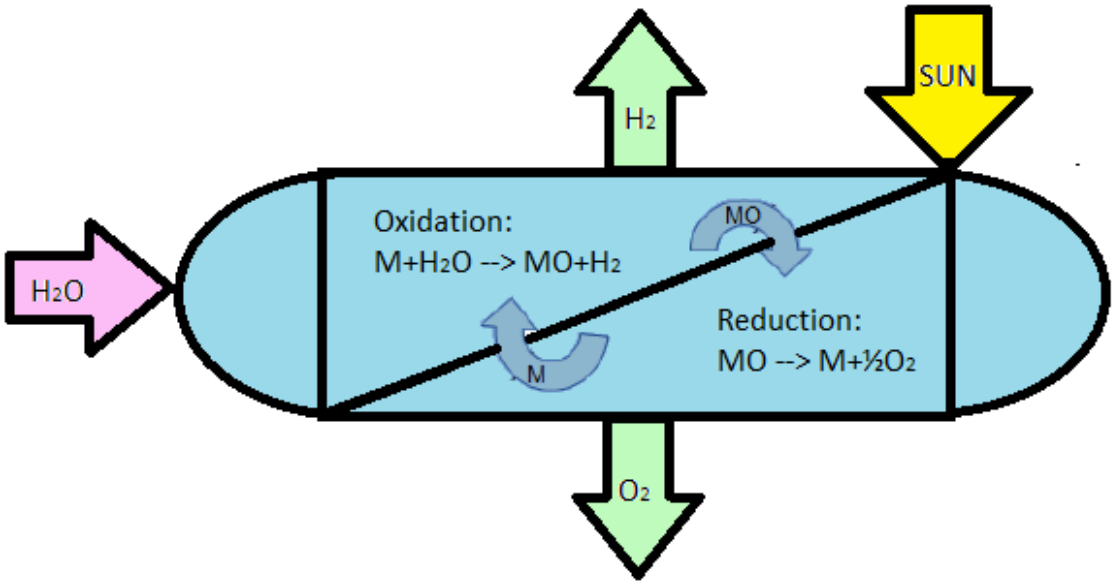

Figure 2: Simplified oxidation-reduction cycle for solar thermal water splitting, where M denotes metal and MO denotes oxidized metal.

In the oxidation step, water reacts with the metal catalyst in its reduced state, transferring its oxygen atom, thus yielding oxidized metal while H_2 is left in the gas phase in the solar reactor and is sent for further processing. When the amount of metal catalyst oxidized is near equilibrium, the partial pressure of steam is reduced, and the oxidized metal will release its oxygen. Before the next cycle can begin, as much oxygen as possible should be released and leave the reactor. This is done by introducing a vacuum pump and allowing for the oxygen to leave the reactor in a separate stream. The governing oxidation reaction is shown in equation (3.2) and the governing reduction reaction is shown in equation (3.3) below [16].

$$\boldsymbol{CoAlO_4 + 2FeAl_2O_4 + H_2O \rightarrow CoFe_2O_4 + 3Al_2O_3 + H_2} \qquad \textbf{(3.2)}$$

$$\boldsymbol{CoFe_2O_4 + 3Al_2O_3 + heat \rightarrow CoAl_2O_4 + 2FeAl_2O_4 + \frac{1}{2}O_2} \qquad \textbf{(3.3)}$$

The heats of reactions at 1350°C for these two reactions are calculated in Aspen HYSYS and are presented together with the simulation methodology in chapter 5.1. The conversion in the oxidation reaction is assumed to be 90% with respect to the metal and 90% with respect to the oxidized metal in the reduction reaction, thus leaving almost pure hydrogen and oxygen as products, with a small fraction of trace water [5]. 90% of the trace water is assumed to be in the hydrogen product and the remaining 10% in the oxygen product [5]. In order to achieve continuous production, there are two solar reactors operating in parallel with cycles opposite of each other. The water is fed to the reactor performing the oxidation step where hydrogen is produced, while oxygen is produced in the other reactor. The cycle time is set to 10minutes [5]. When the oxidation step is completed in the reactor producing hydrogen, the water feed is sent to the other reactor, now performing oxidation and producing hydrogen.

3.1.2 Synthesis gas from reverse water gas shift reaction

The hydrogen produced by the solar thermal water split undergoes a reverse water gas shift (RWGS) reaction by direct injection of a CO_2 feed in order to produce syngas at the desired composition. The RWGS reaction is endothermic (ΔH_{rx}=41 kJ/mol), the reaction is favored by high temperatures and is shown in equation (3.4) below [24].

$$\boldsymbol{H_2 + CO_2 \rightarrow H_2O + CO} \qquad \textbf{(3.4)}$$

The H_2/CO ratio in the syngas product from the RWGS can be manipulated to the desired optimal ratio by adjusting the flowrate of the CO_2 feed and the temperature for the reaction. A simplified block diagram which summarizes the process so far is given in the figure below.

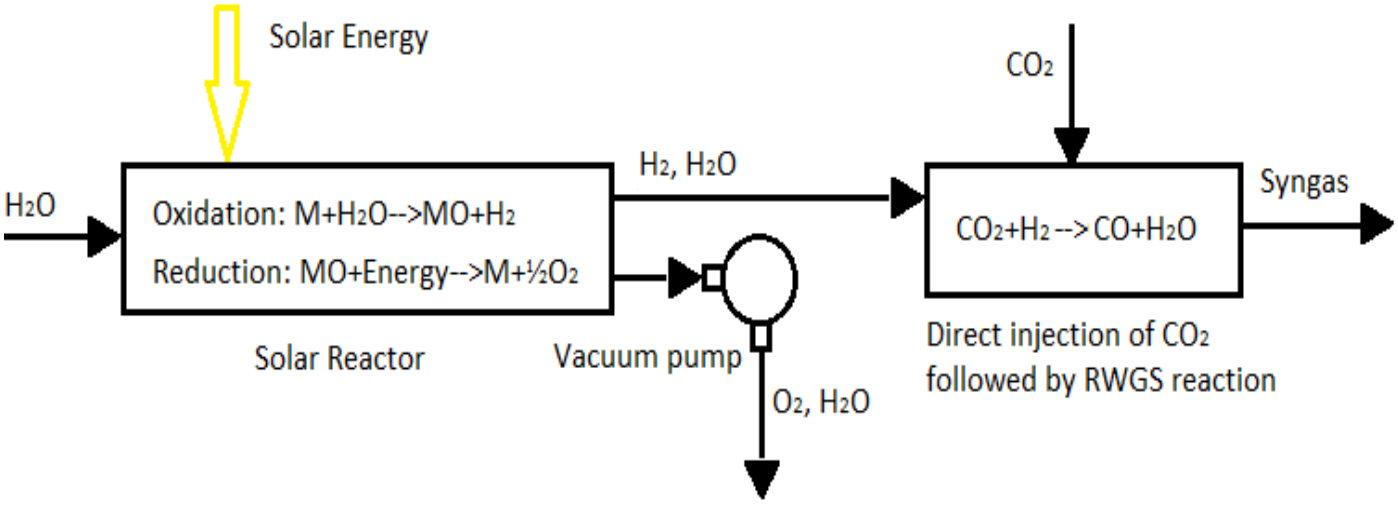

Figure 3: Simplified block diagram of solar thermal water split followed by direct injection of CO_2 and reverse water gas shift. M denotes metal and MO denotes oxidized metal. The governing reactions in the solar reactor are given in more detail in equations (3.2) and (3.3).

Figure 3 shows that solar energy is used for splitting water in the solar reactor. Hydrogen and oxygen is produced continuously due to two solar reactors operating with opposite cycles, and the resulting hydrogen is mixed with CO_2, resulting in a reaction that yields syngas.

3.1.3 Fischer Tropsch synthesis

The syngas produced in the RWGS reaction is sent to Fischer Tropsch (FT) synthesis after being cooled in order to remove water in a separator. The FT reactor is a slurry bubble column, reacting syngas in the presence of fine cobalt based catalyst particles suspended in a liquid phase to form a mixture of hydrocarbons. The reactor is operating isothermally and isobaric at 220°C and 20bar. There are two main reactions occurring in the FT reactor, which are presented in the equations (3.5) and (3.7) below [14].

$$\boldsymbol{CO + (3 - \alpha)H_2 \rightarrow \sum_i^{\infty} v_i C_i H_{2i+2} + H_2O} \qquad \textbf{(3.5)}$$

Where

$$\boldsymbol{v_i = (1 - \alpha)^2 * \alpha^{i-1}} \qquad \textbf{(3.6)}$$

This reaction is yielding hydrocarbons at a widespread of carbon numbers and the propagation probability, $\boldsymbol{\alpha}$, is dependent on the temperature and H_2/CO molar ratio inside the reactor. The reaction is approximated by lumps of components in the process simulation. The reaction kinetics, propagation probability, $\boldsymbol{\alpha}$, and the approximation by lumping of components is described in detail in Hillestad [14]. However, the reaction kinetics, lumping of components, and $\boldsymbol{\alpha}$ is to be implemented for the process simulation this thesis and is further described in chapter 5.

Because alpha is dependent on the temperature, it is essential to maintain isothermal conditions. The overall reaction in the FT reactor is exothermic; hence, in order to achieve isothermal conditions and avoid overheating of catalyst which results in an increased deactivation rate due to sintering and fouling, a cooling water system is integrated in the reactor [25]. Because the cooling water is integrated in the FT reactor, a high heat transfer coefficient is essential in order to reduce the required space for the cooling tubes inside the FT reactor; hence, water at its boiling point is utilized, using the heat of vaporization for cooling. However, cooling water configurations are to be investigated in this thesis and are further described in chapter 6. The second reaction occurring in the FT reactor is shown in the equitation below.

$$\boldsymbol{3H_2 + CO = CH_4 + H_2O} \qquad \textbf{(3.7)}$$

The liquid FT product is separated from the gas phase inside of the slurry bubble column, which enables the liquid product to leave the reactor in a separate stream. By reducing the temperature of the tail gas, more hydrocarbons become liquid and leave a downstream three phase separator as liquid product. The Fischer Tropsch product can be cracked into various products, such as diesel, naphtha and wax, depending on the hydrocarbon chain length, which is described in Sasol Technology Research and Development [2] and Moulijn et al. [7]. A simplified flowsheet summarizing the process so far is shown in the figure below.

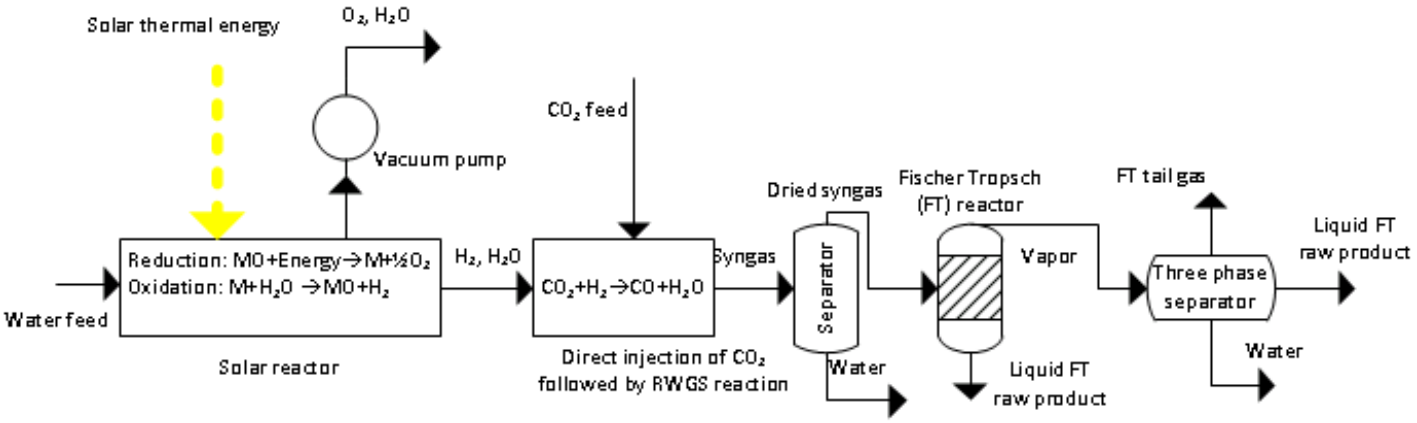

Figure 4: Syngas produced from solar thermal water split fed to FT synthesis. M denotes metal and MO denotes oxidized metal. The governing reactions in the solar reactor are given in more detail in equations (3.2) and (3.3). The syngas is dried before entering the FT reactor. More FT product is liquified by cooling and is taken out in a three phase separator.

Figure 4 shows that syngas derived from solar thermal water split and RWGS reaction is dried before being sent to FT synthesis. More FT product is liquefied from the vapor stream leaving the FT reactor. This is done by cooling, and the liquid product is taken out in a three phase separator.

3.1.4 CO_2 purification of tail gas by an amine plant

The tail gas is purified of CO_2 by an amine plant because of four main reasons

1. The amine plant enables nearly complete recycling of all CO_2. This is beneficial with respect to environmental aspects and carbon efficiency, in addition to reducing the external CO_2 feed needed for production of syngas in the RWGS reaction.

2. It removes the need for any partial purge, except for waste water.

3. It reduces the size of the equipment in the FT synthesis loop

4. It allows for optimization of the CO_2 concentration in the downstream ATR.

The simplified flowsheet presented below illustrates the CO_2 purification of the tail gas by an amine plant.

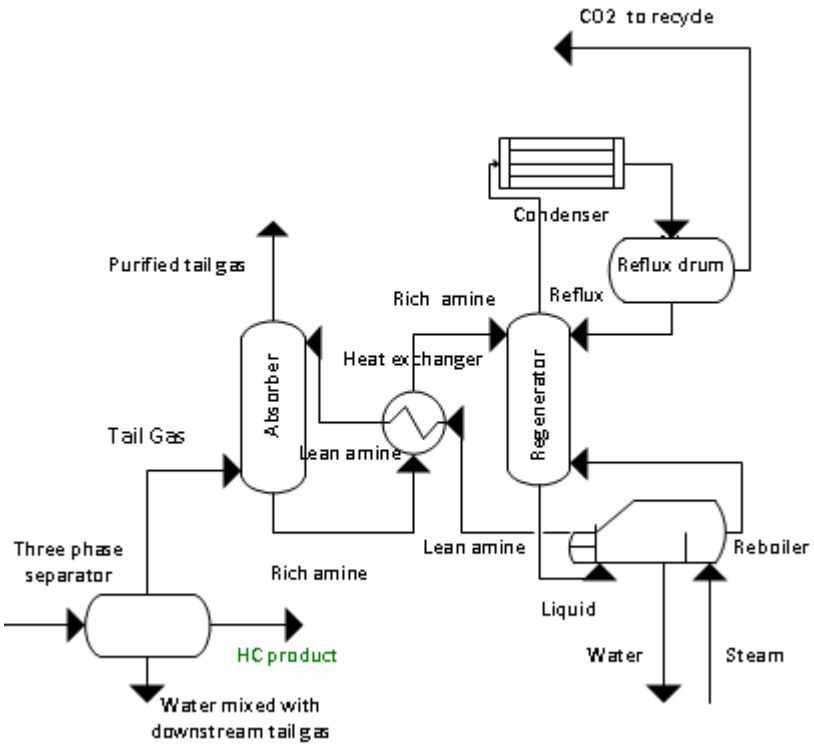

Figure 5: Simplified flowsheet for CO_2 capture of the tail gas by an amine plant.

Figure 5 presents the basic concept of the amine plant. The amine plant utilizes the thermodynamics of the absorption/desorption reactions, whereas the absorption is an exothermic reaction and desorption is an endothermic reaction. Hence, utilizing a temperature swing process, the equilibrium can be driven to either side. The tail gas enters the absorption column bottom and is contacted with CO_2 lean amine solvent fed at the top. CO_2 reacts with the solvent and is absorbed in the liquid. The purified tail gas leaves the top of the absorber. The CO_2 rich solvent leaves the absorption column bottom and is pre-heated in the heat exchanger before injection to the regenerator top. In the regenerator column, heat is added by the reboiler. This drives the equilibrium of the process to release CO_2 from the liquid, since the desorption reaction is endothermic. The CO_2 lean amine leaves the stripper bottom and is sent to the heat exchanger to transfer heat to the rich amine out of the absorber. This process is explained in more detail in Kohl & Nielsen [26].

3.1.5 Autothermal reformer

The autothermal reformer (ATR) is converting methane and lighter hydrocarbons in the FT tail gas into syngas at high temperatures. The high temperature is reached by

utilizing oxygen produced in the solar reactor, resulting in exothermic reactions. Before going through the ATR, the tail gas is enriched with steam and sent through a pre reformer which converts all hydrocarbons, but methane, in order to prevent coke formation. There are five reactions occurring in the ATR, which are shown in the equations below. [27]

$$\boldsymbol{CH_4 + H_2O = 3H_2 + CO} \quad \textbf{(3.8)}$$

$$\boldsymbol{CO_2 + H_2 = CO + H_2O} \quad \textbf{(3.9)}$$

$$\boldsymbol{2H_2 + O_2 = 2H_2O} \quad \textbf{(3.10)}$$

$$\boldsymbol{CH_4 + 2O_2 = CO_2 + 2H_2O} \quad \textbf{(3.11)}$$

$$\boldsymbol{CH_4 + \frac{1}{2}O_2 = CO + 2H_2} \quad \textbf{(3.12)}$$

The reformed tail gas is recycled to the FT reactor after it is cooled and water is removed in a separator. The simplified flowsheet below summarizes the entire base case of the particular process with the solar thermal syngas production units and the FT synthesis units connected.

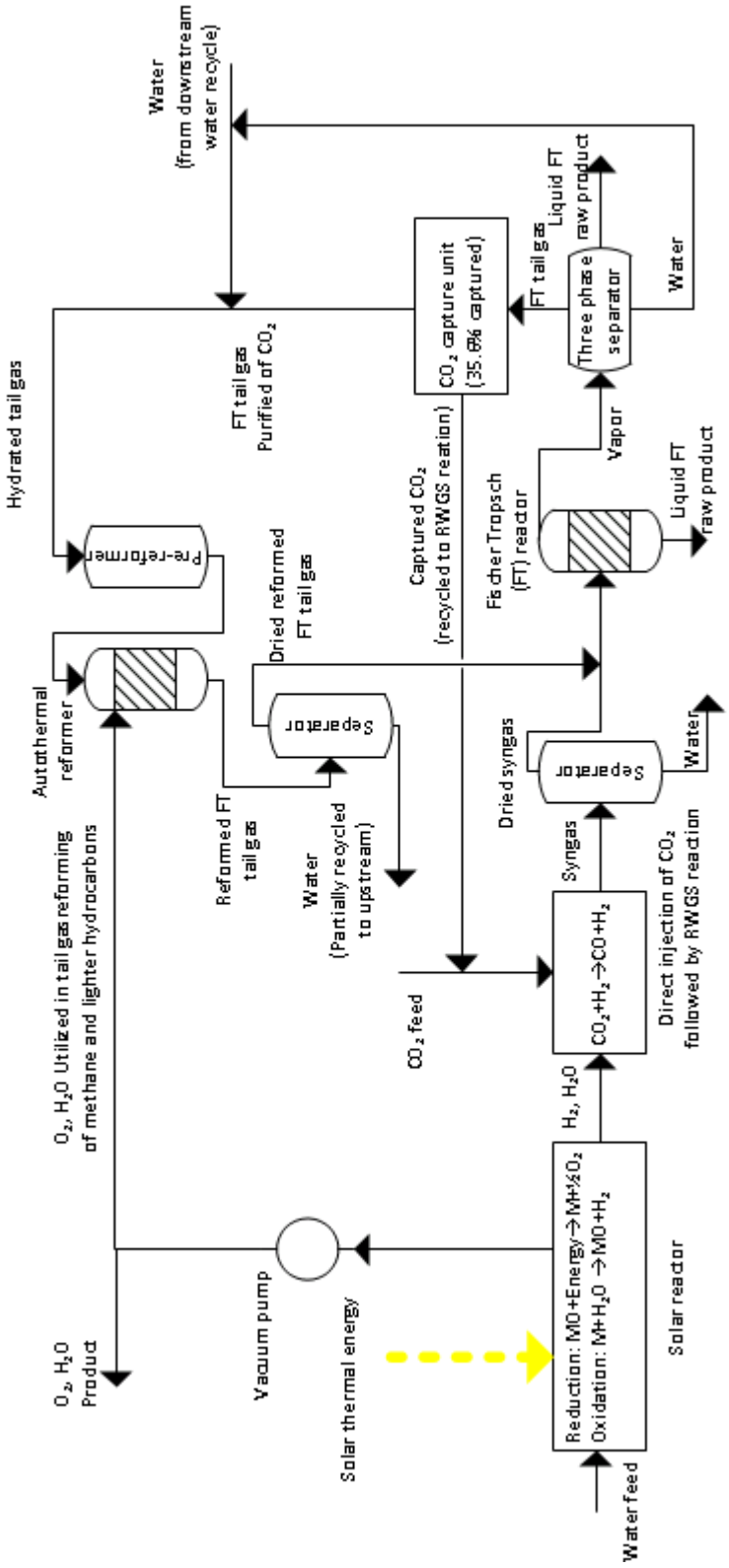

Figure 6: Simplified flowsheet for the entire base case of the particular process. M denotes metal and MO denotes oxidized metal. The governing reactions in the solar reactor are given in more detail in equations (3.2) and (3.3).

Figure 6 shows the basic integration of the base cases from Erevik [4] and Emhjellen [6]. The individual Aspen HYSYS models from the given base cases in Erevik [4] and Emhjellen [6] are presented in Appendix E.

4 CONCEPTUAL DESIGN

4.1 Design basis

This thesis is based upon recent studies at NTNU, whereas Erevik [4] and Souskova et al. [5] are assessments of the design and optimization of syngas production by the hercynite cycle and Erevik [4] is a further development of Souskova et al. [5]. An assessment of the design and optimization of FT synthesis from the solar thermal water split derived syngas in Souskova et al. [5], is performed in Emhjellen [6]. The integration between the solar thermal syngas production and the FT synthesis is conducted in a close cooperation between the authors in the assessments in [4] and Emhjellen [6]. However, the simulations and optimization is these assessments are only performed for the respective parts of the entire plant. The primary focus in Erevik [4] and Souskova [5] is to optimize the temperature of the water fed to the solar reactor by heat exchanging with process streams, in order to reduce the energy required from the heliostats while maintaining the desired product of syngas. The primary focus in Emhjellen [6] is to optimize the design and conditions in the FT synthesis loop in order to maximize the production of FT product from the syngas delivered by the solar thermal water split in Erevik [4]. The assessments in Erevik [4] and Emhjellen [6] are to be considered the base cases to be further developed, fully integrated, adjusted and optimized in this thesis. In order to give an overview of the key differences between the design basis in previous studies and in this thesis, the key design basis and result of these assessments are presented together with the adjusted design basis for this thesis, in the tables below.

Table 1: Overview of the key differences between design basis in previous studies and in this thesis. Erevik [4] and Emhjellen [6] is labeled 1. and 2. respectively, and referred to correspondently in the column "This thesis" for easier comparison. Differences is highlighted in bold in the column "This thesis".

	1.(Erevik [4])	2.(Emhjellen [6])	This thesis
Design basis	- Conversion with respect to metal is 90% for the oxidation and reduction steps in the hercynite cycle. -The cycle time between oxidation and reduction is 10 minutes. - 10% of unconverted water in the solar reactor will be in the oxygen product, while the remaining 90% is in the hydrogen product - Operating pressure of the process is 5bar, while the oxygen product from the solar reactor is 0.5bar. - A ceramic high temperature heat exchanger is required at temperatures above 850°C for heat exchanging syngas with process streams, and at temperatures above 1100°C for heat exchanging oxygen with process streams. The flowrate of water fed to the solar reactor is 699kgmole/h.	-The propagation constant is approximated to be constant for all components in the FT reaction, α=0.94, and to correspond to a H_2/CO ratio of approximately 1.7 into the FT reactor with a temperature of 230°C inside the FT reactor and the reaction kinetics is approximated by the Arrhenius equation, k=[A*e]^((-E/RT)). - CO conversion of approximately 60% over the FT reactor is assumed to be optimal and the FT loop operating pressure is assumed optimal at 20bar	1. Conversion in the oxidation reaction is 90% with respect to the metal and 90% with respect to the oxidized metal in the reduction reaction in the hercynite cycle. - The cycle time between oxidation and reduction is 10 minutes. - 10% of unconverted is in the oxygen product, while the remaining 90% is in the hydrogen product. - The operating pressure of the solar thermal syngas production process is 5bar and the oxygen product from the solar reactor is 0.5 bar. - A ceramic high temperature heat exchanger is required at temperatures above 1100°C for heat exchanging oxygen with process streams, and syngas is required to be cooled to **600°C** in a waste heat boiler before heat exchanging with process streams [10, 28] The flowrate of water fed to the solar reactor is 699kgmole/h 2. The propagation constant, α, is **not** constant for all components in the FT reaction, and the reaction kinetics is dependent on α. This implementation is further described in Hillestad [14]. - CO conversion of approximately 60% over the FT reactor is assumed to be optimal, and the FT loop's operating **pressure is to be investigated**.

Table 2: Key results of previous studies

	(Erevik [4])	(Emhjellen [6])
Results	Overall energy efficiency for syngas production calculated to 84.05%. Highest temperature achievable by process to process heat exchanging before solar heating water in the solar reactor is 917.2°C.	Overall energy efficiency for the FT synthesis (from solar energy to FT product) calculated to 50.3%. Final FT product flowrate is at 8.999kgmole/h (2944kg/h) with 0.4533 mole fraction of a lump with average carbon number 36.666.

While the assessments Erevik [4], Emhjellen [6] and Souskova et al. [5] are addressing and simulating either the solar thermal production of hydrogen or FT synthesis individually, an assessment with simulation of the entire plant will be addressed in this thesis. In addition to addressing the entire plant, adjustments of the design basis and further process development is made in this thesis, with the key differences described in table 3. There are several additional design basis configurations in this thesis.

- In order to achieve continuous production, there are two solar reactors alternating between producing hydrogen and oxygen.
- The solar reactors are assumed to operate during the hours of sunlight, assumed to be 8 hours per day, 334 days a year at the optimal location of the plant in South Africa, and the entire plant is therefore expected to operate during these hours [5].
- A temperature above 850°C is desired for the RWGS reaction to go spontaneously without a catalyst, thus removing the need of a reactor [22].
- The temperature of the mixed CO_2 and H_2 before the RWGS determines the flowrate of CO_2 required to achieve syngas at H_2/CO ratio of 2, as well as the CO_2 content in the syngas. The upper limit CO_2 content in the makeup syngas is assumed to be approximately 12mol%, which results in a mixed CO_2 and H_2 temperature of approximately 1100°C [4].
- The optimized H_2/CO ratio for the makeup syngas is 2 and the optimized FT product distribution, α, versus production rate is assumed to correspond to H_2/CO ratio in the range of 1.2 to 1.4 inside the FT reactor [9, 10].

- For simulation purposes, the CO_2 concentration out of the CO_2 capture unit is set to be 100% and methane feedstock is available as pure methane
- The FT tail gas recycle stream into the pre reformer has a maximum temperature of 400°C and into the ATR it is assumed to have a maximum temperature of 600°C to prevent coke formation [10].

The goal in this thesis is to maximize production of heavy Fischer Tropsch product from solar thermal energy on a mass per time basis with corresponding optimal energy efficiency and heat exchanger network. The main focus areas in this thesis are summarized in the list below.

- Process development for optimizing the conceptual design and optimizing all conditions and variables with respect to total production of heavy FT product

- Optimizing the entire plants energy efficiency with carbon efficiency, purge of valuable components and recycling ratios kept at reasonable values.

- A FT reactor model from Aspen Custom Modeler (ACM) is implemented in the Aspen HYSYS simulation in order to simulate the FT reactor with a more correct FT product distribution and reaction kinetics.

- A major focus is to reduce the need for solar thermal heating of the water fed to the solar reactor by optimizing the heat exchanger network based on simulations in Aspen HYSYS and Aspen Energy Analyzer (AEA).

- Finally, a techno-economical plant evaluation is performed for the final best case.

The feed of water is set to 699kgmole/h and the entire process is scaled from this stream, meaning that the production plant can be re-scaled simply by multiplying every inlet material- and energy stream with a desired factor for reproducing the work in this thesis at different a different scale. Although the scale up of certain equipment in this process is evaluated during the optimization of the conceptual design, the scale-up of the entire process is beyond the scope of this thesis. However, a scale up analysis is recommended to be considered for further investigation and discussed in chapter 8.1. The conceptual design was developed and optimized with the design basis as described. The computer software Microsoft Visio® by Microsoft Corporation has been used for schematic drawing of the process flow diagram. The computer software Aspen HYSYS® by AspenTech has been used for calculations, simulation of the conceptual design and optimizing the process on a production basis. The optimizing was performed

by using the optimizer function in Aspen HYSYS on separate parts of the process, when applicable, to manipulate all independent variables in a wide range simultaneously, and manual adjusting of all independent variables, when the optimizer function was not applicable. The reason for not using the optimizer function for the entire process is described in chapter 7.2.

In the Aspen HYSYS simulation, a fluid package with Peng-Robinson properties was used. The Peng-Robinson model is ideal for Vapor-Liquid Equilibrium calculations and calculations of liquid densities for hydrocarbon systems. In addition, the Peng-Robinson property package is very efficient and highly reliable in solving any single-, two-, or three-phase systems in a wide range of conditions; pressures below 1000bar and temperatures above -271°C, of which this simulation is within. Further, Peng-Robinson is generally the recommended property package for simulation of processes involving hydrocarbons and oil, gas, or petrochemical applications. [29, 30]. The Aspen HYSYS simulation is further described in chapter 5 and in Appendix F.

The computer software Aspen Energy Analyser® by AspenTech is used for simulations and optimization of the heat exchanger networks (HENs), which is further described in chapter 6.

4.2 Process flow diagrams of the best case

The process flow diagrams of the best case developed in this thesis is presented in the figures below.

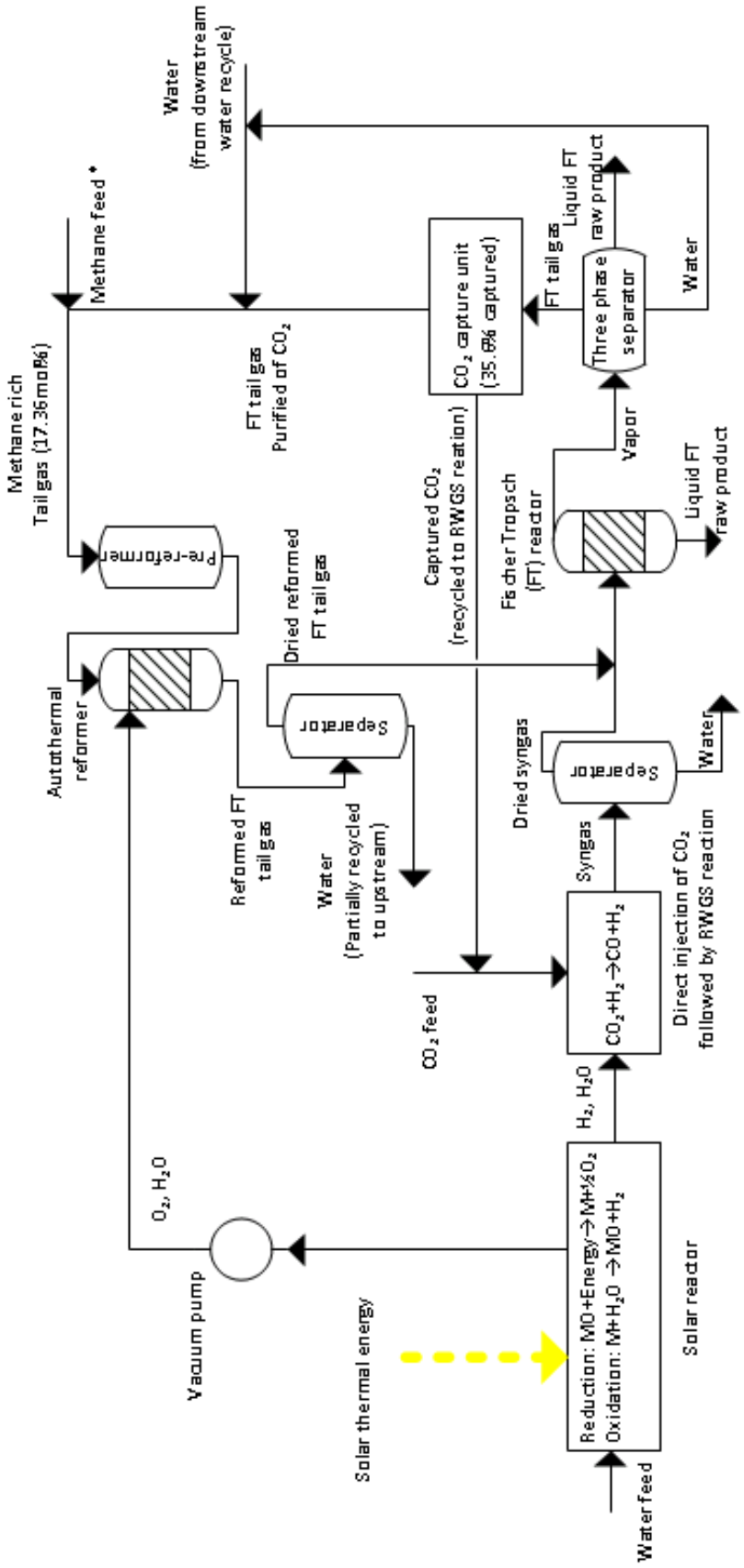

Figure 7: Simplified flowsheet of the best case conceptual design

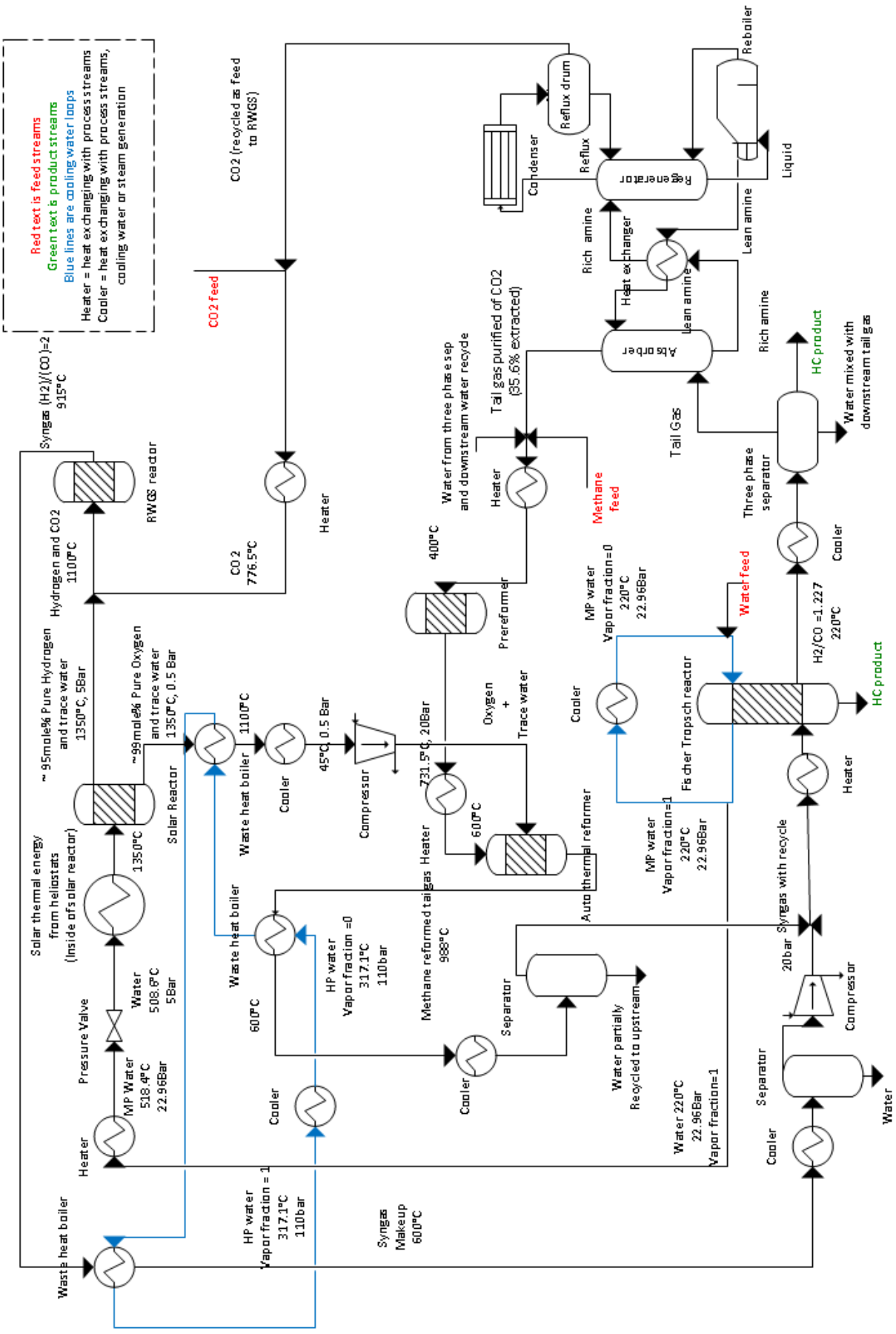

Figure 8: Process flow diagram of the best case

4.3 Process description of the best case

The water feed for the solar reactors is pumped up to 22.96 Bar and goes through the FT reactor's cooling system in order to get vaporized and heated to 220°C by the FT heat of reaction. Together with the solar reactors' feed, additional water is required in the FT reactor's cooling system in order to maintain a constant temperature in the FT reactor. The additional water goes in a loop partially through a condenser, releasing heat to process streams, and partially through a steam turbine, generating electricity, before being recycled back to the FT reactor's cooling system.

In order to reduce the heat exchanger area inside the FT reactor, the cooling water inlet is near its boiling point of 220°C at 22.96bar, meaning the majority of the cooling duty is from the heat of vaporization of boiling water, of which has a higher heat transfer coefficient than liquid water. The amount of additional water required in order to maintain a constant temperature in the FT reactor is calculated in Aspen HYSYS.

However, the solar reactors' feed is leaving the FT reactor's cooling water system and is heated by process to process heat exchanging to 518.4°C. Further, the pressure is reduced to 5bar in a valve, resulting in a final temperature of 508.6°C, before heating with solar thermal energy from the heliostats is required. Heating from solar thermal energy is taking place inside of the solar reactors and this energy comes from concentrated solar radiation by the heliostats, heating the water to 1350°C.

The cooling water loop, heating of water fed to the solar reactor and the basis for the heat exchanger network (HEN) is further described in chapter 6, while the best case HEN is presented in chapter 7.3. The solar reactors are producing H_2 and O_2 in separate streams and the conditions and compositions of the streams in and out of the solar reactors is shown in the table below.

Table 3: Conditions and composition of streams in and out of the solar reactors

Stream	Water feed	Hydrogen product	Oxygen product
Vapour / Phase Fraction	1	1	1
Temperature [C]	1350	1350	1350
Pressure [Bar]	5	5	0.5
Molar Flow [kgmole/h]	699	695.17	334.18
Mass Flow [kg/h]	12593	1953	10640
Component [Molar fraction]			
Hydrogen	0	0.95	0
CO	0	0	0
H2O	1	0.05	0.01
Nitrogen	0	0	0
Oxygen	0	0	0.99

Due to the high temperature of the oxygen, it cannot heat exchange with process streams in a conventional heat exchanger and is therefore sent to a waste heat boiler (WHB), reducing the temperature to 1100°C. The annealing temperature for nickel is at 1150°C, while that of stainless steel (18Cr, 8Ni) is at 1050°C [28]. It is therefore reasonable to assume that Oxygen can be cooled in a conventional heat exchanger at 1100°C, and it is heat exchanged with process streams and cooling water to a temperature of 45°C before being compressed from 0.5 to 20bar. The oxygen compressed to 20bar has a temperature of 730.1°C and is used for methane reforming downstream the plant.

The high temperature hydrogen produced in the solar reactor is mixed with a stream of CO_2, which comes from an external CO_2 feed in addition to recycled CO_2 from downstream the plant. The CO_2 is heated by process streams to 776°C before mixing with hydrogen. The mixed H_2 and CO_2 stream has a temperature of 1099°C and undergoes a RWGS reaction to form syngas. Conditions and composition of the syngas stream after the RWGS reaction in shown in the table below.

Table 4: Conditions and composition of syngas after RWGS reaction

Stream	Syngas from RWGS
Vapour / Phase Fraction	1
Temperature [C]	915.3
Pressure [Bar]	5
Molar Flow [kgmole/h]	1010.2
Mass Flow [kg/h]	15817
Component [Molar fraction]	
CO2	0.0938
Hydrogen	0.4360
CO	0.2181
H2O	0.2522

Due to the high temperature of the syngas, it cannot heat exchange with process streams in a conventional heat exchanger because CO will be subject to coke formation, which also can lead to metal dusting, at temperatures above 600°C [10, 29]. Therefore, the syngas is rapidly cooled to 600°C in a WHB. Further, it is cooled by process to process heat exchanging and by cooling water to 60°C and water is taken out in a separator. The syngas is compressed to 20bar and mixed with a rather large FT tail gas recycle stream before getting heated by process streams and entering the FT reactor. The FT reactor operates at isothermal conditions due to the cooling water configuration previously mentioned. The liquid FT product in the FT reactor is separated from the gas stream inside of the FT reactor. The conditions and composition of the streams in and out of the FT reactor, except for the streams in the cooling water system, is shown in the table below. Heavy hydrocarbons may have a small molar fraction, yet a large mass fraction due to its high molecular weight and the compositions is therefore presented in mass fractions in addition to molar fractions in the table below, in order to give a more detailed overview of the compositions.

Table 5: Conditions and compositions of streams in and out of the FT reactor, except for streams in the FT cooling water system, with compositions given in mass fractions and molar fractions

Stream	FT reactor feed	Liquid product	Gaseous product (Tail gas)
Vapour / Phase Fraction	1	0	1
Temperature [C]	215	221.2	221.2
Pressure [Bar]	20	20	2000
Molar Flow [kgmole/h]	3724.15	11.67	2396.34
Mass Flow [kg/h]	58841	8284	50557
Component [Molar fraction / Mass fraction]			
CO	0.3201 / 0.5674	0.0100 / 0.00039	0.2214 / 0.2939
H2	0.5365 / 0.0685	0.0082 / 0.00002	0.2717 / 0.0260
H2O	0.0172 / 0.0196	0.1152 / 0.00293	0.3021 / 0.2580
Methane	0.0040 / 0.0041	0.0007 / 0.00002	0.0096 / 0.0073
C2	0 / 0	0.0001 / 0.00000	0.0012 / 0.0016
C3	0 / 0	0.0002 / 0.00001	0.0009 / 0.0018
C4	0 / 0	0.0003 / 0.00003	0.0007 / 0.0019
C5+	0 / 0	0.8444 / 0.99530	0.0026 / 0.0134
CO2	0.1222 / 0.3405	0.0209 / 0.00130	0.1899 / 0.3960

The liquid product in the FT reactor leaves the system as FT raw product, while the gaseous product, also known as FT tail gas, is sent to further processing. The gaseous product is cooled by generating steam, heat exchanging with process streams as well as cooling water to a final temperature of 60°C in order to liquefy water and more FT product, which then is separated in a three phase separator. Out of the three phase separator the liquid hydrocarbons (HC) leaves the system as FT raw product, the liquid water leaves in a separate stream and is mixed with tail gas downstream the plant, while the remaining FT tail gas leaves the three phase separator in a third stream and is sent to further processing.

The FT tail gas out of the three phase separator consists of a high fraction of CO_2 and unreacted synthesis gas as well as considerable amounts of methane and light hydrocarbons. Thus, to preserve and optimize recycling of synthesis gas back to the FT reactor, the tail gas is purified of CO_2 in an amine plant before being sent to reforming in an ATR. This design allows for almost all tail gas, but CO_2, to be completely recycled through the downstream ATR with no purging, thus receiving a maximum potential of syngas recovery. The amine plant is extracting 35.6mol% of the CO_2 which is recycled back as feed to the upstream RWGS reaction.

There is an issue that may occur in the downstream ATR of which the Aspen HYSYS simulation does not take into consideration; the hydrocarbons may be subject to coke formation through the ATR at high temperatures. In order to avoid this issue, the stream is preheated and sent through a pre reformer which makes all the hydrocarbons, but methane, fully react, thus preventing the most severe issues of coke formation. The Aspen HYSYS simulation of the pre reformer is discussed in chapter 5; however, it is an important feature that has to be implemented in the realization of the process design.

The purified FT tail gas out of the amine plant is mixed with water recycled from downstream the plant and from the three phase separator, in addition to external methane. The stream is heated by process streams to 400°C and sent through the pre reformer which converts the heavier hydrocarbons. Further, the stream is heated by process streams to 600°C and sent through the ATR together with the oxygen produced in the solar reactor. The amount of water and methane fed to the FT tail gas before reforming is optimized with respect to the amount of available oxygen produced in the solar reactor and the steam to carbon molar ratio is adjusted to 0.6099, which is just above the recommended steam to carbon ratio of 0.6 in Aasberg-Petersen et al. [8].

Due to the high temperature of reformed tail gas out of the ATR, it cannot heat exchange with process streams in a conventional heat exchanger, because CO will be subject to coke formation which may lead to metal dusting at temperatures above 600°C like with the high temperature syngas as mentioned [10, 31]. Therefore, the reformed tail gas is rapidly cooled to 600°C in a waste heat boiler. Further, it is cooled by process to process heat exchanging and by cooling water to a final temperature of 60°C, and water is taken out in a separator. Finally, the tail gas recycle loop is closed by mixing the dried reformed tail gas with the syngas from the downstream RWGS reaction as previously mentioned.

The water utilized in the waste heat boilers is at 110bar at its boiling temperature of 317.1°C and vapor fraction (VF), VF=0, being vaporized to VF=1 through the three WHBs. The steam goes in a loop partially through a condenser, releasing heat to process streams and partially through a steam turbine, generating electricity, before being recycled back to the WHBs as liquid water. The amount of water required in order to cool the hot streams in the WHBs is calculated in Aspen HYSYS.

4.4 Design choices

Several alternative designs were considered during the development and optimization process of the conceptual designs, leading to the current design as the best case. The most important design choices decided upon, together with the respective alternatives they were compared against is presented in this sub-chapter.

The solar reactor may utilize water and CO_2 for production of syngas by using a pressure swing hercynite cycle or a temperature swing hercynite cycle. In this thesis, only water is utilized in the solar reactor, because utilizing CO_2 may cause CO to be subject to coke formation in the reactor at these temperatures [10]. The pressure swing reduction-oxidation cycle has a better potential with respect to hydrogen production than the temperature swing reduction-oxidation cycle, and is therefore chosen in this thesis [16]. Thus, using the solar thermal water split by the pressure swing hercynite cycle is decided upon for this thesis.

Since the 1950s it has been known that slurry bubble column reactors may be used to carry out FT synthesis [15]. However, due to several challenges that had to be solved, the slurry bubble column reactor was not used for commercial-scale FT synthesis until 1993 [25]. One of the challenges that had to be solved was the understanding of the bubble to bubble interactions in the churn turbulent flow regime in the reactor [32]. The churn turbulent flow regime is one of the most complex flow patterns that can be found in gas-liquid two phase flow systems and is described in detail in Montoya et al. [33]. Additional challenges was with respect to high shear created near the gas distributor, side products due to high liquid to solid ratio and difficult catalyst-liquid separation, especially when fine catalyst particles are used [32].

Despite these challenges, the slurry bubble column reactor has several advantages over the agitated and packed bed reactors and is therefore chosen as the basis for the FT synthesis in this thesis. The advantages of the slurry bubble column are with respect to better temperature control due to a large liquid volume in the reactor, low operating and maintenance cost partly due to simple design, low investment cost due to small space needed, large active surface area per reactor volume due to the fine catalyst particles, a higher yield per reactor volume and longer runs without reactor shutdown due to better, continuous catalyst replacement [25, 32, 34, 35].

Two different conceptual design configurations, utilizing external methane together with all oxygen produced from the solar reactor in order to produce additional syngas,

was developed. In one of these design configurations, all of the oxygen produced in the solar reactor is utilized together with the tail gas from FT and the external methane feed in the ATR inside the FT synthesis recycle loop. The other design choice utilizes the oxygen necessary for conversion of the methane in FT tail gas in the ATR, inside the FT loop, while the remaining oxygen is utilized in a separate ATR together with external methane feed, recycled CO_2 and recycled water. These two conceptual design configurations were developed in order to compare the outcomes and decide upon which one is the better design.

Optimizing the conversion of methane to syngas with the composition desired for the FT synthesis in this thesis requires a CO_2 feed [7, 9]. This means that the conceptual design configuration last mentioned utilizes CO_2 recycled from the amine plant. However, the design configuration first mentioned may utilize CO_2 that is already present in the tail gas and both of the designs yielded the same production of FT product after being optimized. Thus, it is evident that the conceptual design configuration first mentioned is better with respect to the cost of the amine plant, because this design allows for a lower molar fraction of CO_2 capture. In addition, scale up of the pre reformer and ATR inside the FT synthesis loop is cheaper than having an additional ATR outside the FT synthesis loop, which is reflected in the cost correlation of ATR scaling presented in Appendix G with cost scaling factors from Kreutz et al. [36]. The ATR's in the conceptual design configuration last mentioned was operating at the same pressure, however, operating the two ATR's at different pressures is recommended for further investigation as described in chapter 8.1.

Three different designs were fully developed and near optimized, in order to be compared on a total production and energy efficiency basis under quite similar conditions. The first designs FT synthesis loop operates at 20bar and uses only the oxygen necessary for reforming the methane in the FT tail gas, without introducing external methane, leaving the remaining oxygen as a valuable product. Two of the designs utilize all oxygen produced from the solar reactor in the ATR inside the FT synthesis recycle loop, by introducing external methane and converting it to syngas. In one of these designs, the FT synthesis loop is operating at 20bar, while in the other design it is operating at 25bar. The results are presented and discussed in chapter 7.1.

A CO_2 capture unit has been simulated as a component splitter in Aspen HYSYS as shown in chapter 5, whereas the component spiller is intended for simulating an amine

plant using MDEA as chemical solvent. However, a design choice of using physical solvents for acid gas removal, i.e. CO_2 capture, is investigated. Physical solvent processes for acid gas removal, including the Fluor solvent process, Selexol process, Purisol process and Rectisol process are described in detail in Kohl & Nielsen [26]. This literature describes how physical solvents may be considered the best economical option for acid gas removal in situations with appreciable concentrations of acid gas.

When using physical solvents, small fractions of methane, CO and H_2 will be removed together with CO_2, however, hydrocarbons are removed to a large extent together with the acid gases, and the solubility of hydrocarbons in physical solvents is increasing with the molecular weight of the hydrocarbon [26]. This means that the design simulated in Aspen HYSYS in this thesis would remove a considerable amount of heavy hydrocarbons together with CO_2 in the CO_2 capture unit, which is to be recycled as feed to the RWGS reaction upstream the plant. This would increase the complexity in the RWGS reaction and require pre reforming of hydrocarbons prior to the mixing of the CO_2-rich and H_2-rich streams, in order to prevent coke formation.

Therefore, as a solution to avoid the complexity of having heavy hydrocarbons removed together with CO_2, an alternative design is presented. This alternative design has the CO_2 capture unit located downstream of the ATR in the FT synthesis loop and directly after the separator that takes out water from the loop. Downstream of the ATR, all hydrocarbons, except for methane, have been completely converted and are therefore not present at the CO_2 capture unit, thus avoiding the complexity of having higher hydrocarbons present in the CO_2 recycled to the RWGS reaction. In addition, after the separator that takes out water, the temperature is quite low, of which promotes the solubility of CO_2 [26].

The Selexol process uses a mixture of polyethylene glycol dimethyl ethers. The process is suitable for operating at temperatures up to 175°C and the purity of the CO_2 removed can be as high as 99.4mol% [26]. Further, it has proven applications for CO_2 removal from synthesis gas derived from partial oxidation of heavy hydrocarbons in industry and as of 1992, 53 Selexol plants had been installed, which means that the selexol process presumably is a readily available technology for the best case in this thesis [26]. For the best case in this thesis, the Selexol process is considered to be the most suitable CO_2 capture unit, over the physical solvent process alternatives mentioned. Physical solvents for acid gas removal is considered, but not implemented in this thesis, however, further investigation of physical solvents is recommended as described in chapter 8.1.

5 SIMULATION METHODOLOGY – ISSUES AND TECHNIQUES

This chapter is giving a brief overview of the simulation methodology, issues encountered while simulating in Aspen HYSYS and the techniques used to overcome these issues. The optimization of the external methane feed with respect to production of FT product performed by simulations in Aspen HYSYS is described in chapter 7.1.2, and the observations from the simulation is presented in chapter 7.2. The basis for simulation in Aspen Energy Analyzer is described in chapter 6.

5.1 Simulation of the solar reactors

Several techniques are used in order to avoid the dynamic simulations required for simulating the vacuum pump being turned on and off and the water fed to the solar reactors alternating between the reactors. In a dynamic simulation the vacuum pump would be turned off in the reactor performing the oxidation step and the water would be fed to this reactor. When the reactor is done performing the oxidation step, the vacuum pump would be turned on, water would be fed to the other reactor, of which now has the vacuum pump turned off.

However, the solar reactors are modelled as conversion reactors in series in the Aspen HYSYS simulation, with one reactor continuously performing the oxidation step, while the other reactor is continuously performing the reduction step. Water is fed to the reactor performing the oxidation step, hydrogen and unconverted water leaves this reactor in a separate stream, while the oxidized metal catalyst is simulated to leave in a

separate stream, and enter the reactor performing the reduction step. Pure oxygen leaves the reactor performing the reduction step in a separate stream and the metal catalyst is simulated to leave in a separate stream, and enter the reactor performing the oxidation step. Thus, the catalyst is simulated to be recycled through the conversion rectors.

The conversion reactor models are set to initialize from product with respect to the catalyst and the reactions are defined by the stoichiometry and conversion as described in chapter 3.1.1, with the catalyst defined as hypothetical components and the heat of reaction is set to -44586kJ/kgmole and 286400kJ/kgmole at 25°C for the oxidation and reduction reactions, respectively [4, 5]. These heats of reactions are estimated to 395kJ/kgmole and 250038kJ/kgmole at 1350°C in Aspen HYSYS, for the oxidation and reduction reaction, respectively.

An energy input in the reactors required to perform the reactions is defined in the Aspen HYSYS simulation, which represents the solar thermal energy input on a continuous basis. However, the plant is only running during hours of sunlight, and this is accounted for when performing the plant evaluation, as described in chapter 7.5. Further, a component splitter is used for adjusting the water content in the oxygen and hydrogen streams. The Aspen HYSYS model developed for simulations in this thesis is presented in Appendix F, together with further description of the simulation methodology in Aspen HYSYS.

5.2 Import Fischer Tropsch reactor from Aspen Custom Modeler

New fluid packages and component lists were designed and implemented in order to implement a FT- reactor with more correct kinetics and stoichiometry than standard reactors in Aspen HYSYS. This FT reactor was modeled in Aspen Custom Modeler (ACM) as a continuous mixed stirred tank reactor, approximated as a slurry bubble column reactor. The model was imported from ACM to Aspen HYSYS, and requires Aspen property databanks for its fluid package.

Four lumps of hydrocarbons were created as hypothetical components in this new fluid package, still using Peng Robinson properties. A set of two different lumps is representing olefins of carbon numbers 5 and higher, with two different average carbon numbers of 6.5 and 7.85, corresponding to α-values in the FT reaction of $\alpha = 0.6$ and $\alpha = 0.74$, respectively. In addition, a set of two different lumps is representing paraffins of carbon numbers 11 and higher, with two different average carbon numbers of 13.33

and 43.33, corresponding to α-values in the FT reaction of $\alpha = 0.7$ and $\alpha = 0.97$, respectively.

Having sets of two lumps with different alpha values makes the simulation of the FT reaction more accurate and makes it possible to determine a more accurate product distribution. The lumps are coupled and related to each other with respect to the sum of the components produced for each set, and in this way it is possible to simulate a dynamic α, dependent on the individual carbon number produced. The alpha values in the FT reaction are also dependent on the partial pressure of H_2 and CO. The reactor is modeled with slurry volume fraction of 0.67 and mass fraction 0.2 of catalyst in slurry, and the catalyst density is 3000kg/m^3.

The lumping methodology and modeling of the FT reactions is performed as is described in detail in Hillestad [14].

5.3 Implement Fischer Tropsch reactor from Aspen Custom Modeler

Implementing the FT-reactor (ACM-model) in the FT synthesis loop faced a convergence error. The ACM- model requires an "initial guess" of all variables and constants, and the model is not very robust with respect to significant deviations from this initial guess in terms of converging. In order to get the recycle loop to converge, several techniques were tried out and a technique that requires manual iterations to converge the recycle loop solved the convergence error.

The first step needed is to disconnect the recycle loop, which allows for an easier convergence of the reactors. The second step is to create a low flowrate "test-stream" with similar composition and conditions as the recycle stream (tail gas recycle) and mix this "test-stream" with the makeup stream (connect the "test-stream" to the mixer, together with the makeup stream, instead of the actual recycle stream that was connected when the loop was closed).

By doing this, it is possible to slightly increase the flowrate of the "test-stream" to match that of the recycle stream, while observing, monitoring and adjusting parameters that may have caused the convergence error. Now the manual iterations are performed by alternately adjusting the "test-stream's" flowrate and composition, and adjusting the parameters to acceptable values. Such parameters can be conversion over the reactor,

compositions or H_2/CO ratio in and out of the reactor, volume of the reactor, alpha-values, flowrates and more. In this particular instance, it was the boundaries of the alpha-values that caused the convergence error.

Finally, the parameters have been adjusted in such a way that allows for the flowrate and composition of the "test-stream" to approach the flowrate and composition of the recycle stream and the recycle loop can be closed without the convergence error.

5.4 Connecting external methane feed to the Fischer Tropsch loop

In order to make the FT loop converge after the external methane feed is connected to the FT loop, the technique that requires manual iterations and allows for observing, monitoring and manipulating parameters which is described in detail in chapter 5.3 had to be used.

While using this technique, is became evident from the observations that the boundary of the higher α-values needed to be increased and a new initial guess in the ACM model had to be implemented for the recycle loop to converge. Thus the FT reactor model was adjusted in ACM and new fluid packages and component lists of which corresponded to the new lumped components were created and implemented in Aspen HYSYS. The new lumps for the higher α-value representing olefins of carbon numbers 5 and higher and paraffins of carbon numbers 11 and higher, had an increase in the average carbon number from 7.85 to 8 and from 43.33 to 60, respectively. This is corresponding to an increase in the α-value in the FT reaction from $\alpha = 0.74$ to $\alpha = 0.75$ and from $\alpha = 0.97$ to $\alpha = 0.98$, respectively.

Whenever simulating with hypothetical components, the fluid package has to be changed through the ATR. The ATR is simulated as a Gibbs reactor, which is not compatible with hypothetical components. Therefore, an identical fluid package, excluding the hypothetical components was used over the simulated Gibbs reactor. In order to change fluid package over the simulated Gibbs reactor, stream cutters was applied to every inlet and outlet streams of the simulated Gibbs reactor. Prior to the stream cutters, the hypothetical components are removed in a component splitter, and an approximation is made while these hypothetical components, accounting for about 4.78wt% of the total FT product in the best case, is simulated to mix with the total FT product.

For this reason, in addition to that Aspen HYSYS does not account for coke formation in the simulation; a pre reformer is not simulated in Aspen HYSYS. Instead, the FT tail gas, including the external methane feed, is heated to the desired pre reformer inlet temperature of 400°C in a separate heat exchanger, before it is heated to the desired ATR inlet temperature of 600°C. This is done in order to achieve more accurate heat integration when optimizing the heat exchanger network.

6 HEAT EXCHANGER NETWORK

6.1 Basis for Aspen Energy Analyzer

Aspen Energy Analyzer (AEA) is used to simulate near optimum heat exchanger networks (HENs) for the best case Aspen HYSYS simulation. AEA imports streams from Aspen HYSYS and develops near optimum heat exchanger networks with respect to heating and cooling utilities cost [US$/s] or total area of heat exchangers with total investment cost of the network [US$]. The results of the simulation is compared manually and the best case is chosen with respect to total utility cost and the investment cost of the HEN, with the criteria of no infeasible heat exchangers, no heat exchanging of streams forbidden to match, and no unsatisfied streams in the HEN.

In order to reduce complexity in the AEA simulation, the best case Aspen HYSYS simulation is simplified by removing process equipment and disconnecting streams, leaving only segments of the streams with their respective temperature intervals and corresponding heaters or coolers. The segmented streams are defined as identical to the streams in the best case Aspen HYSYS simulation at their starting and ending temperature through a heater or a cooler. Aspen Energy Analyzer requires input from manual calculations of heat transfer in order to handle streams vaporizing and condensing. The simplification process by segmentation of streams and the input from manual calculations of vaporizing and condensing streams, as well as the basic concept

of how AEA works is described in detail in the user reference guide [37]. AEA uses an incorrect equation with respect to the investment rate and plant life for calculating the annualized capital cost, however this is accounted for, adjusted to the correct equation before simulation and confirmed by Aspen HYSYS Technical Support [38]. The interest rate is set to 10% and plant life is set to 20 years, with average operating hours of 8 hours per day, 334 days a year, for all simulations.

In order to further reduce complexity in the AEA simulation, all heat exchanging of streams that are known to heat exchange with each other, such as high temperature syngas and water in a waste heat boiler, is performed manually in Aspen HYSYS and the results is used for the basis in the AEA simulation. The FT heat of reaction is producing a lot of steam. The amount of steam generated in the FT cooling water loop is calculated in Aspen HYSYS and used for the basis in AEA.

A segment is made of the oxygen stream from 1350°C to 1100°C, of which may heat exchange with process streams in a ceramic high temperature heat exchanger or generate steam in a waste heat boiler. According to a customer representative for Heat Transfer International [39], a company that produces high temperature ceramic heat exchangers, a gas-to-gas ceramic high temperature heat exchanger would cost from 10 to 20 times more than that of a conventional heat exchanger. The customer representative advised using the factor 20 to be conservative in early estimates. The cost of the ceramic high temperature heat exchanger is therefore set to 10 times or 20 times the cost of a conventional heat exchanger in separate simulations to compare the outcomes; however, the advised factor of 20 is used for the final best case.

A hot utility, “very high temperature”, is defined, which simulates the solar thermal energy used for heating water fed to the solar reactor to 1350°C, after it has been heated by hot process streams. This hot utility is restricted to only allow for heating of water fed to the solar reactor in the AEA simulation. The solar thermal energy utility is defined by an investment cost and operation cost directly proportional to the required duty. Operating and maintenance (O&M) cost for the solar thermal energy plant, including insurance and all other miscellaneous costs is estimated to be in the range of US$ 0.02/kWh to US$ 0.03/Kwh in International Renewable Energy Agency [22]. Therefore, to be conservative, the total O&M cost of the solar thermal energy is defined as US$ 0.03/kWh in AEA. The investment cost of the solar heliostats is estimated to be US$ 127/m^2 in 2015 in Kolb et al. [17] and the energy provided by the heliostats per m^2,

e_{helio} used is 0.58kW [19]. It is assumed that the energy required for heating the water fed to the solar reactor is achieved by increasing the amount of heliostats, leaving the investment cost for the solar thermal energy utility as the investment cost of the heliostats.

Additional investment costs related to heating of the water fed to the solar reactor are accounted for in the calculation of investment cost for the solar reactor in chapter 7.5.1 and are further described in Appendix G. The O&M cost and investment cost of the solar thermal energy utility is derived as a cost dependent on the heating duty required, with the units as defined in AEA, in the equations 5.1 and 5.2 below, respectively.

$$\frac{US\$\ 0.03/kWh}{3600s/h} = \frac{US\$\ 8.33*10^{-6}}{kJ} \quad \textbf{(6.1)}$$

$$\frac{US\$\ 127/m^2}{0.58kW/m^2} * \frac{3600s}{h} = \frac{US\$\ 218.966}{kJ/s} * \frac{3600s}{h} = \frac{US\$\ 0.06082}{kJ/h} \quad \textbf{(6.2)}$$

6.2 Design configurations for Aspen Energy Analyzer basis.

There are three design configurations for the AEA simulation basis which are compared in this thesis. For all three configurations two sets of simulations was performed and compared separately for ceramic high temperature heat exchanger cost of 10 times and 20 times the cost of a conventional heat exchanger. For each simulation of a design configuration, 60 near optimum HENs are developed, whereas one of the HENs is chosen as the best case for that configuration. The best cases of the three configurations is then compared, manually adjusted in Aspen HYSYS, and compared again in order to ultimately decide upon a final best case HEN configuration.

All three design configurations for the AEA simulation basis has the general basis as described in chapter 6.1, whereas the difference in the configurations is the design for heating of the water fed to the solar reactor and its initial conditions. The three design configurations are presented in simplified flowsheets in the figure below.

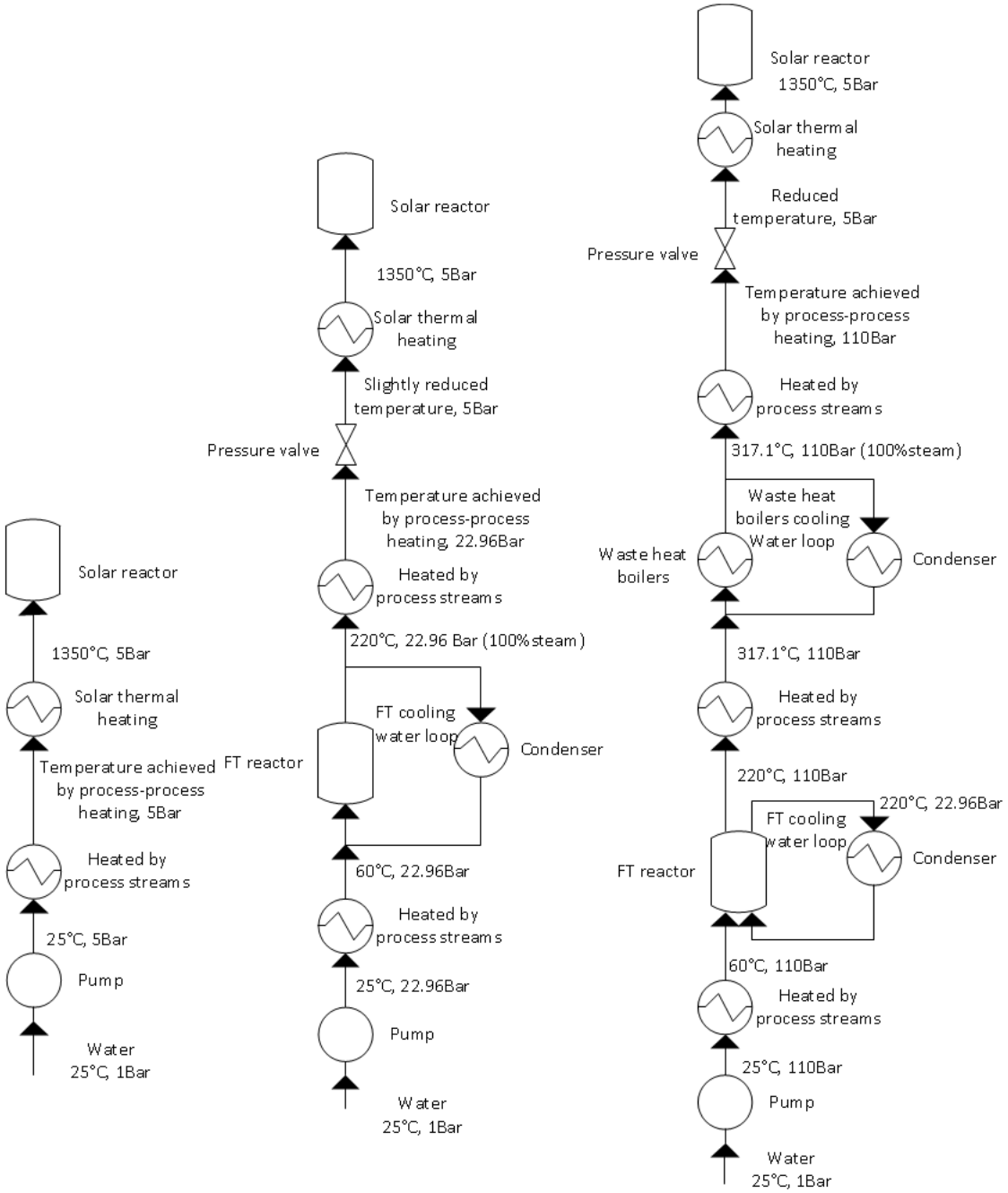

Figure 9: Simplified flowsheets for the three design configurations for water fed to the solar reactor, which is imported as a basis to Aspen Energy Analyzer together with the rest of the streams simulated in Aspen HYSYS.

Configuration 1 is considering the water fed to the solar reactor's initial conditions of 25°C and 1bar being pumped up to 5bar. It is heated by process streams as much as possible and fed directly to the solar reactor where it is being heated by solar thermal energy to 1350°C, before entering the active site of the reactor where it is converted to

oxygen and hydrogen as described in chapter 3. In the both the FT cooling water loop and the waste heat boilers it is desired to have water at its boiling point due to its high heat transfer coefficient. Water at 5bar will be completely vaporized at 158.1°C, a temperature lower than the desired operating temperature of the FT reactor and the waste heat boilers. Therefore, the water fed to the solar reactor does not go through the FT cooling water loop or through the waste heat boilers.

Configuration 2 is considering the water feed to the solar reactor's initial conditions of 25°C and 1bar being pumped up to 22.96bar, which is the pressure of which water boils at 220°C. The water feed is then heated by process streams to 60°C before entering and directly mixing with the water in the FT reactor's cooling water loop and the exact same amount of water is leaving the loop in a stream splitter after the FT reactor as steam at 220°C. This steam leaving the FT reactor's cooling water loop is heated by process streams as much as possible before going through a valve, leaving the steam with a slightly reduced temperature at 5bar, which is the pressure required for entering the solar reactor. Finally, the steam is sent to the solar reactor, where it is being heated by solar thermal energy to 1350°C, before entering the active site of the reactor.

Configuration 3 is considering the water feed to the solar reactor's initial conditions of 25°C being pumped up to 110bar, which is the pressure that is set for the cooling water loop in the waste heat boilers. The water is then heated by process streams to 60°C and enters the FT reactor in a separate cooling water system, in addition to the previously mentioned cooling water loop, and leaving the FT reactor as liquid water at 220°C and 110bar. After leaving the FT reactor, the water is heated by process streams to its boiling temperature of 317.1°C before directly mixing with the water in the waste heat boilers cooling water loop. The exact same amount of water fed to the waste heat boilers cooling water loop leaves the loop in a stream splitter after the last waste heat boiler as steam at 317.1°C. This steam leaving the waste heat boilers cooling water loop is heated by process streams as much as possible before going through a valve, leaving the steam with a reduced temperature at 5bar. Finally, the steam is sent to the solar reactor, where it is being heated by solar thermal energy to 1350°C, before entering the active site of the reactor.

7 RESULTS AND DISCUSSION

The results of conceptual design simulations and optimization of total FT production presented in this chapter are from simulations in Aspen HYSYS. In addition, several observations made during simulations in Aspen HYSYS are presented and discussed in this chapter. The results of heat exchanger network designs and optimization of energy efficiency are based upon the best case conceptual design simulation in Aspen HYSYS. In addition to simulations in Aspen HYSYS, Aspen Energy Analyzer is used as a tool for simulating heat exchanger networks and comparing configurations.

7.1 Comparison of three different conceptual design configurations

In Aspen HYSYS, three different conceptual design configurations are optimized and compared with respect to total production of FT product and energy efficiency. This comparison is done in order to choose a conceptual design configuration as the best conceptual design to be considered for further investigation. The three design configurations are described in chapter 4.5. The energy efficiencies are merely presented as indications for comparison, due to the heat exchanger network not being optimized for the individual conceptual designs. The energy efficiencies presented in this section is based on conservative, preliminary non-optimized estimates of the heat exchanger network. The three designs are all set to require solar thermal energy to heat the water feed to the solar reactor from 220°C to 1350°C, in addition to the solar thermal energy required in the solar reactor, and the energy required by the compressors is assumed to be an external energy input. This conservative, non-optimized estimate is

chosen in order to approximate the energy efficiency comparison to be performed on a similar basis. The heat exchanger network for the conceptual design configuration chosen as the best conceptual design is optimized and discussed together with the corresponding energy efficiency of this configuration in chapter 7.3.

7.1.1 Conceptual design using no external methane feed

Conceptual design configuration 1 is only utilizing the oxygen necessary for optimal methane conversion of the FT tail gas. The oxygen is fed to the ATR in the FT tail gas recycle loop, in order to promote the conversion of methane and lighter hydrocarbons, and the FT synthesis loop is operating at 20bar. Using the optimal conditions of the independent variables found in Emhjellen [6] as a guideline, the independent variables in the FT synthesis loop was manually adjusted to optimize the production of FT product. The independent variables found to be optimal is presented in the table below.

Table 6: Values of independent variables in the FT synthesis loop found to be optimal during simulation in conceptual design configuration 1.

Independent variable	Value
CO conversion over FT reactor [%]	51.149
H_2/CO molar ratio in FT reactor	1.358
α-value C11+ lump paraffin	0.967
α-value C5+ lump olefin	0.738
Fraction of CO_2 captured in CO_2 capture unit	0.6
Steam/Carbon molar ratio into the ATR	0.614
Flowrate oxygen fed to the ATR [kgmole/h]	28
Molar fraction methane slip out of the ATR	1.75E-03

The design does not utilize any external methane, and utilizes 28 kgmole/h of the oxygen produced in the solar reactor, leaving the remaining oxygen to be considered as a product. The optimal conditions of the independent variables found in Emhjellen [6] are presented in Appendix E. The molar flows and mass flows of the products and feeds for this configuration are shown in the table below

Table 7: Flowrates of feed streams and product streams for optimized conceptual design configuration 1

Stream	[kgmole/h]	[kg/h]
Feed streams		
CO_2 feed	190	8367
H_2O feed	699	12593
Product streams		
O_2	294	9304
FT product	6.076	2687
Waste water	498	8966

Although oxygen is considered a valuable product, the most valuable and noteworthy product is the FT product of 2687kg/h. The energy input, LHV of the FT products, energy efficiencies, carbon efficiency and recycle ratio are presented in the table below.

Table 8: Energy efficiencies calculated from lower heating values (LHVs) of FT product divided by thermal energy input, carbon efficiency and FT synthesis recycle loop for the optimized conceptual design configuration 1. Calculated in Microsoft excel with data from Aspen HYSYS.

20Bar without CH4 feed	Column1	Column2	Column3
LHV HC Product Total SUM	118	[GJ/h]	
Compressor Work Total SUM (entire plant)	6.07	[GJ/h]	(2 compressors: Oxygen(only the used) and syngas 5 --> 20bar)
Qsun (Solar thermal energy duty)	205	[GJ/h]	
Carbon efficiency entire system	99.93 %		
Energy Efficiency entire system	56.01 %		(LHV product / (Qsun+Wcompressor)
Energy Efficiency (Solar not Counted)	1948.92 %		(LHV product / (Wcompressor)
FT loop			
Total LHV syngas fed to FT	161	[GJ/h]	
Compressor Work (FT loop)	6.40	[GJ/h]	(1 Compressor: Methane)
Energy Efficiency FT loop	70.70 %		(LHV product / (LHV syngas fed to FT + Wcompressor)
FT synthesis loop recycle molar ratio	0.7356		

A carbon efficiency of 99.93% means that the amount of FT product theoretically possible to produce in the system with these feed streams is 2689kg/h, only 2kg/h higher than achieved under the optimization in this simulation. Due to the limit of CO_2 content in the makeup syngas of 12mole%, the molar flow of CO_2 feed is at the maximum allowed for the temperature 1100°C of the mixed H_2 and CO_2 before the RWGS reaction. Thus, the total production of FT product can not be significantly increased without introducing a feed containing carbon. The recycle ratio of 0.74 means that it is a considerably lower molar flow in the FT synthesis loop recycle stream than in the makeup feed, which results in quite low equipment sizes in the FT synthesis loop. The entire systems energy efficiency of 56.01% means that 56.01% of the total energy input to the system is converted to energy as the LHV of the FT product, and the rest of the energy input goes to either steam generation or losses.

7.1.2 Conceptual design utilizing external methane feed

Conceptual design configuration 2 is utilizing all the oxygen produced in the solar reactor in the ATR in the FT tail gas recycle loop which is operating at 20bar. External methane is fed to this ATR and the flowrate of methane, the steam/carbon ratio and the CO_2 is optimized with respect to the flowrate of H_2+CO out of the ATR, with the constraints of keeping a constant flowrate of oxygen feed, H_2/CO ratio out of the ATR and keeping a reasonable CO_2 and methane content out of the ATR. The optimization with respect to the external methane feed proved to be quite difficult due to the issues causing non-convergence of the FT synthesis loop, which are described and discussed in chapter 7.2.

In order to overcome these issues, the optimization of the external methane feed is performed in a separate ATR which is not inside the FT synthesis loop. The syngas produced in this ATR is mixed with the syngas produced in the RWGS reaction before entering the FT synthesis loop. In this way, it is possible to determine how much oxygen is needed for methane conversion in the ATR in the FT synthesis loop, now that the additional syngas makeup is included. The oxygen required for methane conversion in the FT synthesis loop and the amount of syngas produced by utilizing the remaining oxygen produced in the solar reactor is optimized by manual iterations.

The oxygen utilized in both ATRs was adjusted and the syngas makeup was updated with respect to the syngas produced with the remaining oxygen, which was optimized by using the optimizer function in Aspen HYSYS. The algorithm used to perform the optimization by manual iterations is summarized in the table below.

Table 9: The algorithm used for optimizing the external methane feed by manual iterations.

Step	Action
1	Make sure enough oxygen is utilized for sufficient methane reforming in the ATR in the FT synthesis loop
2	Adjust the oxygen utilized in both ATRs to match the oxygen produced in the solar reactor.
3	Use the optimizer function on the syngas produced in the ATR outside of the FT loop
4	Update the syngas makeup feed with respect to the additional syngas produced in the ATR outside of the FT synthesis loop
5	The oxygen utilized in methane reforming in the ATR inside the FT synthesis loop is reduced in order to increase the oxygen available for methane reforming in the ATR outside the loop.
6	The sequences 1-5 is repeated until the oxygen utilized for methane reforming in the ATR in the FT synthesis loop is no longer enough for sufficient methane reforming. Thus, the previous iteration is found to be the optimum.

The independent variables for the optimizer function used on the ATR outside of the FT synthesis loop and its constraints are presented in the table below.

Table 10: Variables adjusted, constrains and target maximized during optimizer function on the ATR outside the FT synthesis loop in Aspen HYSYS.

Adjusted independent variables	Variable description	Low bound	Current value	High bound
Methane feed	Molar Flow [kgmole/h]	250	464.1	1000
CO2 from recycle	Molar Flow [kgmole/h]	0	111	240
Water to NG	Molar Flow [kgmole/h]	175	345	700
Constrains				
Product syngas	H_2/CO molar ratio	2	2	2
ATR feed	Steam/carbon molar ratio	0.6	0.6	
Methane slip	CH_4 concentration		0.01	0.01
Product syngas	CO_2 concentration		0.09	0.12
Target maximized				
H_2+CO	Molar flow [kgmole/h]		1291	

Using the optimal flowrates of the independent variables from the optimizer function and using the optimal conditions of the independent variables found in Emhjellen [6] as guidelines, the independent variables in the FT synthesis loop were manually adjusted to optimize the production of FT product, and the independent variables found to be optimal are presented in the table below.

Table 11: Optimal independent variables in the FT synthesis loop for conceptual design configuration 2.

Independent variable	Value
CO conversion over FT reactor [%]	55.48
H_2/CO molar ratio in FT reactor	1.227
α-value C11+ lump paraffin	0.972
α-value C5+ lump olefin	0.742
Fraction of CO_2 captured in CO_2 capture unit	0.356
Steam/Carbon molar ratio into the ATR	0.61
Flowrate oxygen fed to the ATR [kgmole/h]	334.2
Molar fraction methane slip out of the ATR	0.0039

The design utilizes all oxygen and external methane in the ATR in the FT tail gas recycle loop, and the products and feeds of the entire system are shown in the table below.

Table 12: Flowrates of feed and product streams for conceptual design configuration 2.

Stream	[kgmole/h]	[kg/h]
Feed streams		
CO_2 feed	153	6737
H_2O feed	699	12593
CH_4 feed	464.1	7445
Product streams		
O_2	0	0
FT product	15.5	8716
Waste water	1002.4	18059

This is a significantly higher total carbon feed and total production of FT product than in conceptual design configuration 1. The energy input, LHV FT product, energy efficiencies, carbon efficiency and recycle ratio are presented in the table below.

Table 13: Energy efficiencies calculated from lower heating values (LHVs) of FT product divided by thermal energy input, carbon efficiency and FT synthesis recycle loop for the optimized conceptual design configuration 2. Calculated in Microsoft excel with data from Aspen HYSYS.

20Bar with CH4 feed	Value	Unit	Description
LHV HC Product Total SUM	383	[GJ/h]	
LHV Methane feed total	372	[GJ/h]	
Compressor Work Total SUM (entire plant)	18.8	[GJ/h]	(3 compressors: Oxygen. Methane and syngas 5 --> 20bar)
Qsun (Solar thermal energy duty)	205	[GJ/h]	
Carbon efficiency entire plant	99.95 %		
Energy Efficiency entire system	64.33 %		(LHV product / (LHV Methane feed +Qsun+Wcompressor)
Energy Efficiency (Solar not Counted)	98.00 %		(LHV product / (LHV Methane feed + Wcompressor)
FT loop			
Total LHV syngas fed to FT	169	[GJ/h]	
Compressor Work (FT loop)	6.40	[GJ/h]	(1 Compressor: Methane)
Energy Efficiency FT loop	70.00 %		(LHV product / (LHV Methane feed+ LHV syngas fed to FT + Wcompressor)
Fischer Tropsch synthesis loop recycle molar ratio	1.48		

A carbon efficiency of 99.95% means that the amount of FT product theoretically possible to produce in the system with these feed streams is 8720kg/h, only 4kg/h higher than achieved under the optimization in this simulation. Because both feed sources of carbon have been optimized, the total production of FT product can not be significantly increased. Thus, a near optimum with respect to the total production of FT product has been found for this conceptual design configuration. The recycle ratio of 1.48 means that it is a considerably higher molar flow in the FT synthesis loop recycle

stream than in the makeup feed, which results in higher relative equipment sizes in the FT synthesis loop than in design configuration 1. The entire systems energy efficiency of 64.33 % means that 64.33% of the total energy input to the system is converted to energy as the LHV of the FT product, and the rest of the energy goes to either steam generation or losses. This is a significantly higher energy efficiency for the entire plant than in conceptual design configuration 1.

7.1.3 Conceptual design utilizing external methane at higher pressure

In order to see how the operating pressure of the FT synthesis loop affects the total production of FT product, the FT synthesis loop is set to operate at 25bar in configuration 3. This conceptual design configuration is utilizing all the oxygen produced in the solar reactor in the ATR in the FT tail gas recycle loop. External methane is fed to this ATR and the flowrate of methane, CO_2, and the steam/carbon ratio are optimized with respect to the flowrate of H_2+CO out of the ATR, with the constraints of keeping a constant flowrate of oxygen feed, H_2/CO ratio out of the ATR and keeping a reasonable CO_2 and methane content out of the ATR. The optimization procedure and its constraints are the same as for the optimization procedure in conceptual design configuration 2, as described in chapter 7.1.2.

Using the optimal flowrates of the independent variables from the optimizer function and using the optimal conditions of the independent variables found in Emhjellen [6] as guidelines, the independent variables in the FT synthesis loop were manually adjusted to optimize the production of FT product, and the independent variables found to be optimal are presented in the table below.

Table 14: Optimal independent variables in the FT synthesis loop for conceptual design configuration 3.

Independent variable	Value
CO conversion over FT reactor [%]	50
H_2/CO molar ratio in FT reactor	1.1
α-value C11+ lump paraffin	0.973
α-value C5+ lump olefin	0.743
Fraction of CO_2 captured in CO_2 capture unit	0.44
Steam/Carbon molar ratio into the ATR	0.67
Flowrate oxygen fed to the ATR [kgmole/h]	334.2
Molar fraction methane slip out of the ATR	0.0006

The design utilizes all oxygen and external methane in the ATR inside the FT tail gas recycle loop, which is operating at 25bar, and the products and feeds for the entire system are shown in the table below.

Table 15: Feed and product streams for optimized design configuration 3.

Stream	[kgmole/h]	[kg/h]
Feed streams		
CO_2 feed	136	5972
H_2O feed	699	12593
CH_4 feed	410	6578
Product streams		
O_2	0	0
HC product	14	7710
Waste water	965	17429

This is a slightly lower flowrate of both the CO_2 feed and the methane feed than in conceptual design configuration 2. The lower CO_2 feed is due to a higher molar fraction CO_2 capture is required and since CO_2 captured is recycled to the RWGS reaction, the CO_2 makeup feed required is reduced. The lower methane feed can be explained directly by the increased operating pressure of the FT synthesis loop. A higher operating

pressure is reducing the methane conversion in the ATR, as is evident from the reaction stoichiometry shown in chapter 3.1.5, since a higher pressure shifts the reactions equilibrium towards fewer moles of gas molecules. Methane only leaves the FT synthesis loop together with the FT product and this methane is almost at a neglect able molar fraction of the methane in the FT synthesis loop of 0.00037. This means that almost no methane leaves the FT synthesis loop, therefore the methane has to be converted in the ATR Thus a lower conversion of methane in the ATR allows for a lower flowrate of methane fed to the ATR

The energy input, LHV of the FT product, energy efficiencies, carbon efficiency and recycle ratio are presented in the table below.

Table 16: Energy efficiencies calculated from lower heating values (LHVs) of FT product divided by thermal energy input, carbon efficiency and FT synthesis recycle loop for the optimized conceptual design configuration 3. Calculated in Microsoft excel with data from Aspen HYSYS.

25Bar with CH4 feed	Value	Unit	Description
LHV HC Product Total SUM	339	[GJ/h]	
LHV Methane feed total	372	[GJ/h]	
Compressor Work Total SUM (entire plant)	20.3	[GJ/h]	(3 compressors: Oxygen. Methane and syngas 5 --> 20bar)
Qsun (Solar thermal energy duty)	205	[GJ/h]	
Carbon efficiency entire system	99.94 %		
Energy Efficiency entire system	56.70 %		(LHV product / (LHV Methane feed +Qsun+Wcompressor)
Energy Efficiency (Solar not Counted)	86.28 %		(LHV product / (LHV Methane feed + Wcompressor)
FT loop			
Total LHV syngas fed to FT	169	[GJ/h]	
Compressor Work (FT loop)	6.22	[GJ/h]	(1 Compressor: Methane)
Energy Efficiency FT loop	61.88 %		(LHV product / (LHV Methane feed+ LHV syngas fed to FT + Wcompressor)
Fischer Tropsch synthesis loop recycle molar ratio	1.56		

A carbon efficiency of 99.94% means that the amount of FT product theoretically possible to produce in this system is 7715kg/h, only 5kg/h higher than achieved under the optimization in this simulation. Because both feed sources of carbon have been optimized, the total production of FT product can not be significantly increased. Thus, a near optimum with respect to the total production of FT product has been found for this conceptual design configuration. The recycle ratio of 1.56 means that it is a considerably higher molar flow in the FT synthesis loop recycle stream than in the makeup feed, which results in higher relative equipment sizes in the FT synthesis loop than in design configuration 1, and slightly higher than that in design configuration 2. The entire system's energy efficiency of 56.70 % means that 56.70% of the total energy input to the system is converted to energy as the LHV of the FT product, and the rest of the energy goes to either steam generation or losses. This conceptual design

configuration has a lower overall energy efficiency than conceptual design configuration 2 and only slightly higher than that of conceptual design configuration 1.

7.1.4 Comparison of conceptual design configurations

Three conceptual design configurations have been optimized with respect to total production of FT product in order to be compared on a FT production and energy efficiency basis. Key results from the three conceptual design configurations are shown in the table below.

Table 17: Key results of the three conceptual design configurations

Conceptual design configuration	Total FT product	Entire system's energy efficiency	Carbon efficiency	Molar Recycling ratio FT synthesis loop	CO2 captured in capture unit
1	2687kg/h	56.01 %	99.93 %	0.74	60 %
2	8716kg/h	64.33 %	99.95 %	1.48	35.6 %
3	7710kg/h	56.70 %	99.94 %	1.56	44 %

From table 24 it is clear that conceptual design configuration 2 is performing significantly better than the other configurations in all of these key results, except for the molar recycling ratio in the FT synthesis loop. Conceptual design configuration 3 is performing significantly worse than configuration 2 in all of the key results, which leaves this configuration out of the question. Conceptual design configuration 1 has the best performance with respect to the molar recycling ratio in the FT loop, with about half of that in conceptual design configuration 2, which corresponds to the lowest relative sizes of equipment in the FT synthesis loop, resulting in the lowest relative investment cost for the FT synthesis loop. The apparent high molar recycling ratios in conceptual design configuration 2&3 can partially be explained by the molar flowrate of the methane feed being converted to a higher molar flowrate of syngas over the ATR, due to the stoichiometry in the reactions occurring inside the ATR. Therefore, the molar recycling ratios are not entirely representative for direct comparison of the conceptual design alternatives.

However, scaling up the flowrates in the FT synthesis loop due to the external methane feed does not increase the investment cost linearly, the correlation is better described as a function with an exponent less than one, which is reflected by the correlations for investment cost presented in Appendix G. In addition, increasing the investment cost of the equipment in the FT synthesis loop is not equivalent with increasing the investment cost for the entire plant, since the FT synthesis loop is only a part of the entire plant. As of year 2002, when the slurry bubble column reactor had been used for FT synthesis on commercial scale for about 9 years, the production of the purified syngas accounted for 60-70% of the capital and the operation cost of the total plant of a typical FT synthesis with purified syngas derived from a methane conversion plant [25]. While this cost correlation does not apply directly to the syngas production from the solar reactor system, it is assumed that the solar reactor system, being the new technology, has an investment cost accounting for a high fraction of the investment cost for the entire plant. This assumption will be investigated and discussed in chapter 7.5.1.

These factors significantly reduces the negative impact from the equipment in FT synthesis loop's scale up on the entire plant's profitability. Therefore, the conceptual design configurations are best compared with respect to the total production and energy efficiency. Although it is not completely obvious which configuration is better without performing a thorough evaluation on both configurations, configuration 2 is chosen as the best case to be considered for further investigation. This is because of its apparent better potential for profitability due to significantly higher production and energy efficiency. In addition, under the right conditions, the upscaling of the ATR and FT synthesis loop due to the external methane, with oxygen readily available on site, has the potential for being even more profitable than the FT synthesis plants utilizing methane reformed syngas that are operating profitably without this being readily available, when considering this upscaling process as an individual process.

However, when the external methane feed is introduced, the entire process goes from being completely CO_2 neutral and even having the potential for having a negative CO_2 footprint, depending on the source of the CO_2 feed, to being significantly less environmentally friendly with respect to overall CO_2 emissions if the source of the methane feed is fossil natural gas. Even though the methane feed comes from natural gas, the manufacturing process has no CO_2 emissions due to complete recycling of CO_2, but it will contribute to CO_2 emissions when the fraction of the FT product that is cracked into fuel is ultimately utilized for energy consumption by the end customer.

Obviously, the process is still more environmentally friendly with respect to CO_2 emissions than FT synthesis utilizing only syngas derived from fossil natural gas reforming. However, the potential for using biomass as feedstock for the external methane feed is investigated, and the results are presented in the following chapter.

7.1.5 Biomass as feedstock for external methane feed

By using biomass in a gasifier, it is possible to achieve a gas with quite high methane composition.

If the gas derived from biomass may be utilized as external methane feed in the best case conceptual design configuration, while still having complete recycling of CO_2, the environmental friendliness of the entire plant with respect to overall CO_2 emissions will be significantly improved. The CO_2 composition of the biogas derived from biomass is found to be from 35 to 40%, 30 to 40% and 30 to 40%, depending on whether the biogas is derived from sewage digesters, organic waste digesters or in landfills, respectively [40]. It is therefore desired to investigate if by increasing the amount of CO_2 captured by the amine plant allows for the external methane feed having this high concentration of CO_2, while still operating at optimal conditions with complete recycle of CO_2.

This is possible if the CO_2 composition in the methane feed is sufficiently high, without the CO_2 recycle exceeding the amount of CO_2 required in the RWGS reaction downstream of the solar reactor. This is simulated in Aspen HYSYS, and the results are presented in the figure below.

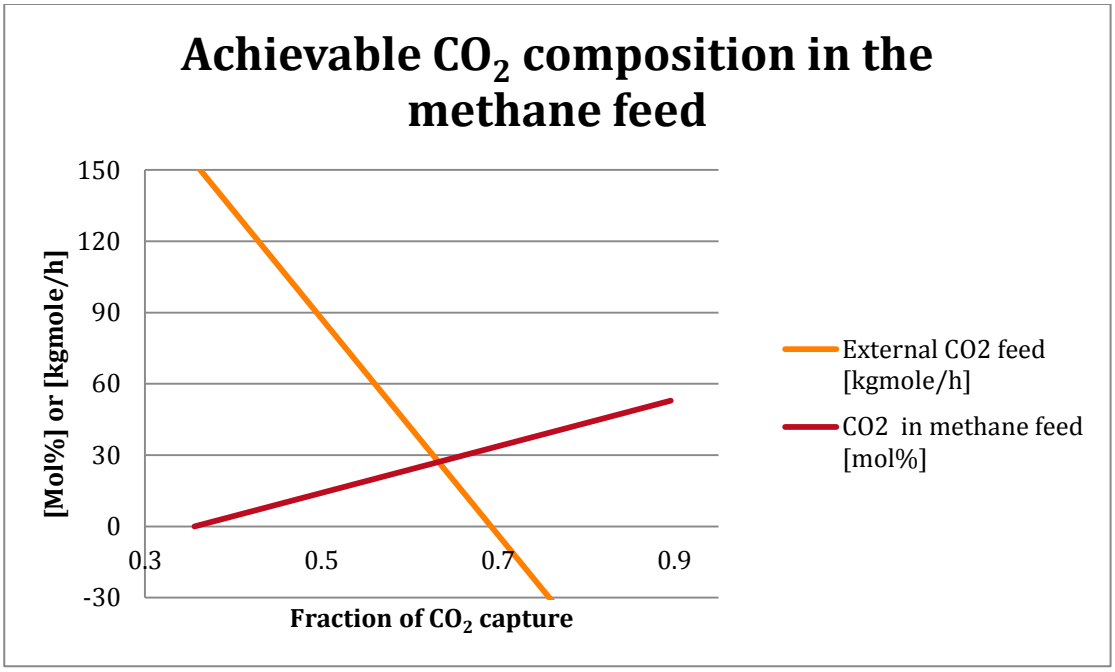

Figure 10: Achievable CO_2 composition in the methane feed. The fraction of CO_2 captured is adjusted in order to observe the composition of CO_2 that can be achieved while maintaining optimal operating conditions and recycling of all CO_2.

Figure 10 shows that the maximum CO_2 capture fraction that can be used before complete recycle of CO_2 is no longer possible is when the external CO_2 feed graph intersects with the x-axis at approximately 0.69. The mole% of CO_2 achievable in the methane feed while maintaining optimal operating conditions and complete recycle of CO_2 is when the CO_2 in methane feed graph's y-value has this x-value at approximately 33mole%. The CO_2 content in biogas derived for organic waste digesters and landfills can be as low as 30mole% [40]. This means that the system allows for a CO_2 content high enough for using biogas derived from organic waste digesters and landfills as feedstock for the external methane feed in the best case conceptual design configuration.

However, using biomass as feedstock requires additional process equipment and additional purification of the gas due to the presence of components that are inert in the FT synthesis loop. Although FT synthesis with syngas derived from biomass is an overall CO_2 neutral process, due to the CO_2 emissions from the manufacturing process has its origin in non-fossil carbon, the integration of FT synthesis from solar thermal water split and biomass derived syngas with complete recycling of CO_2 may prove to be a very viable option for renewable energy production in the future. However, the implementation of biomass as feedstock for the external methane feed in the best case

conceptual design configuration is beyond the scope of this master thesis, but it is recommended for further investigation and is further discussed in chapter 8.1.

7.2 Observations from the simulation in Aspen HYSYS.

When the design choice of using the oxygen produced from the solar reactor as feed to the ATR in the FT synthesis loop, together with external methane, recycled water and recycled CO_2 in order to produce additional syngas, it was desired to use the optimizer function in Aspen HYSYS. The optimizer function would estimate the optimal flowrates of external methane, recycled water and recycled CO_2 fed to the ATR by iterations of all independent variables simultaneously. Aspen HYSYS did not manage to perform the iterations required in the optimizer when this additional "makeup syngas stream", derived from external methane, oxygen produced in the solar reactor, recycled CO_2 and recycled water, was connected to the FT loop. There were three main issues observed that caused non-convergence of the FT synthesis loop during the Aspen HYSYS optimizer function and during manual iterations, which are summarized in the table below.

Table 18: Three main issues observed that caused non-convergence of the FT synthesis loop during manual iterations and during iterations by Aspen HYSYS's optimizer function.

Issue	Cause	Result
1	The α-values in the FT reaction may exceed their upper boundary during iterations.	This is causing an error in the ACM model, resulting in non-convergence
2	The combined methane fed to the FT synthesis loop and produced in the FT reactor may exceed the methane leaving with the FT product and methane converted in the ATR combined, during iterations.	This is causing an infinite accumulation of methane in the loop, resulting in non-convergence.
3	Significant deviations from the initial guess in the ACM model may occur during iterations.	This is causing an error in the ACM model, which results in non-convergence.

Firstly, the desired optimal production of FT product was corresponding to α-values close to their upper boundaries. Therefore, the α-values could go above their boundaries during the iterations in the Aspen HYSYS calculations, causing an error in the ACM model of which results in non-convergence. This might occur even though α would be within its boundaries at "steady state", or convergence, since the simulation of the loop stops when an error arises in the ACM model, causing non-convergence of the loop. This is an issue occurring during manual iterations as well because Aspen HYSYS is performing iterations while calculating the outcome of all process equipment included in simulating a loop, in order to make the loop converge (i.e. the conditions in for example a reactor will be different and "updated" when the loop has been calculated the first time, a second time, a third time and so on, until it reaches convergence. This is the standard calculation procedure for most loops).

Secondly, methane fed to the FT synthesis loop has limited options for leaving this loop. Additional methane is produced in the FT reactor and although small amounts of methane leave the loop together with the FT product, the remaining methane has to be converted in the ATR. If the combined flowrate of the methane feed and methane produced in the FT reactor exceeds the amount of methane leaving with the FT product and converted in the ATR combined, the result will be an infinite amount of methane accumulated in the FT loop, causing non-convergence.

Finally, significant deviations from the initial guess in the ACM model which may arise during manual iterations as well as during the optimizer function, is resulting in an error in the ACM model, which causes non-convergence.

Because of these issues, the optimizer function was used to estimate the optimal flowrates of external methane, recycled water and recycled CO_2 fed to the ATR while it was disconnected from the FT loop. This is why the independent variables in the FT loop were optimized by manual iterations, while any degree of an extensive sensitivity analysis of the performance of the conceptual design proved impossible for this system. A sensitivity analysis would be useful for understanding the system's behavior and for comparing the optimum values of every performance parameter. However, the best case conceptual design has a carbon efficiency of 99.95%, meaning that the production of FT product could not be significantly improved by performing a sensitivity analysis. Developing another basis for the simulation model in order to perform a sensitivity analysis is recommended for further investigation as described in chapter 8.3.

7.3 Heat exchanger network

Conceptual design configuration 2 is chosen as the best conceptual design and is the foundation for the heat exchanger network basis described in chapter 6.

7.3.1 Three base cases for optimizing heat exchanger network

There are three configurations of base cases for the HEN that are developed from the best case Aspen HYSYS simulation, which are imported into Aspen Energy Analyzer (AEA). The HEN chosen as the best case is presented and discussed in chapter 7.3.3. The basis for the AEA simulation is described in detail in chapter 6.1 and the three base case configurations are described in detail in chapter 6.2.

In general, the same amount of energy is required to heat water from 25°C to 1350°C, no matter which process configuration is used. In addition, an observation from the Aspen HYSYS simulation is that water requires more energy to increase its temperature and less energy to vaporize, at higher pressures. Therefore one might easily jump to the premature conclusion that configuration 1 is the optimal configuration, because this configuration does not pump water to a higher pressure just to go through a valve of which reduces its temperature downstream the process. However, it is a lot of energy from the exothermic FT reaction that can be used to heat and vaporize the water fed to the solar reactor through the coils in the FT reactor's cooling water system, while the same can be said for the hot streams required to be cooled in waste heat boilers, which may be utilized to vaporize this water. The process configurations that utilize the readily available heat exchangers in the FT reactor and in the waste heat boilers may prove to be more economical configurations. Therefore, it is not obvious which configuration is resulting in the most economical HEN, and AEA is used as a tool, alongside Aspen HYSYS, to optimize all three configurations in order to ultimately decide upon a best case HEN.

Configuration 1

The water fed to the solar reactor is in this configuration at 5bar, as described in chapter 6.2. The composite curves for this configuration with a pinch temperature of $\Delta T_{min}=10°C$ are shown in the figure below.

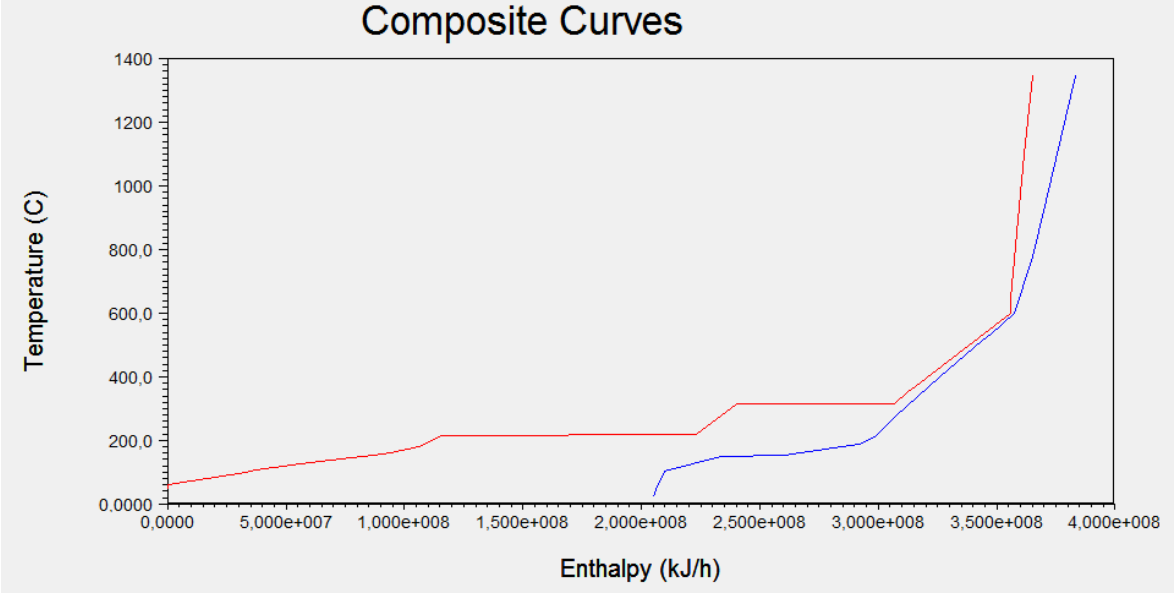

Figure 11: Composite curves with a pinch temperature of ΔTmin=10°C for configuration 1

This composite curve shows that it is possible to recover heat by process to process heat exchanging in the area where both curves are present, approximately from $2.05*10^8$ to $3.65*10^8$ kJ/h on the x-axis. In addition, it shows that it is possible to heat all streams to a temperature of 780°C or 700°C before external heating is required, when the oxygen stream segment from 1350°C to 1100°C is heat exchanging with process streams in a ceramic high temperature heat exchanger or when it is producing steam in a waste heat boiler, respectively. The additional cooling required is done by utilizing cooling water or by generating steam. At temperatures above 776.5°C, every stream, but the water fed to the solar reactor has reached its target temperature, and the external heating required is from solar thermal energy. Two sets of 60 near optimum HENs are developed during the simulation of this design configuration in AEA, whereas for the first set, the ceramic high temperature heat exchanger cost factor is set to 20 times the cost of a conventional heat exchanger, while in the second set a cost factor of 10 is used. The HENs developed during these AEA simulations is quite comprehensive and it is therefore chosen only to show the HEN network which is evaluated to be the best case, in chapter 7.3.3. However, the economic parameters of the HEN chosen as the best case for the AEA simulation of the first set are shown in the table below.

Table 19: Economic parameters for configuration 1 with cost factor 20 for ceramic high temperature heat exchanger. Total cost index is the sum of the operating cost and the annualized capital cost converted to US$/h

Total cost index [US$/h]	Area [m^2]	Number of units	Number of shells	Capital cost index [MM US$]	Heating [GJ/h]	Cooling [GJ/h]	Operation cost index [US$/h]
-51.84	21100	36	94	7.39E+06	26.1	213	-150.84

The total cost index is the sum of the operating cost and the annualized capital cost converted to US$/h. Negative total cost index means that the HEN is actually "making money", due to large amounts of steam being generated for producing electricity in steam turbines. This HEN was chosen due to having the best performance in every single economic parameter in this simulation. An important observation of this simulation is that the water fed to the solar reactor had a temperature of 486.9°C before solar thermal heating is required and the oxygen stream segment from 1350°C to 1100°C is not heat exchanging with process streams, but producing steam in a waste heat boiler. Even though this requires more heat from solar thermal energy, it was the most economical option for the oxygen stream segment in this simulation. The economic parameters of the HEN chosen as the best case for the second set are shown in the table below.

Table 20: Economic parameters for configuration 1 with cost factor 10 for ceramic high temperature heat exchanger. Total cost index is the sum of the operating cost and the annualized capital cost converted to US$/h

Total cost index [US$/h]	Area [m^2]	Number of units	Number of shells	Capital cost index [MM US$]	Heating [GJ/h]	Cooling [GJ/h]	Operation cost index [US$/h]
-72	15700	33	79	6.38	24.8	212	-157.68

This HEN was also chosen due to having the best performance in every single economic parameter in this simulation. In this simulation, the most economical option was when oxygen stream segment from 1350°C to 1100°C is heat exchanging with process

streams which reduces the heat needed from solar thermal energy. The water fed to the solar reactor has a temperature of 534.6°C before solar thermal heating is required, which is a significantly higher temperature than in the first set. The overall economic parameters are also significantly better than in the first set.

Configuration 2

The water fed to the solar reactor is in this configuration at 22.96 bar and is sent through a valve which slightly decreases its temperature, as described in chapter 6.2. The effect this slight temperature decrease has on the HEN performance is accounted for and described in chapter 7.3.2.

The composite curves for this configuration with a pinch temperature of ΔTmin=10°C are shown in the figure below.

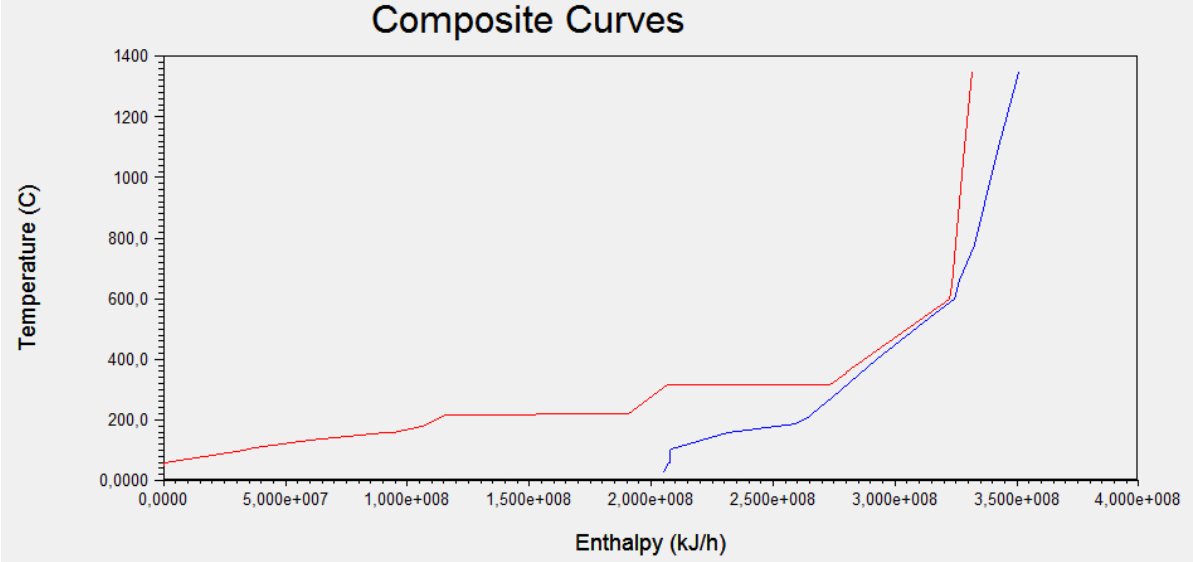

Figure 12: Composite curves for configuration 2 with a pinch temperature ofΔTmin=10°C.

This composite curve shows that it is possible to recover heat by process to process heat exchanging in the area where both curves are present, approximately from $2.05*10^8$ to $3.35*10^8$ kJ/h on the x-axis. In addition, it shows that it is possible to heat all streams to a temperature of 760°C or 720°C before external heating is required, when the oxygen stream segment from 1350°C to 1100°C is heat exchanging with process streams in a ceramic high temperature heat exchanger or when it is producing steam in a waste heat boiler, respectively. This is 20°C lower than in configuration 1 when the oxygen stream

segment is heat exchanging with process streams, and 20°C higher when it is producing steam in a waste heat boiler. The additional cooling required is done by utilizing cooling water or by generating steam. At temperatures above 776.5°C, every stream, but the water fed to the solar reactor has reached its target temperature, and the external heating required is from solar thermal energy. Similarly to in configuration 1, two sets of 60 near optimum HENs are developed during the simulation of this design configuration in AEA, whereas for the first set, the ceramic high temperature heat exchanger cost factor is set to 20 times the cost of a conventional heat exchanger, while in the second set a cost factor of 10 is used. The economic parameters of the HEN chosen as the best case for the AEA simulation of the first set are shown in the table below.

Table 21: Economic parameters for configuration 2 with cost factor 20 for ceramic high temperature heat exchanger. Total cost index is the sum of the operating cost and the annualized capital cost converted to US$/h

Total cost index [US$/h]	Area [m^2]	Number of units	Number of shells	Capital cost index [MM US$]	Heating [GJ/h]	Cooling [GJ/h]	Operation cost index [US$/h]
-54.36	19300	30	78	6.78	25.4	212	-145.44

This HEN was chosen due to having the best performance in every single economic parameter in this simulation. An important observation is that this simulations most economical option for the oxygen stream segment from 1350°C to 1100°C is the same as in configuration 1 with ceramic high temperature heat exchanger cost factor of 10. The water fed to the solar reactor has a temperature of 518.4°C before solar thermal heating is required, which is a significantly higher temperature than in configuration 1 with the same cost factor for ceramic high temperature heat exchanger. The overall cost parameters are also better in this configuration than in configuration 2 with the same cost factor. The economic parameters of the HEN chosen as the best case in the AEA simulation of the second set are shown in the table below.

Table 22: Economic parameters of HEN for configuration 2 with cost factor 10 for ceramic high temperature heat exchanger. Total cost index is the sum of the operating cost and the annualized capital cost converted to US$/h

Total cost index [US$/h]	Area [m^2]	Number of units	Number of shells	Capital cost index [MM US$]	Heating [GJ/h]	Cooling [GJ/h]	Operation cost index [US$/h]
-72.36	14300	25	63	5.90	24.3	211	-151.20

This HEN was also chosen due to having the best performance in every single economic parameter in this simulation. In this simulation, the most economical option for the oxygen stream segment from 1350°C to 1100°C was also the same as in configuration 1 with the same cost factor of the ceramic high temperature heat exchanger. The water fed to the solar reactor has a temperature of 560.5°C before solar thermal heating is required, which is a significantly higher temperature than achieved in both the first set for configuration 2 and for both sets in configuration 1. The overall economic parameters are also significantly better in this HEN than in all the HENs previously presented.

Configuration 3

The water fed to the solar reactor is in this configuration at 110bar and sent through a valve which decreases its temperature, as described in chapter 6.2. The effect this temperature decrease has on the HEN performance is discussed in chapter 7.3.2.

The composite curves for this configuration with a pinch temperature of ΔT_{min}=10°C are shown in the figure below.

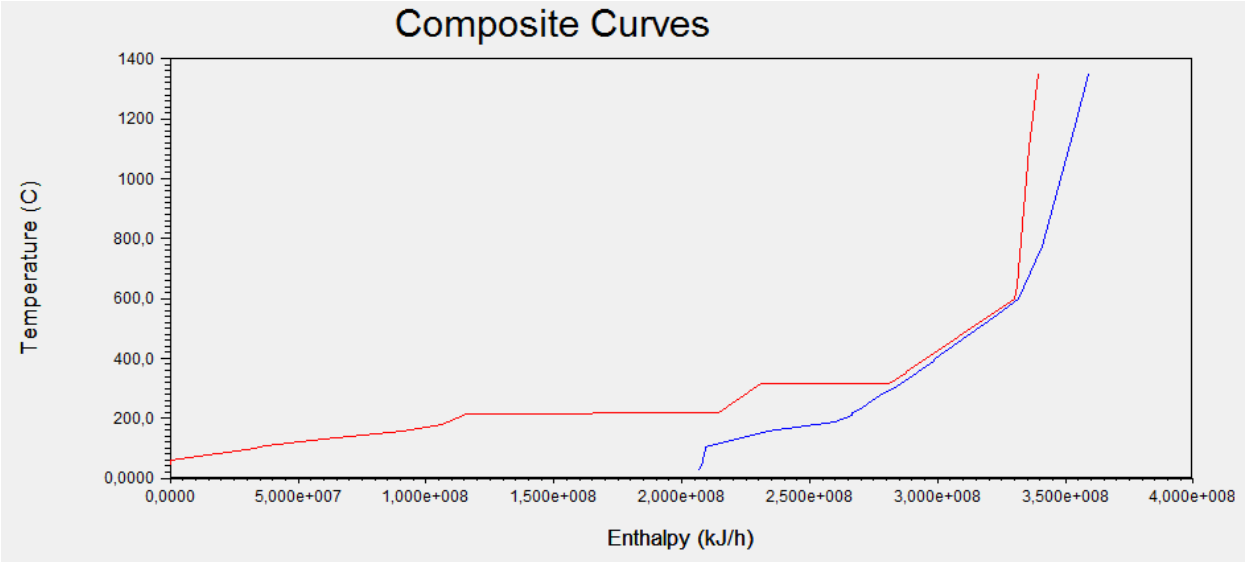

Figure 13: Composite curves for configuration 3 with a pinch temperature of ΔTmin=10°C.

This composite curve shows that it is possible to recover heat by process to process heat exchanging in the area where both curves are present, approximately from $2.05*10^8$ to $3.4*10^8$ kJ/h on the x-axis. In addition, it shows that it is possible to heat all streams to a temperature of 760°C or 680°C before external heating is required, when the oxygen stream segment from 1350°C to 1100°C is heat exchanging with process streams in a ceramic high temperature heat exchanger or when it is producing steam in a waste heat boiler, respectively. This is the same temperature as in configuration 2 when the oxygen stream segment is heat exchanging with process streams and 40°C lower when it is producing steam in a waste heat boiler. . The additional cooling required is done by utilizing cooling water or by generating steam. At temperatures above 776.5°C, every stream, but the water fed to the solar reactor has reached its target temperature, and the external heating required is from solar thermal energy. Similarly to in configuration 1&2, two sets of 60 near optimum HENs are developed during the simulation of this design configuration in AEA, whereas for the first set, the ceramic high temperature heat exchanger cost factor is set to 20 times the cost of a conventional heat exchanger, while in the second set a cost factor of 10 is used. The economic parameters of the HEN chosen as the best case for the AEA simulation of the first set are shown in the table below.

Table 23: Economic parameters for configuration 3 with cost factor 20 for ceramic high temperature heat exchanger. Total cost index is the sum of the operating cost and the annualized capital cost converted to US$/h

Total cost index [US$/h]	Area [m^2]	Number of units	Number of shells	Capital cost index [MM US$]	Heating [GJ/h]	Cooling [GJ/h]	Operation cost index [US$/h]
-35.57	18100	36	81	6.65	27.0	214	-124.92

This HEN was also chosen due to having the best performance in every single economic parameter in this simulation. An important observation is that this simulations most economical option for the oxygen stream segment from 1350°C to 1100°C is the same as in configuration 1&2 with ceramic high temperature heat exchanger cost factor of 10. The water fed to the solar reactor has a temperature of 513.6°C before solar thermal heating is required. This temperature is higher than in configuration 1 and lower than in configuration 2 with the same cost factor for ceramic high temperature heat exchanger. However, the overall economic parameters are better in both configuration 1&2 with the same cost factor. The economic parameters of the HEN chosen as the best case for the AEA simulation of the second set are shown in the table below.

Table 24: Economic parameters for configuration 3 with cost factor 10 for ceramic high temperature heat exchanger. Total cost index is the sum of the operating cost and the annualized capital cost converted to US$/h

Total cost index [US$/h]	Area [m^2]	Number of units	Number of shells	Capital cost index [MM US$]	Heating [GJ/h]	Cooling [GJ/h]	Operation cost index [US$/h]
-59.4	12400	34	72	5.67	25.3	212	-135.36

This HEN was also chosen due to having the best performance in every single economic parameter in this simulation. In this simulation, the most economical option for the oxygen stream segment from 1350°C to 1100°C was also the same as in configuration 1&2 with the same cost factor of the ceramic high temperature heat exchanger. The water fed to the solar reactor has a temperature of 568°C before solar thermal heating is required. This temperature is higher than achieved in any of the other HENs, however, the overall economic parameters is slightly better in configuration 1&2 with the same cost factor for ceramic high temperature heat exchanger. It proved to be more

economical to have the oxygen stream segment heat exchanges with process streams instead of producing steam in a waste heat boiler and using additional solar thermal energy to heat process streams when the cost factor was set to 10 instead of 20, and vice versa.

7.3.2 Comparison of base case results

Three base case configurations for the heat exchanger network has been simulated to develop near optimum heat exchanger networks as described in chapter 6.1. Key results from the three configurations with a cost factor of 20 for ceramic high temperature heat exchanger are shown in the table below.

Table 25: Key results from the three configurations with a cost factor of 20 for ceramic high temperature heat exchanger. Water temperature is the temperature of the water fed to the solar reactor achieved by heat exchanging with process streams before solar thermal heating is required.

Key results	Configuration 1 (Water feed 5bar)	Configuration 2 (Water feed 22.96bar)	Configuration 3 (Water feed 110bar)
Water temperature [°C]	486.9	518.4	513.6
Total cost index [US$/h]	-51.84	-54.36	-35.57
Capital cost index [MM US$]	7.39	6.78	6.65
Heating [US$/h]	217.8	212.0	225.4
Cooling [US$/h]	-367.2	-357.5	-350.3
Operation cost index [US$/h]	-150.8	-145.44	-124.9

The negative total cost index means that the cost is negative and the HEN system is making money by generation of electricity in steam turbines. Table 32 shows that configuration 2 has the best overall economic parameters, with total cost index of –US$ 54.36/h, slightly better than configuration 1 with -US$ 51.84/h, and significantly better than configuration 3 with –US$ 51.84/h. It is noteworthy that configuration 1 has the best operation cost index and configuration has the best capital cost index, while configuration 2 has the best total cost index, making it the best case configuration in this comparison. However, the water fed to the solar reactor's decrease in temperature over

the valve has to be accounted for and its effect on the total cost index of the HEN in configuration 2 is presented in the table below.

Table 26: The temperature reduction over the valve's effect on the total cost index of the HEN in configuration 2, calculated in Microsoft Excel.

Description	Value
Temperature drop over valve[°C]	9.8
Solar heating after valve (508.6°C to 1350°C at 5bar) [GJ/h]	25.6
Solar heating performed in AEA (518.4°C to 1350°C at 23bar) [GJ/h]	25.5
Heat required in addition to what accounted for in AEA [GJ/h]	0.04
Additional operation cost [US$/h]	0.10
Additional capital cost [US$]	2431.4
interest rate	0.1
Plant life [years]	20
Annualizing factor	0.1175
Additional annualized cost [US$/year]	285.6
Annualized cost [US$/h]	0.03
Total cost index from AEA [US$/h]	-54.36
Total cost index (Temperature reduction over valve accounted for) [US$/h]	-54.22

From table 33 it is clear that the temperature reduction over the valve does not affect the total cost index in configuration 2 to a large extent, and it is still the best configuration. The total cost index in configuration 3 is also affected by the temperature reduction over the valve. However, this will not affect the choice of best configuration, because accounting for the temperature reduction over the valve increases this total cost index, of which is already higher than for the other configurations.

Key results from the three configurations with a cost factor of 10 for ceramic high temperature heat exchanger are shown in the table below.

Table 27: Key results from the three configurations with a cost factor of 10 for ceramic high temperature heat exchanger. Water temperature is the temperature of the water fed to the solar reactor achieved by heat exchanging with process streams before solar thermal heating is required.

Key results	Configuration 1 (Water feed 5bar)	Configuration 2 (Water feed 22.96bar)	Configuration 3 (Water feed 110bar)
Water temperature [°C]	534.6	560.5	568.8
Total cost index [US$/h]	-72	-72.36	-59.4
Capital cost index [MM US$]	6.38	5.90	5.67
Heating [US$/h]	207.0	202.3	210.6
Cooling [US$/h]	-363.6	-353.5	-346.0
Operation cost index [US$/h]	-157.7	-151.2	-135.4

For the configurations using the cost factor of 10 for the ceramic high temperature heat exchanger, using it for heat exchanging water fed to the solar reactor and the segmented oxygen stream from 1350°C to 1100°C is the most economical option. These configurations using the cost factor 10 have significantly better total cost index for every individual configuration. However, it is advised to use the cost factor 20 for the ceramic high temperature heat exchanger, as described in chapter 6.1. Therefore, using a ceramic high temperature heat exchanger is recommended for further investigation and is further discussed in chapter 8.1, and the HEN in configuration 2 with the cost factor of 20 is ultimately chosen as the best HEN.

7.3.3 Best case heat exchanger network

The stream heat exchanging with each other in the best case HEN and their temperature intervals are presented in the diagram below.

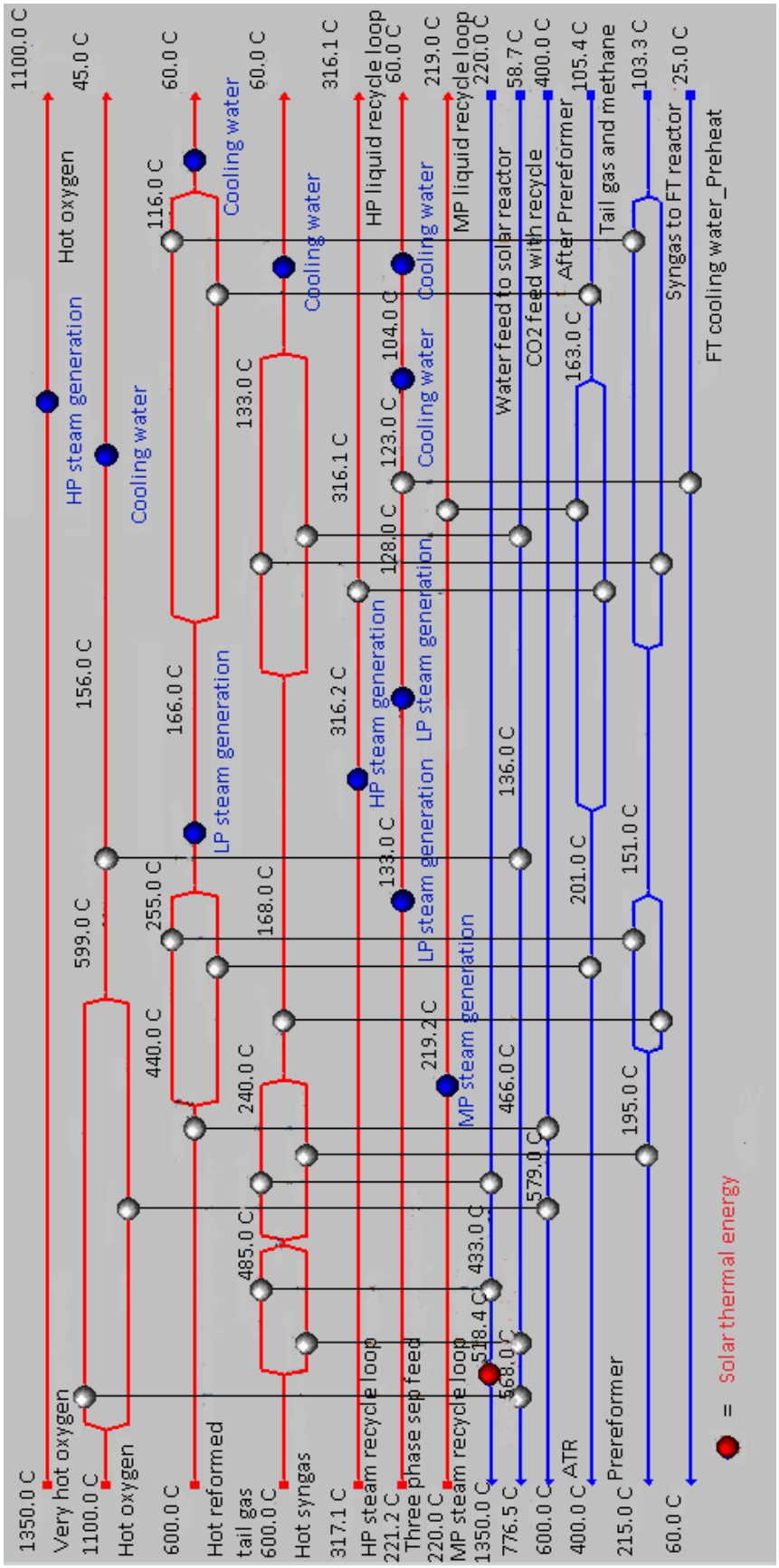
1100.0 C
Hot oxygen
45.0 C
60.0 C
Cooling water
60.0 C
316.1 C
HP liquid recycle loop
60.0 C
219.0 C
MP liquid recycle loop
220.0 C
58.7 C
400.0 C
105.4 C
103.3 C
25.0 C
HP steam generation
Cooling water
Cooling water
Cooling water
Water feed to solar reactor
CO2 feed with recycle
After Prereformer
Tail gas and methane
Syngas to FT reactor
FT cooling water_Preheat
116.0 C
133.0 C
316.1 C
123.0 C
104.0 C
163.0 C
156.0 C
166.0 C
316.2 C
128.0 C
136.0 C
LP steam generation
HP steam generation
LP steam generation
LP steam generation
599.0 C
255.0 C
168.0 C
133.0 C
201.0 C
151.0 C
440.0 C
240.0 C
219.2 C
466.0 C
MP steam generation
485.0 C
433.0 C
579.0 C
195.0 C
518.4 C
568.0 C
1350.0 C
Very hot oxygen
1100.0 C
Hot oxygen
600.0 C
Hot reformed
tail gas
600.0 C
Hot syngas
317.1 C
HP steam recycle loop
221.2 C
Three phase sep feed
220.0 C
MP steam recycle loop
1350.0 C
776.5 C
600.0 C
ATR
400.0 C
Prereformer
215.0 C
60.0 C
= Solar thermal energy

Figure 14: Heat exchanger network diagram. The temperatures are shown above the streams, and names are shown below. Process to process, external heating and cooling are gray, red and blue heat exchangers, respectively.

Figure 14 presents which streams is heat exchanging with each other and what kind of external heating or external cooling is required. No external heating, but the solar thermal energy input is required, while external cooling is utilizing cooling water as well as producing steam, of which may be used for generation of electricity in a steam turbine. The splitting of the streams in the diagram is representing actual splitting of the streams and the segments are heat exchanged in different heat exchangers before being mixed again. The heat load over the heat exchangers and their respective surface areas are excluded in figure 14 in order to simplify the HEN diagram for the rather complex HEN. However, the streams heat exchanging with each other, the heat load, area and inlet- and outlet temperatures in the heat exchangers in the best case HEN design are presented in the table below for a more detailed overview of the HEN.

Table 28: Detailed overview of streams heat exchanging with each other.

load [MJ/h]	Area [m^2]	Hot stream	Hot T in [°C]	Hot T out [°C]	Cold stream	Cold T in [°C]	Cold T out [°C]
25448	106	Very high temperature (Solar thermal energy)	3000	2999	Water feed (from FT)_To_Water feed to Solar reactor	518.4	1350
3046	83	Very hot oxygen	1350	1100	HP Steam Generation	250	250
2464	459	Hot Oxygen	1100	599	After Prereformer_To_ATR	579	600
3463	1236	Hot Oxygen	1100	599	CO2 feed with recycle	568	777
1609	1347	Hot syngas	600	485	CO2 feed with recycle	466	568
2358	338	Hot syngas	600	485	Water feed (from FT)_To_Water feed to solar reactor	433	518
20658	4572	Hot reformed tail gas	600	440	After Prereformer_To_ATR	400	579
4785	3239	Hot Oxygen	599	156	CO2 feed with recycle	136	466
2333	98	Hot syngas	485	240	syngas to FT reactor	195	215
5924	1561	Hot syngas	485	240	Water feed (from FT)_To_Water feed to Solar reactor	220	433
2800	55	Hot reformed tail gas	440	255	syngas to FT reactor	151	195
21225	2713	Hot reformed tail gas	440	255	Tail gas and methane_To_Prereformer	201	400
63040	87	HP steam_To_liquid recycle loop	317	316.2	HP Steam Generation	249	250
3169	10	HP steam_ To_liquid recycle loop	316.2	316	tailgas and methane_To_Prereformer	163	201
17185	231	Hot reformed tail gas	255	166	LP Steam Generation	125	125
2359	506	Hot syngas	240	168	syngas to FT reactor	151	195
23363	472	Three phase sep. feed	221	133	LP Steam Generation	124	125
55990	115	MP steam_To_liquid recycle loop	220	219.2	MP Steam Generation	174	175
18322	244	MP steam_To_liquid recycle loop	219.2	219	Tail gas and methane_To_Prereformer	163	201
89	24	Hot syngas	168	133	syngas to FT reactor	103	151
1042	329	Hot syngas	168	133	CO2 feed with recycle	59	136
19778	381	Hot reformed tail gas	166	116	Tail gas and methane_To_Prereformer	105	163
5488	811	Hot reformed tail gas	166	116	syngas to FT reactor	103	151
1146	383	Hot Oxygen	156	45	Cooling Water	20	24
1966	80	Three phase sep. feed	133	128	LP Steam Generation	125	125
11824	85	Hot syngas	133	60	Cooling Water	20	24
1902	5	Three phase sep. feed	128	123	FT cooling water_preheat	25	60
7072	19	Three phase sep. feed	123	104	Cooling Water	24	25
19111	75	Hot reformed tail gas	116	60	Cooling Water	20	24
8590	39	Three phase sep. feed	104	60	Cooling Water	20	24

The flowrate ratio between the streams in the stream segments after splitting can be derived from the heat loads in the respective segments as shown in the equation below.

$$\frac{Load_{ss1}}{Load_{ss2}} = \frac{Flowrate_{ss1}}{Flowrate_{ss2}} \quad (7.1)$$

The subscripts ss1 and ss2 stands for split-segment1 and split segment 2, respectively. Now that the best case HEN of which required less energy from solar thermal heating than in the preliminary conceptual designs HENs has been chosen, a better energy efficiency is achieved as presented in the table below. The final energy efficiency of the best case when the electric energy generated in steam turbines is taken into account is presented in chapter 7.5.4.

Table 29: The energy efficiencies when using the best case HEN configuration.

20Bar with CH4 feed	Value	Unit	Description
LHV HC Product Total SUM	383	[GJ/h]	
LHV Methane feed total	372	[GJ/h]	
Compressor Work Total SUM (entire plant)	18.8	[GJ/h]	(3 compressors: Oxygen 0.5 → 20bar, Methane and syngas 5 → 20bar)
Qsun (Solar thermal energy duty)	191	[GJ/h]	
Entire system			
Energy Efficiency entire system	65.86 %		(LHV product / (LHV Methane feed +Qsun+Wcompressor)
Energy Efficiency (Solar not Counted)	98.00 %		(LHV product / (LHV Methane feed + Wcompressor)
FT loop			
Total LHV syngas fed to FT	169	[GJ/h]	
Compressor Work (FT loop)	6.40	[GJ/h]	(1 Compressor: Methane 5 → 20bar)
Energy Efficiency FT loop	70.00 %		(LHV product / (LHV Methane feed+ LHV syngas fed to FT + Wcompressor)

The energy efficiency for the entire system increased from 64.33% to 65.86% when the best case HEN is used for the best case conceptual design, instead of the preliminary estimate described in chapter 7.1. Although this might not look like a big improvement, the reduction of solar thermal energy required is potentially saving MM US$ 0.311 in annual direct operating costs alone. The total investment cost of the solar reactor will also be reduced, in addition to improving the overall economic performance of the HEN when deciding upon using this best case HEN. Due to deciding upon a best case

conceptual design configuration and a best case HEN, a project evaluation is only performed for the configuration ultimately decided to be the best case. The project evaluation is presented in chapter 7.5, of which finalizes the techno-economic feasibility.

7.4 Conditions and composition of total Fischer Tropsch product

The total production of FT product has a very high fraction of the lump of components representing paraffin with carbon number 11 and higher, with an average carbon number of 60, as explained in chapter 5. The conditions of the total FT product are shown in the table below.

Table 30: Conditions of total FT products from Aspen HYSYS simulation

Conditions	Value
Vapor / Phase praction	0.0
Temperature [°C]	213.3
Pressure [Bar]	20.0
Molar Flow [kgmole/h]	15.5
Mass Flow [kg/h]	8716.4

Table 30 shows the conditions of the total FT product from Aspen HYSYS simulation. The composition of the total FT product is shown in the table below.

Table 31: Composition of total FT products from Aspen HYSYS. OL, PL, OH and PH denotes olefin low, paraffin low, olefin high and paraffin high, respectively, whereas high and low refers to the propagation probability, *α*, which corresponds to the average molecular weight of the lump, which is explained in chapter 5.

Component	Molar fraction	Mass fraction
CO	7.54E-03	3.76E-04
H_2	6.15E-03	2.21E-05
H_2O	0.087	2.79E-03
Methane	5.38E-04	1.54E-05
Ethane	2.10E-05	1.12E-06
Ethylene	9.34E-05	4.67E-06
Propylene	1.28E-04	9.58E-06
Propane	3.42E-05	2.68E-06
Butylene	1.57E-04	1.57E-05
Butane	5.59E-05	5.78E-06
Pentane	9.02E-05	1.16E-05
Hexane	1.46E-04	2.23E-05
Heptane	2.37E-04	4.23E-05
Octane	3.99E-04	8.11E-05
Nonane	6.85E-04	1.56E-04
Decane	1.22E-03	3.08E-04
C5+OL*	8.46E-03	1.37E-03
C11+PL*	5.35E-03	1.80E-03
C5+OH*	0.235	0.047
C11+PH*	0.631	0.945
CO_2	0.016	1.25E-03

Table 31 shows the total FT product distribution as simulated in Aspen HYSYS. The components marked with an asterix are lumped components of olefins and paraffin with carbon numbers of higher than 5 and 11 respectively, as explained in chapter 5. The majority, mass fraction 0.945 of the total FT products, consists of the lump of component, C11+PH*, with average carbon number 60.

7.5 Project evaluation

In this chapter only a brief overview of the key basis for the project evaluation is presented. The basis for calculating the investment cost of the specific types of equipment, the operating costs, net present value and profitability analysis are presented in more detail in Appendix G, along with a description of the methods used to achieve the results presented in this chapter. The procedure used for deriving the sizing and investment cost estimations is described in detail in Sinnot & Towler [41]. The method used for estimating operating costs is described in detail in Turton et al. [42]. The economic lifetime of the plant is set to be 20 years, operating during the hours of sunlight of 2672 hours per year. However, the shutdown and start-up processes are not accounted for, but is recommended for further investigation. All values are converted into 2015-US$ [43]. All of the equipment, except for the solar reactor, is chosen to be of stainless steel in order to avoid corrosion, because the plant is expected to last for at least 20 years.

7.5.1 Sizing of equipment and investment cost estimations

- The heliostats cost is derived from cost correlations from Kolb et al. [17] and Stine & Geyer [19] and is directly proportional to the solar thermal energy required.
- The two phase separators, the FT reactor and the solar reactors are costed as stainless steel vertical pressure vessels using cost correlations found in Sinnot & Towler [41].
- The solar reactors are made of ceramic material similar to that of the ceramic high temperature heat exchanger; therefore an investment cost factor of 20times more than a conventional stainless steel vertical pressure vessel is used [39].
- A complexity factor accounting for towers, secondary concentrators, catalyst and that water is heated to such a high temperature inside the reactors, as well as accounting for that this is new technology makes the investment cost of the solar reactors 2 times higher.
- Initial catalyst required in the FT reactor is accounted for in the investment cost and a complexity factor accounting for internal equipment makes the investment cost for the FT reactor 2 times higher.
- The three phase separator is costed as a stainless steel horizontal pressure vessel using cost correlations found in Sinnot & Towler [41].

- The amine plant is costed as an MDEA-amine plant, using the cost correlations found from personal communication with Sogge, and a factor accounting for the low CO_2 capture fraction, makes the investment cost for the MDEA-amine plant 2 times lower [44].
- The investment cost of an ATR including a pre reformer is derived by scale parameters of base volumetric flow capacity and a base cost using the cost correlations found in Kreutz et al. [36].
- The compressors are costed as centrifugal compressors using the cost correlations found in Sinnot & Towler [41]

The fixed capital cost of the equipment is derived as described in Appendix G, and the results, including the total fixed capital cost, are shown in the table below.

Table 32: Fixed capital cost of all major equipment.

Equipment	Fixed capital cost	Unit
FT reactor	40.92	MM US$
ATR + pre reformer	16.90	MM US$
Compressors	44.06	MM US$
Heliostats	51.16	MM US$
Solar reactors	52.43	MM US$
Heat exchangers, including the waste heat boilers	36.03	MM US$
Two phase separators	0.59	MM US$
Three phase separator	0.12	MM US$
Amine plant MDEA	26.90	MM US$
Total fixed capital cost of all major equipment	269.12	MM US$

Table 32 is presenting the fixed capital cost for all major equipment, including the total fixed capital cost. The fixed capital investment cost distribution is shown in the figure below.

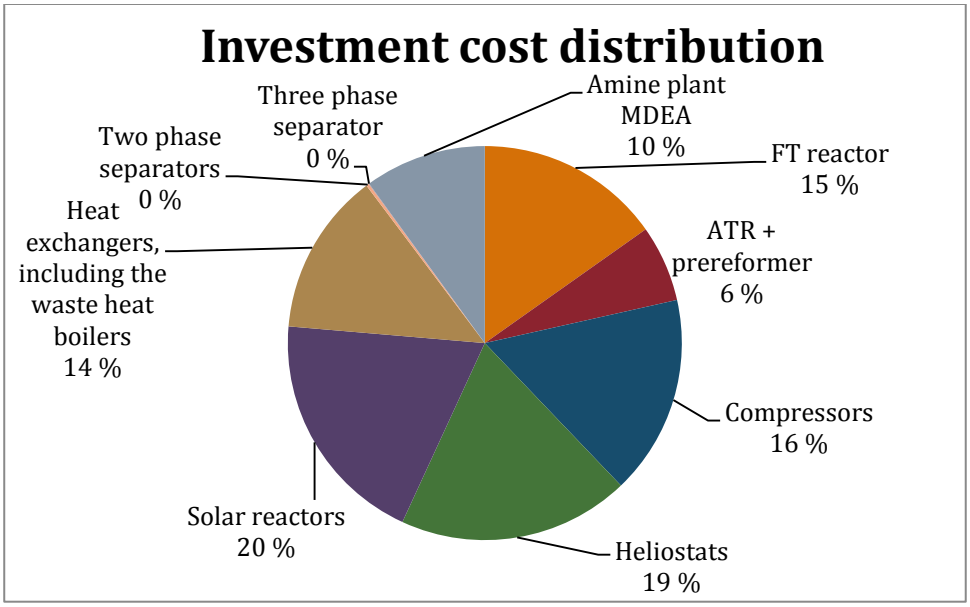

Figure 15: The fixed capital investment cost distribution. The fixed capital cost for all major equipment is presented as a fraction of the total fixed capital cost. The investment cost calculations are described in Appendix G.

The solar thermal energy plant with the investment cost of heliostats and solar reactor is accounting for about 39% of the total investment cost. This validates the assumption made in chapter 7.1.4 of that the solar reactor system has an investment cost accounting for a high fraction of the total investment cost for the entire plant. The amount of CO_2 captured by the amine plant in the best case conceptual design in only 35.6% of the CO_2 in the inlet stream, and this percentage is not accounted for by the scale factor correlations in the investment cost estimation, only the flowrate of CO_2 captured is considered. Therefore, a low capture fraction factor is introduced. It is noteworthy that the amine plant's investment cost of 10% of the total investment cost is considerably high, even after accounting for the low CO_2 capture fraction. Because the percentage of CO_2 captured in the basis for the cost correlation is unknown, the effect this percentage has on the investment cost is recommended for further investigation. In addition, the high investment cost of the MDEA-amine plant increases the incentive for further exploring the implementation of other CO_2 removal processes such as the Selexol process described in chapter 4.5.

7.5.2 Operating cost

The method used for estimating the operating costs is described in detail in Turton et al. [42]. The key basis that is accounted for in the operating cost estimation is listed below and is basis is described in more detail in Appendix G.

- Direct manufacturing cost is accounting for raw materials, utilities, operating labor, direct supervisory and clerical labor, maintenance, repairs and laboratory charges as described in Turton et al. [42]
- Fixed manufacturing cost is accounting for depreciation, taxes, insurance and plant overhead cost as described in Turton et al. [42].
- The average commercial charge for water use during 2015-2016 is US$ 0.00336/L [45].
- The average industrial price of electricity in South Africa during 2014-2015 is 51.79 South African cent/kWh = US$ 0.035/kWh [46].
- The default values from Aspen Energy Analyzer are used for calculating the electricity generated in the steam turbines. The average efficiency from hot stream to steam generation to electrical energy is calculated to be 0.26 for high pressure steam generation, 0.23 for medium pressure steam generation and 0.19 for low pressure steam generation [37].
- The average price for natural gas the past 5 years, is about US$ 3/GJ = US$ $3*10^{-6}$/kJ [47].
- The cost of CO_2 is set to zero.

The estimated direct manufacturing cost is presented in the table below.

Table 33: Direct manufacturing cost

Direct manufacturing cost factors	Value	Unit
Cost of raw materials	3.10	MM US$/year
Cost of utilities	4.56	MM US$/year
Cost of operating labor*1.33	0.48	MM US$/year
Fixed capital investment cost*0.069	11.40	MM US$/year
Sum direct manufacturing cost	19.60	MM US$/year

Table 31 is presenting the direct manufacturing cost, whereas the cost of raw materials is the sum of the cost of water and methane feeds, due to the cost of CO_2 is set to zero. The cost of the utilities is from the solar thermal energy required alone, since enough electric energy is produced in steam turbines to power the compressors and amine plant. The electric energy utilized in the compressors and amine plant is subtracted from the energy provided in the steam turbines in further estimations. The direct manufacturing cost and the fixed manufacturing cost adds up to the total manufacturing cost, which is presented in the table below.

Table 34: Direct, fixed and total manufacturing cost

Manufacturing cost	Value	Unit
Total direct manufacturing cost	19.60	MM US$/year
Total fixed manufacturing cost	11.50	MM US$/year
Total annual manufacturing cost	31.10	MM US$/year

The total annual manufacturing cost presented in is not accounting for the depreciation; however, the depreciation will be accounted for in the net present value estimations in chapter 7.5.3.

7.5.3 Net present value

The procedure for estimating the net present value is described in detail in Sinnot & Towler [41] and Turton et al. [42].

- The economic plant life is set to 20 years, operating 334 days a year, 8 hours a day.
- Tax rate is set to 28% and a constant depreciation rate of 10% is used.
- Although it is always a wide range of FT products, the final FT product distribution has a mass fraction of 0.945 of hydrocarbons with average carbon number 60 and is approximated to be sold as pure FT wax due to the high concentration of heavy hydrocarbons for comparing with the market price of FT wax [2, 3].
- An approximation is made that the average sale price in 2012 for FT wax of US$1300/Metric Ton can be used for comparison of the sale price for the entire FT product [48]. High melting point and low viscosity FT wax sale price can be as high as US$ 2500/Metric Ton, and is used for comparison during calculation of net present value [48]

The annual revenues is estimated to MM US$ 30.7 when using the average sale price in 2012 for FT wax of US$ 1300/Metric Ton. This makes the annual profit before taxes -MM US$ 0.35, which means that the plant is not profitable for this price of FT wax. The discount factor is set to 10% and makes the net present value –MM US$ 272.

The annual revenues is estimated to MM US$ 58.7 when using the price for high melting point and low viscosity FT wax of US$ 2500/Metric Ton. This makes the annual profit before taxes MM US$ 27.60, which means that the plant has the potential for being profitable for this price of FT wax. The internal rate of return is calculated to be 8.0%.

The figure below presents the required sale price for achieving different internal rates of return.

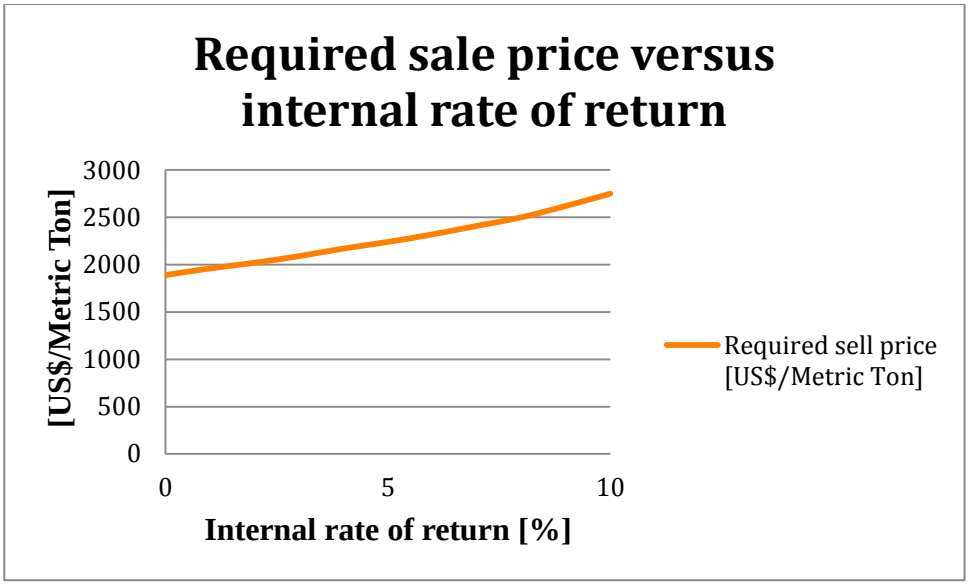

Figure 16: Required sale price of the entire FT product versus internal rate of return.

Figure 16 shows the required sale price plotted against the resulting internal rate of return. The sale price making the internal rate of return zero is US$ 1890/Metric Ton, and the sale price making the internal rate of return 10% is US$ 2750/Metric Ton.

This plant evaluation is performed without accounting for the shutdown and startup costs due to limited hours of sunlight, the cost of upgrading FT product or the cost related to the effects of coke formation, alongside several approximations and other details that are recommended by the Association for Advancement of Cost Engineering (AACE) in Christensen & Dysert [49]. In addition, the incentives for environmentally friendly production and a very low CO_2 footprint are not accounted for in any way.

A plant evaluation with the inclusion of these factors is recommended for further investigation as described in chapter 8.1. In addition, by operating the solar thermal derived syngas production at full capacity and by storage of the syngas and oxygen produced from the solar reactors, the FT synthesis may be operating continuously 24 hours per day without sunlight at one third of the capacity. However, this implementation in the conceptual design is beyond the scope of this thesis and is also recommended for further investigation as described in chapter 8.1.

The FT synthesis produces a lot of water, which in this plant evaluation is considered as waste water. In areas where drought occurs, the produced water, if treated, may be considered a valuable resource, however, the implementation of treating waste water is recommended for further investigation as described in chapter 8.1.

7.5.4 Final energy efficiencies of the best case

By performing the project evaluation, the electrical energy generated in steam turbines was found to exceed the energy required in the compressors and the amine plant. As a result, the energy input and output is different from what is used in the previously presented energy efficiency estimations. The final energy efficiencies of the best case are presented in the table below.

Table 35: Final energy efficiencies of the best case

20Bar with CH4 feed	Value	Unit	Description
LHV HC Product Total SUM	383	[GJ/h]	
LHV Methane feed total	372	[GJ/h]	
Excess electrical energy generated in steam turbines	17.1	[GJ/h]	
Qsun (Solar thermal energy duty)	191	[GJ/h]	
Energy Efficiency entire system	71.07 %		(LHV product+excess electric energy) / (LHV Methane feed +Qsun)
Energy Efficiency (Solar not Counted)	102.94 %		(LHV product+ excess electric energy) / (LHV Methane feed)

Table 35 presents the final energy efficiencies of the best case for the entire system. The final energy efficiency for the entire system is 71.07%. There are operating costs associated with deriving the solar thermal energy. However, if this energy is considered as energy free of charge because it comes from the sun, the overall energy efficiency for the entire system is 102.94%. This means that the energy output is exceeding the energy input from the external methane feed by 2.94%. The energy footprint of the total energy input is presented in the figure below.

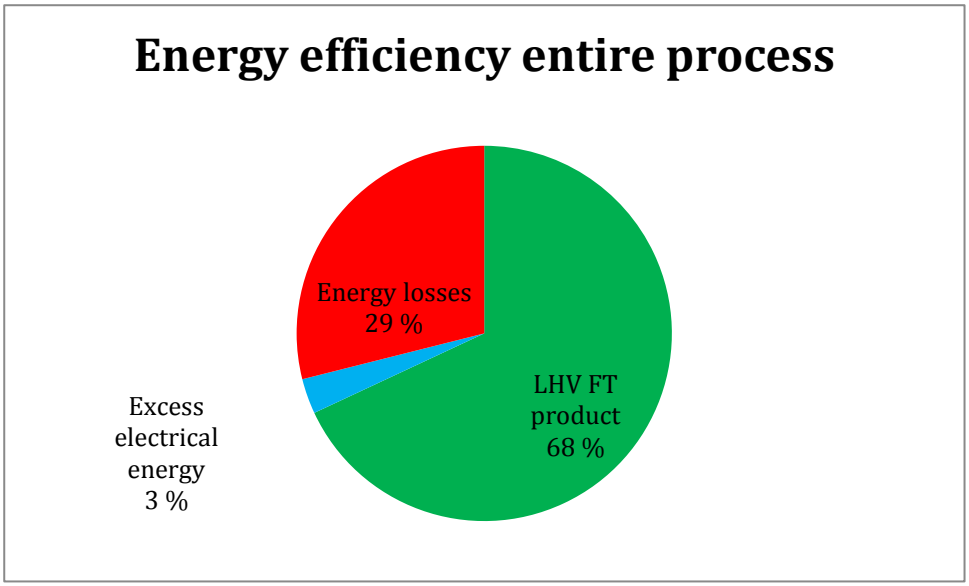

Figure 17: Energy footprint of total energy input. LHV FT product is the lower heating value of the total Fischer Tropsch product.

The footprint of the total energy input is presented in figure 16. The energy in the LHV FT product and the excess electrical energy represents the energy output of the entire process, while the energy losses represents the energy lost is the process.

8 CONCLUSIONS

This projects main scope was to develop, optimize and perform a techno-economic feasibility of a process design using solar thermal energy for producing syngas by the hercynite cycle integrated with Fischer Tropsch synthesis.

Several conceptual designs and heat exchanger network configurations was considered in order to optimize production of FT product and the entire plants energy efficiency. By using an ACM model for the FT reactor in order to simulate the FT reaction, more accurate product distribution and reaction kinetics was achieved. However, the ACM model proved to reduce the ability to optimize and perform a sensitivity analysis in Aspen HYSYS simulations, especially when the ACM model is inside of a loop. Even though the ACM model caused difficulties for optimization inside of a loop, optimization tools was applicable for parts of the process outside the loop. In addition, parts that can be optimized while disconnected from the loop gives room for adjusting the ACM model and then integrating the optimized parts with the loop. Several design configurations was continuously optimized by this method when applicable, in addition to manual optimizing when it was not applicable.

By introducing an external methane feed, the production of FT product increased by about 3.25 times and the final FT product consisted of 94.5wt% of hydrocarbons with average carbon number of 60. This was found to be the best conceptual design configuration with an overall energy efficiency for the entire plant of 64.33%, a carbon efficiency of 99.95% and the total production of FT product of 8716.4 kg/h. The inclusion of an optimized heat exchanger network, and accounting for the electric energy generated in steam turbines, changed the energy efficiency to 71.07%.

The project evaluation resulted in an average sale price for the entire FT product of US$ 1890/Metric Ton for the project to break even. The average market price of FT wax is US$ 1300/Metric Ton, and the market price of the most valuable FT wax is US$ 2500/Metric Ton. The break even price between average and most valuable FT wax shows a potentially promising economy for the proposed plant.

When applicable, the estimations have been consistently conservative. However, neither the shutdown and startup costs due to limited hours of sunlight, the cost of upgrading FT product, or the cost related to the effects of coke formation are accounted for when arriving at this number. These factors, alongside several approximations and other details that are recommended by the Association for Advancement of Cost Engineering (AACE) in Christensen & Dysert [49], makes this an estimate of high uncertainty and is therefore not entirely representable for comparing with the FT wax market prices.

On the other hand, the incentives for environmentally friendly production and a very low CO_2 footprint are not accounted for in any way. This means that for the proposed plant to be viable, the sale price for the FT product found in this thesis has to be near equal to the market price when all these factors has been accounted for.

In conclusion, the debate about green house gas emissions is creating continuously increasing incentives for environmentally friendly production plants, which indicates a potentially bright future for the proposed plant in this thesis.

8.1 Recommendations for improvements and further study

There are several further investigations that have potential for improving the proposed plant.

Thermal storage by increasing the amount of heliostats and heating a thermal element for isolated storage during sunlight hours, such as molten salts, is recommended for further investigation. The implementation of thermal storage may increase the operating hours of the plants and thereby improving its potential viability.

Using two ATR’s, one inside the FT synthesis loop utilizing the oxygen necessary for conversion of methane in the loop, and one for utilizing the remaining oxygen produced in the solar reactors together with an external methane feed, is considered in this thesis, but is not chosen as the best case. However, in this thesis, both of the ATR’s were operating at the same pressure. Although the operating pressure is considered to be optimal at 20bar inside the FT synthesis loop in Emhjellen [6], the ATR outside the

loop may be operating at a lower pressure which allows for a higher methane conversion and in return a higher external feed of methane. The high carbon efficiency indicates that in order to significantly increase the production of FT product, more carbon has to be feed to the plant. Thus, a significantly higher external methane feed may allow for a significantly higher production of FT product and the benefit this design choice may yield is recommended to compare against the downsides of including an additional ATR and increasing the fraction of CO_2 captured by the amine plant. This implementation and comparison is recommended for further investigation.

A more detailed investigation of the benefits of having the amine plant before the FT reactor instead of at the current location is recommended for further study with more accurate simulation of the composition of the stream extracted by the amine plant.

Due to the investment cost of the amine plant being estimated to a considerably high percentage of the total investment cost in for the entire plant, a more detailed investigation of the implementation of a different CO_2 capture unit, such as the Selexol process, is recommended for further investigation.

The cost of the heat exchanger network and the profit from generation of electricity in steam turbines are presented in chapter 7.3.2. From the results presented it is evident that by using the recommended cost factor for the ceramic high temperature heat exchanger, the implementation of this heat exchanger is not beneficial to the plant. However, reducing the cost factor to the lowest range, using a ceramic high temperature heat exchanger is significantly improving the economic parameters of the heat exchanger network. Therefore, it is recommended to further investigate the price of the ceramic high temperature heat exchanger.

For the proposed plant to be even more environmentally friendly, and even having the potential for having a negative CO_2 footprint by having CO_2 fed to the plant and maintaining complete recycle of CO_2, the external methane feed can be derived from biomass. In chapter 7.1, it is presented that the proposed plant potentially may utilize external methane feed derived from biomass; however, this implementation is recommended for further investigation.

A scale-up analysis for the proposed plant is recommended for further investigation. A scale-up analysis of the entire plant gives valuable insight of how the plant is performing on a larger or smaller scale, and makes it easier to compare the plants economics against the market prices. In addition, a scale-up analysis on the solar

heliostats alone may give insight in whether or not using additional solar thermal energy for thermal storage or improving the gas purity of the gasification of biomass process is beneficial.

In order to achieve a more accurate simulation of the process, a different type of simulation model should be made, of which allows for converting the heavier hydrocarbons in the tail gas in an ATR, as well allowing for more extensive use of optimization tools by implementing a more robust model for the FT reactor.

Coke formation needs to be studied in more details, as the coke formation is not accounted for in the projects results. Even though several precautions such as having a pre reformer before the ATR, limiting the temperature and adjusting the steam/carbon ratio into the ATR is accounted for, a further study is recommended in order to give a more precise precaution strategy in addition to accounting for the cost associated with coke formation.

In the FT synthesis a lot of water is produced and considered as waste water in this thesis. However, in areas where drought occurs, the waste water may be treated and be considered as a valuable asset. The implementation of treating water is recommended for further investigation.

Moreover, achieving continuous operation of the FT synthesis loop 24 hours per day is recommended for further investigation. This can be done by operating the solar reactor at full capacity during sunlight hours, and reduce the capacity of the FT synthesis loop. This means the conceptual design, its capacity and heat exchanger network has to be redesigned, and solutions for storage of syngas, oxygen and their thermal energies have to be implemented

Finally, a more detailed project evaluation, accounting for the cost of the shutdown and start-up processes, the cost of upgrading FT product, the cost associated with coke formation and the incentives of an environmentally friendly plant, in addition to more accurate approximations from experimental values, is recommended for further investigation.

9 BIBLIOGRAPHY

[1] M. Gonzales and M. Lucky, “Fossile fuels dominate primary energy consumption,” Worldwatch Institute, 2013.

[2] Sasol Technology Research and Development, Upgrading of Fischer-Tropsch Products to produce Diesel, Sasol, 2010.

[3] J. P. Collins, J. J. Font Freide and B. Nay, “A history of Fischer-Tropsch Wax upgrading at BP- From catalyst screening studies to full scale demonstration in Alaska,” *Journal of natural gas chemistry Vol. 15 No. 1,* pp. 1-10, 2006.

[4] T. O. Erevik, “Syngas production from solar thermal splitting of water with CO2 quenching,” Master Student Spesialization Project (Norwegian University of Science and Technology), 2015.

[5] K. Souskova, M. K. Lundgren, W. Ge and Å. D. Nannestad, “The Hercynite cycle for solar thermal upload of CO2 to Syngas,” Master Students Process Design Project (Norwegian University of Science and Technology), 2015.

[6] M. T. Emhjellen, “Fischer Tropsch Synthesis Loop with an Autothermal Reformer: Integration with a Solar Thermal Energy Derived Syngas Facility,” Master Student Specialization Project (Norwegian University of Science and Technology), 2015.

[7] J. A. Moulijn, M. Makkee and A. E. Van Diepen, Chemical Process Technology, Wiley, 2013.

[8] K. Aasberg-Petersen, T. S. Christensen, I. Dybkjaer, J. Sehested, M. Østberg, R. M. Coertzen, M. J. Keyser and A. P. Steynberg, "Chapter 4 - Synthesis Gas Production for FT Synthesis," in *Studies in Surface Science and Catalysis*, Elsevier, 2004, pp. 258-405.

[9] S. F. Rice and D. P. Mann, "Autothermal Reforming of Natural Gas to Synthesis Gas," Sandia National Laboratories, 2007.

[10] K. Aasberg-Petersen, J. -H. Bak Hansen, T. S. Christensen, I. Dybkjaer, P. Seier Christensen, C. Stub Nielsen, S. L. Winter Madsen and J. R. Rostrup-Nielsen, "Technologies for large-scale gas conversion," in *Applied Catalysis A: General*, Elsevier, 2001, pp. 379-387.

[11] W. G. Appleby, J. W. Gibson and G. M. Good, "Coke formation in catalytic cracking," in *I&EC Process design and development Vol.1 NO.2*, Emeryville, California, Emeryville Research Center, The Shell Development Co., 1962, pp. 102-110.

[12] M. Halabi, M. De Croon, J. van der Schaaf, P. Cobden and J. Schouten, "Modeling and analysis of autothermal reforming of methane to hydrogen in a fixed bed reformer," *chemical engineering journal 137,* pp. 568-578, 2008.

[13] A. Rafiee and M. Hillestad, "techno-economical analysis of a gas to liquid process with different placements of a CO2 removal unit," Academia, 2011.

[14] M. Hillestad, "Modeling the Fischer-Tropsch Product Distribution and Model Implementation," in *Chem. Prod. Process Model.*, DE GRUYTER, 2015, pp. 147-159.

[15] L. Sehabiague, R. Lemoine, A. Behkish, Y. J. Heintz, M. Sanoja, R. Oukaci and B. I. Morsi, "Modeling and optimization of a large-scale slurry bubble column reactor for producing 10,000bbl/day of FT liquid hydrocarbons," *Journal of the Chinese Institute of Chemical Engineers 39, Elsevier*, pp. 169-179, 2008.

[16] C. L. Munich, B. W. Evanko, K. C. Weston, P. Lichty, X. Liang, J. Martinek, C. B. Musgrave and A. W. Weimer, "Efficient Generation of H2 by splitting water with an isothermal redox cycle," Science (Sciencemag), 2013.

[17] G. J. Kolb, S. A. Jones, M. W. Donnelly, D. Gorman, R. Thomas, R. Davenport and R. Lumia, “Heliostat Cost Reduction Study,” Sandia National Laboratories, 2007.

[18] Sargent & Lundy LLC Consulting group, “Assessment of Parabolic Trough and Power Tower Solar Technology cost and performance forecasts,” U.S Department of Energy, 2003.

[19] W. B. Stine and M. Geyer, “Power from the Sun,” [Online]. Available: http://www.powerfromthesun.net/Book/chapter10/chapter10.html. [Accessed 2. April 2016].

[20] Practical solar, “CSP today,” Practical solar, 23 february 2009. [Online]. Available: http://social.csptoday.com/technology/company-information-how-much-energy-does-practical-solar-heliostat-deliver. [Accessed 10 june 2016].

[21] R. Perret, “Solar Thermochemical Hydrogen Production Research (STCH),” Sandia National Laboratories, 2011.

[22] International Renewable Energy Agency, “Renewable Energy Technologies: Cost Analysis Series, Concentrating Solar Power,” International Renewable Energy Agency, 2012.

[23] Kitokinimi: The Highlanders, “Wordpress.com,” 6 September 2013. [Online]. Available: https://kitskinny.wordpress.com/2013/09/06/the-solar-power-towers-of-seville-spain/. [Accessed 6 June 2016].

[24] D. D. Wagman, J. E. Kilpatrick, W. J. Taylor, K. S. Pitzer and F. D. Rossini, “Heats, Free Energies, And equilibrium constants of some reactions involving O2, H2, H2O, C, CO, CO2 and CH4,” U. S. Department of Commerce, National Bureau of Standards, 1945.

[25] M. E. Dry, “The Fischer-Tropsch Process,” in *Catalyst today 71*, Elsevier, 2002, pp. 227-241.

[26] A. Kohl and R. Nielsen, “Gas Purification,” in *Gas Purification*, Elsevier, 1997, pp. 1187-1234.

[27] U.S Department of Energy, “Hydrogen Production: Natural Gas reforming”.

[28] R. Sinnot and G. Towler, Chemical Engineering Design: Principles, practice and economics of plant and process design, Elsevier/Butterworth-Heinemann, 2008.

[29] National Technical University of Athens, "Aspen HYSYS - Fluid Package selection".

[30] R. Hesketh, "Conversion Reactors: HYSYS," Rowan University, 2003.

[31] P. Gunawardana, J. Walmsley, A. Holmen, D. Chen and H. J. Venvik, "Metal dusting corrosion initiation in conversion of natural gas to synthesis gas," in *Energy Procedia 26*, Elsevier, 2012, pp. 125-134.

[32] K. Nigam and A. Schumpe, "Three-phase sparged reactors," Gondon and Breach publishers, Amsterdam, The Netherlands, 1996.

[33] G. Montoya, D. Lucas, E. Baglietto and Y. Liao, "A review on mechanisms and models for the churn-turbulent flow regime," *Chemical Engineering Science 141*, pp. 86-103, 2016.

[34] C. Satterfield and G. Huff, "Product distribution from iron catalyst in Fischer-Tropsch slurry reactors," Ing. Eng. Chem. Process Des. Dev., 21 (3), 465, 1982.

[35] W. Zimmermann and D. Bukur, "Reaction kinetics over iron catalysts used for the Fischer-Tropsch synthesis," Can. J. Chem. Eng., 68 (2), 292, 1990.

[36] T. Kreutz, E. Larson, G. Liu and R. Williams, "Fischer Tropsch fuels from coal and biomass," Princeton Environmental institute, Princeton University, 2008.

[37] AspenTechnology, "Aspen Energy Analyzer - User Reference Guide," 2014.

[38] Aspen HYSYS Technical Support, 2016.

[39] Heat Transfer International, "Customer representative," Personal communication, 2016.

[40] O. Jonsson, E. Polman, J. Jensen, R. Eklund, H. Schyl and S. Ivarsson, "Sustainable gas enters the European gas distribution system.," Danish Gas Technology Center, 2003.

[41] R. Sinnot and G. Towler, Chemical Engineering Design: Principles, practice and economics of plant and process design, Elsevier/Butterworth-Heinemann, 2009.

[42] R. Turton, R. C. Bailie, W. B. Whiting and J. A. Shaeiwitz, Analysis, Synthesis, and design of chemical processes, Upper Saddle River, NJ: Prentice Hall, 2009.

[43] “Chemical Engineering's Plant Cost Index,” [Online]. Available: http://www.chemengonline.com/pci-home. [Accessed 5 june 2016].

[44] J. Sogge, “Personal communication,” Statoil ASA.

[45] “SA Water,” 2015-2016. [Online]. Available: https://www.sawater.com.au/accounts-and-billing/current-water-and-sewerage-rates/commercial-water-prices. [Accessed 9 june 2016].

[46] M. Motiang and R. Nembahe, “South African Energy Price Report,” Department of Energy, Republic of South Africa, 2016.

[47] “Investmentmine,” 8 june 2016. [Online]. Available: http://www.infomine.com/investment/metal-prices/natural-gas/5-year/. [Accessed 9 june 2016].

[48] K. J. Jensen, J. R. Menard and B. C. English, “Market Analysis for Fischer-Tropsch Waxes,” ICIS, 2012.

[49] P. Christensen and L. R. Dysert, “Cost Estimate Classification System - As applied in Engineering, Procurement, and Construction for the Process Industries,” AACE International, 2005.

[50] “Metalprices.com,” 2015. [Online]. Available: https://www.metalprices.com/metal/cobalt/cobalt-99-3-n-america. [Accessed 7 june 2016].

10 APPENDICES

APPENDIX A – ENERGY EFFICIENCY

The energy efficiency of the entire plant is a measure for how much of the energy coming into the system comes out of the system as valuable energy. The valuable energy leaving the system in this thesis is considered to be the lower heating value (LHV) of the hydrocarbon streams and the electric energy generated in steam turbines. The energy entering the system is the solar thermal energy and the LHV of the methane feed. The energy efficiency is calculated as shown in the respective tables in this thesis. However, the LHV of the lump of components, described in chapter 5, is found from the correlation of lower heating values for hydrocarbons with known LHVs, as presented in the figure below.

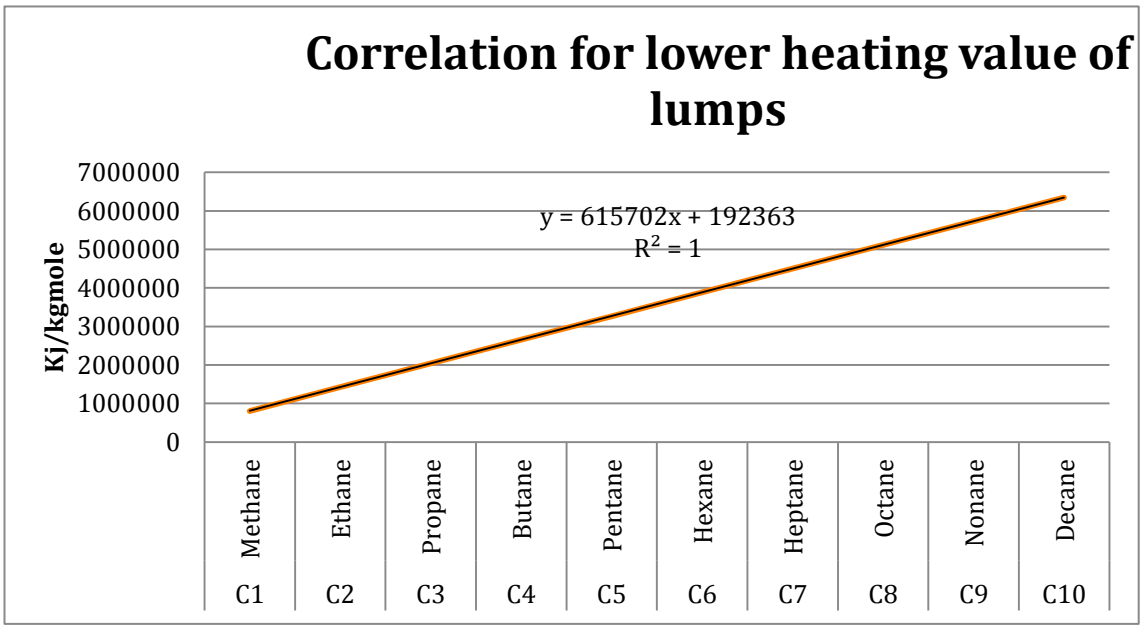

Figure 18: Correlation for lower heating values of lumps. Lower heating value is plotted against the carbon number of the hydrocarbons.

Figure 18 shows the lower heating values of hydrocarbons are linearly increasing with the carbon number. The lumps are representing average carbon numbers and their lower heating values are therefore hard to find in the literature. However, this correlation makes is possible to determine the lower heating values of the lumps. The trend line presented in figure 18 is used when calculating the energy efficiencies.

APPENDIX B – MASS BALANCE IN ASPEN HYSYS SIMULATION

$$\boldsymbol{Imbalance = total\ flow\ of\ outlet\ streams - total\ flow\ of\ inlet\ streams} \quad \textbf{(10.1)}$$

$$(\mathbf{63857.37 - 63857.29})\boldsymbol{kg/h} = \mathbf{0.08}\boldsymbol{kg/h} \quad \textbf{(10.2)}$$

$$\boldsymbol{Relative\ Imbalance}\ (\%) = \frac{\boldsymbol{Imbalance}}{\boldsymbol{total\ flow\ of\ inlet\ streams}} * \mathbf{100}\% \quad \textbf{(10.3)}$$

$$\frac{\mathbf{0.08}\boldsymbol{kg/h}}{\mathbf{63857.37}\boldsymbol{kg/h}} * \mathbf{100}\% = \mathbf{0.0001}\% \quad \textbf{(10.4)}$$

This is a low imbalance, and the imbalance is found to correspond to the imbalance over the recycle block in the Fischer Tropsch loop in Aspen HYSYS.

APPENDIX C – ENERGY BALANCE IN ASPEN HYSYS SIMULATION

$$\boldsymbol{Imbalance = \ total\ flow\ of\ outlet\ streams - total\ flow\ of\ inlet\ streams} \quad \textbf{(10.5)}$$

$$\boldsymbol{\left(-390042669.4 - (-282787607.12)\right) kJ/h = -107255062.2 kJ/h} \quad \textbf{(10.6)}$$

$$\boldsymbol{Relative\ Imbalance}\ (\%) = \frac{\boldsymbol{Imbalance}}{\boldsymbol{total\ flow\ of\ inlet\ streams}} * \mathbf{100}\% \quad \textbf{(10.7)}$$

$$\frac{\boldsymbol{-107255062.2 kJ/h}}{\boldsymbol{-282787607{,}12 kJ/h}} * \mathbf{100}\% = \mathbf{37.93}\% \quad \textbf{(10.8)}$$

This is a very high imbalance. However, this is expected because the ACM model of the FT reactor is modeled to be exothermic with cooling water near its boiling point at 220°C as 22.96bar. The cooling water through the FT reactor is not accounted for in the Aspen HYSYS model, therefore this energy is shown as an imbalance in the Aspen HYSYS simulation. However, this cooling water is accounted for manually.

The energy lost due to the absence of the FT cooling water in the Aspen HYSYS simulation is subtracted from the outlet streams and the result is shown in the equation below.

$$\frac{\boldsymbol{(-107255062.2 - (-107253348.97) kJ}}{\boldsymbol{h}} = \boldsymbol{-1713.2 kJ/h} \quad \textbf{(10.9)}$$

The actual imbalance in the Aspen HYSYS simulation is calculated in equation 10.9 and the actual relative imbalance is calculated as shown in the equation below.

$$\frac{\boldsymbol{-1713.23 kJ/h}}{\boldsymbol{-282787607{,}12 kJ/h}} * \mathbf{100}\% = \mathbf{0.0006}\% \quad \textbf{(10.10)}$$

This means that the actual relative imbalance in Aspen HYSYS is low.

APPENDIX D – CARBON EFFICIENCY

The carbon efficiencies for the entire plant are calculated with the equation presented below.

$$\boldsymbol{Carbon\ efficiency} = \frac{\boldsymbol{Moles\ of\ C\ in\ product}}{\boldsymbol{Moles\ of\ C\ in\ feed}} = \frac{\boldsymbol{F_{CH_4,in} + F_{CO_2,in} - F_{CO_2,out}}}{\boldsymbol{F_{CH_4,in} + F_{CO_2,in}}} \qquad \textbf{(10.11)}$$

The F in equation 10.9 represents the molar flowrate of the respective components. The carbon efficiency for the proposed plant is calculated in the formula below.

$$\frac{(\mathbf{464.1 + 153.1 - (0.2879)})\boldsymbol{kgmole/h}}{(\mathbf{464.1 + 153.1})\boldsymbol{kgmole/h}} * \mathbf{100} = \mathbf{99.95}\% \qquad \textbf{(10.12)}$$

APPENDIX E – ASPEN HYSYS MODELS OF GIVEN BASE CASES.

The Aspen HYSYS model of the given base case for solar thermal energy derived syngas is presented in the figure below.

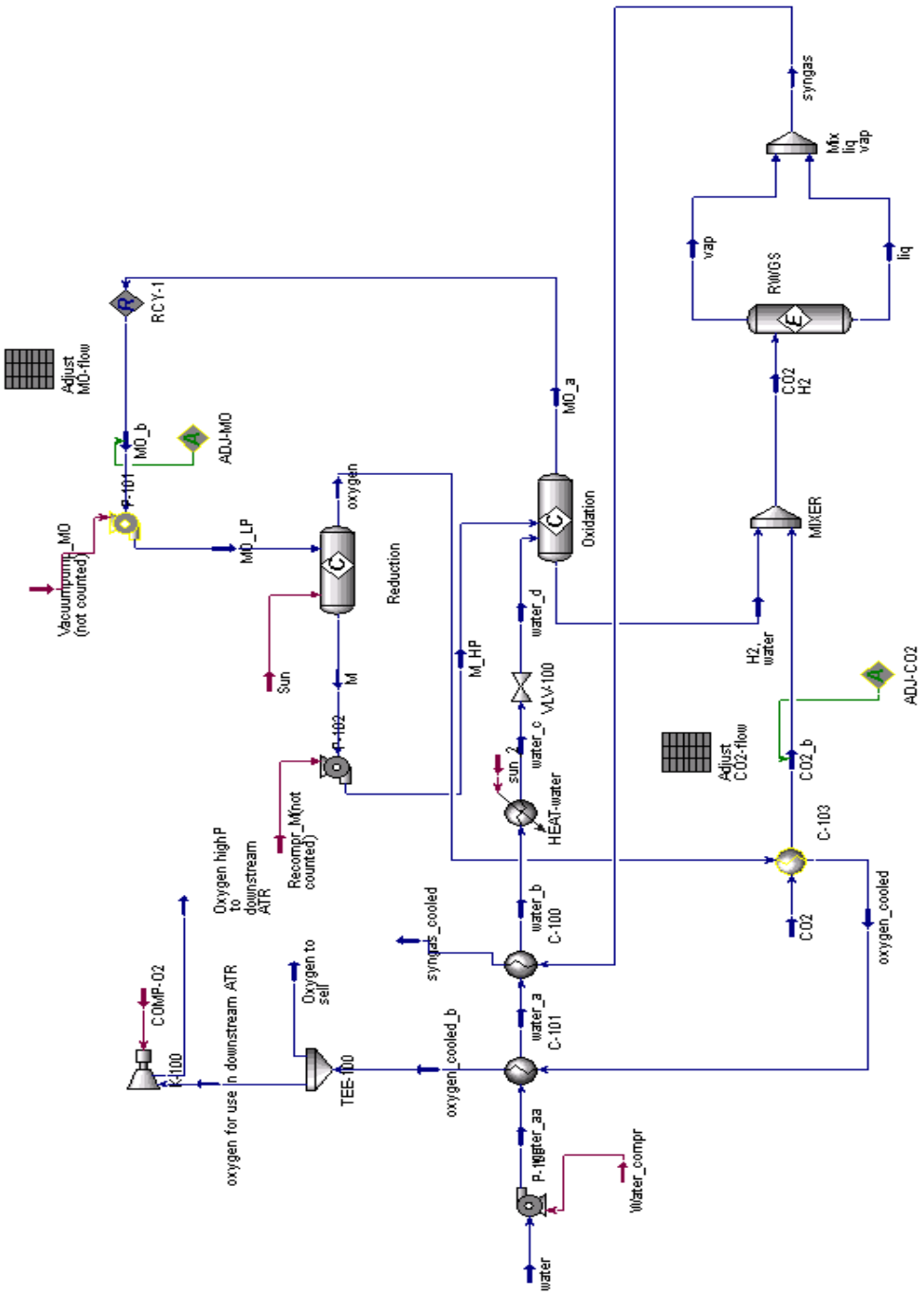

Figure 19: Aspen HYSYS model of given base case for syngas production [4].

Figure 18 shows the Aspen HYSYS model of the base case for solar thermal energy derived syngas. The Aspen HYSYS model of the given base case for FT synthesis is presented in the figure below.

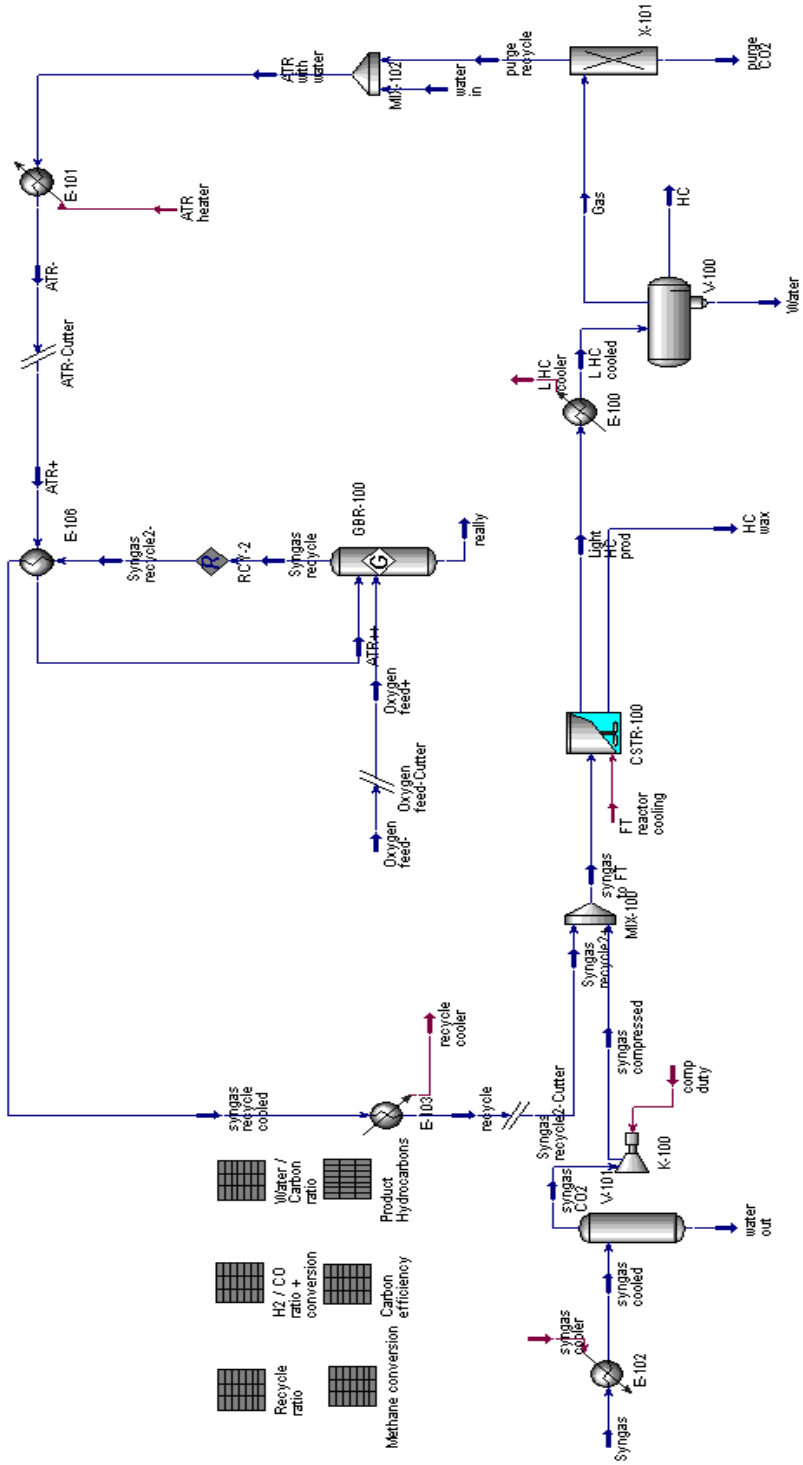

Figure 20: Aspen HYSYS simulation of the Fischer Tropsch synthesis loop given as base case from Emhjellen [6].

Table 36: Conclusion of independent variables target to maximize production and constrains in Emhjellen [6].

Independent Variables	Fixed	Target to maximize production	Constrains
Oxygen fed to the ATR		Minimize	Avoid over stoichiometry of H_2/CO molar ratio into the FT reactor
Split factor CO_2		Minimize	Avoid over stoichiometry of H_2/CO molar ratio into the FT reactor
Water fed to stream into the ATR		Minimize	Avoid over stoichiometry of H_2/CO molar ratio into the FT reactor
Temperature into the ATR	yes	Fixed (maximize)	Higher temperatures causes Coking of hydrocarbons and material issues
FT reactor volume	yes	Fixed	conversion over the FT reactor
α in FT reaction stoichiometry	yes	Fixed	0.94

Table 37: Conclusion of dependent variables target to maximize production, constrains and dependencies in Emhjellen [6].

Dependent variables	Adjusted to fixed value	Target to maximize production	Constrains
H_2/CO molar ratio into the FT reactor	Yes		Correspond to α in FT reaction stoichiometry
Product hydrocarbons		maximize	
CO_2 recycled		minimize	highly related to Product hydrocarbons
Water/carbon molar ratio into the ATR		Minimize	Highly related to water fed to the stream that goes into the ATR (Avoid over stoichiometry of H_2/CO molar ratio into the FT reactor)
Temperature out of the ATR		Maximize	Highly related to oxygen fed to the ATR
Carbon efficiency		Maximize	
Conversion over the FT reactor	Yes		Approximately 60 %

APPENDIX F - SIMULATION METHODOLOGY AND ISSUES

In order to present the Aspen HYSYS model developed for simulations in this thesis, the most important features is highlighted and marked with squares and streams that are disconnected, but set to be identical are marked with circles of the same color. The Aspen HYSYS model developed for simulations in this thesis is presented in the figure below.

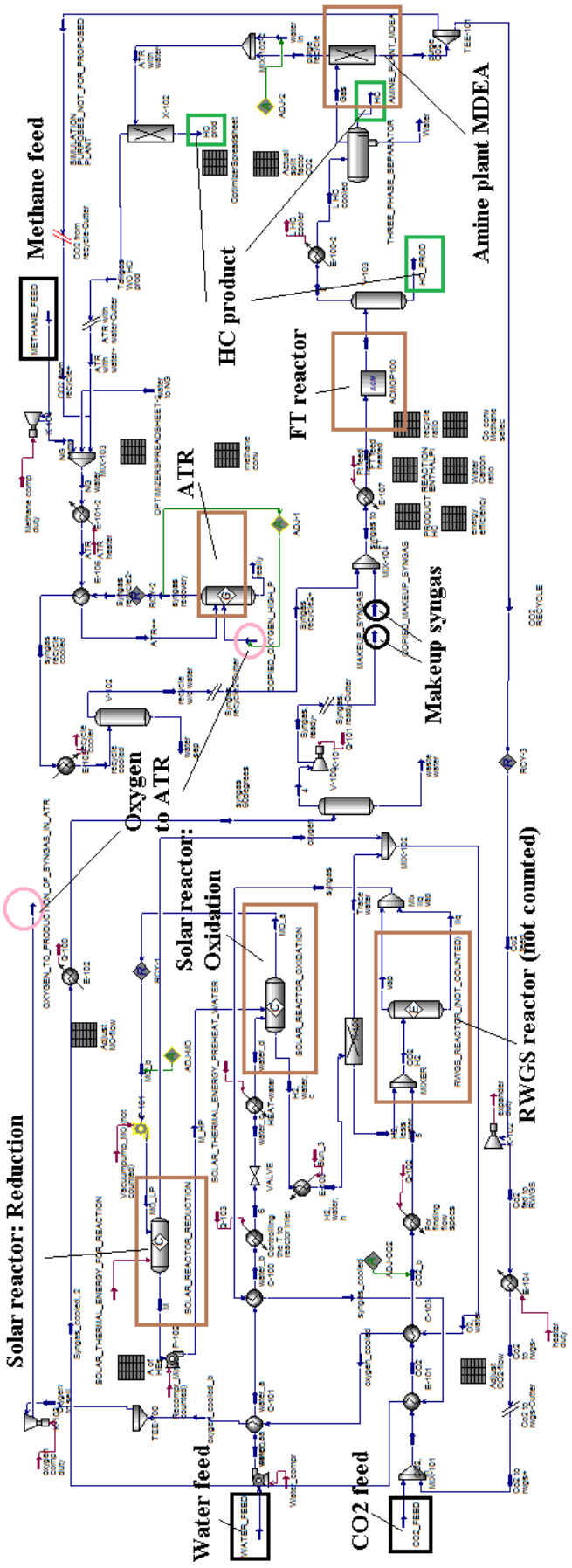

Figure 21: Aspen HYSYS model developed in this thesis.

The Aspen HYSYS model presented in figure 20 is not representing the plant proposed in this thesis, partly due to the heat exchanger network being developed in Aspen Energy Analyzer. However, it is the model that was developed for simulating the process. The brown squares in figure 20 are highlighting the most important equipment, black squares highlights the feed streams, green squares highlights the FT product streams and circles of the same color are highlighting streams that are disconnected, but set to be identical. The splitting of the CO_2 recycle stream out of the amine plant, the RWGS reactor, the HC product out of the component splitter before the ATR and the disconnected streams shown in the figure is not in the proposed plant, they are only in the model for easier convergence and simulations purposes. The liquid streams out of the ATR and the RWGS reactor have zero flowrate. Additional simulation methodology and issues encountered is described in the list below.

1. Connecting plants

The basis for fluid packages was fixed in so that all present components and reactions were included in a fluid package, and then the process development of the solar thermal syngas production plant including the FT synthesis loop was modeled and simulated in Aspen HYSYS.

2. Flaw in Aspen HYSYS – Reads incorrect molecular weight of CO

When the ACM model for the FT reactor was imported, a flaw in the Aspen HYSYS software caused the program to read an incorrect molecular weight of component CO. This flaw was fixed by copying the fluid package containing the flaw, and having an identical component-list attached to it, without using this new fluid package in the simulation environment. This solution was confirmed to be valid by Aspen HYSYS Technical Support [38].

3. Flaw in Aspen HYSYS – Program falsely reads CO_2 as a liquid

When the new FT-reactor (ACM model) was imported and the new fluid packages corresponding to the new adjusted components were implemented, another flaw in Aspen HYSYS occurred. The flaw made Aspen HYSYS falsely read CO_2 as a liquid under any conditions (temperature, pressure). The flaw was fixed by creating a new fluid package with an identical component list attached and implementing this fluid package in the simulation environment, like done with the CO molecular weight issue.

APPENDIX G – BASIS FOR PROJECT EVALUATION

The cost of most of the equipment is estimated from the equation below.

$$C_{e,i,2015} = (a + bS^n) * \frac{CEPCI_{2015}}{CEPCI_{year}} \quad \textbf{(10.13)}$$

$C_{e,i,2015}$ is the cost of the equipment, i, in 2015, a and b are cost constants, S is the size parameter and n is the exponent for a specific type of equipment, *i*. CEPCI is the Chemical Engineering Plant Cost Index, which is used for comparing the cost of equipment for different years, and all values are converted to 2015-US$ [43]. The cost constants, units for size parameters and exponent used for carbon steel centrifugal compressors, carbon steel U-tube shell and tube heat exchangers and horizontal and vertical 304 stainless steel pressure vessels of equipment in 2007 costs are found in Sinnot & Towler [41]. The cost constant, unit for size parameter and exponent for an autothermal reformer in 2007 costs is found in Kreutz et al. [36]. In addition, the cost constant, unit for size parameter and exponent for a MDEA amine plant in 2008 cost is achieved from personal communication with Sogge [44]. The installation cost of the equipment has to be accounted for and the installation factors are shown in the table below [41].

Table 38: Factors used for calculating installation cost and fixed capital cost

Factors used	Value
Installation factors	
f_{er} (equipment erection)	0.3
f_p (piping)	0.8
f_i (instrumentation and control)	0.3
f_{el} (electrical)	0.2
f_c (civil)	0.3
f_s (structures and buildings)	0.2
f_l (lagging and paint)	0.1
Factors for calculating fixed capital cost	
OS (offsites)	0.3
D&E (design and engineering)	0.3
X (contingency)	0.1

In addition to the factors presented in table 44, a factor accounting for the material of the equipment, f_m is used. The material stainless steel is used for most of the equipment and its material cost factor relative to carbon steel is f_m=1.3 [41].

When the cost of equipment is derived from a cost correlation based on carbon steel, the inside battery limit (ISBL) cost is calculated by the following equation [41].

$$\boldsymbol{C_{ISBL} = C_{e,CS} * [(1 + f_p) * f_m + (f_{er} + f_i + f_{el} + f_c + f_s + f_l)]} \qquad \textbf{(10.14)}$$

$C_{e,CS}$ is the cost of the equipment in carbon steel and C_{ISBL} is the ISBL cost. The fixed capital cost is calculated from the following equation.

$$\boldsymbol{C_{FC} = C_{ISBL} * (1 + OS) * (1 + D\&E + X)} \qquad \textbf{(10.15)}$$

C_{FC} is the fixed capital cost and the working capital, WC, is set to be 15% of C_{FC}. Together, this adds up to be the total capital investment, T_{CI}, which is the sum of C_{FC} and WC.

When using the cost correlations for pressure vessels in stainless steel, the mass of the vessel is the size parameter in Sinnot & Towler [41]. In order to calculate the mass of the vessels, the wall thickness has to be derived. The procedures used for all investment cost calculations, including how to derive the wall thickness is described in detail in Sinnot & Towler [41]. However, the pressure tolerance is set to 110% of the operating pressure, as recommended in Sinnot & Towler [41], and the allowable stress for 304 stainless steel, S, found in Sinnot & Towler [41] is presented in the table below.

Table 39: Allowable stress, S, for the material 304 stainless steel for different temperatures.

T_{max} [°C]	S [ksi]
38	20
93	16.7
149	15
204	13.8
260	12.9
316	12.3
343	12
371	11.7
399	11.5
427	11.2
454	11
482	10.8

The values of allowable stress, S, presented in table 39 are plotted against their corresponding temperatures, T_{max}, with a logarithmic trend line, in order to obtain S for the operating temperature of the respective equipment, which is presented in the figure below.

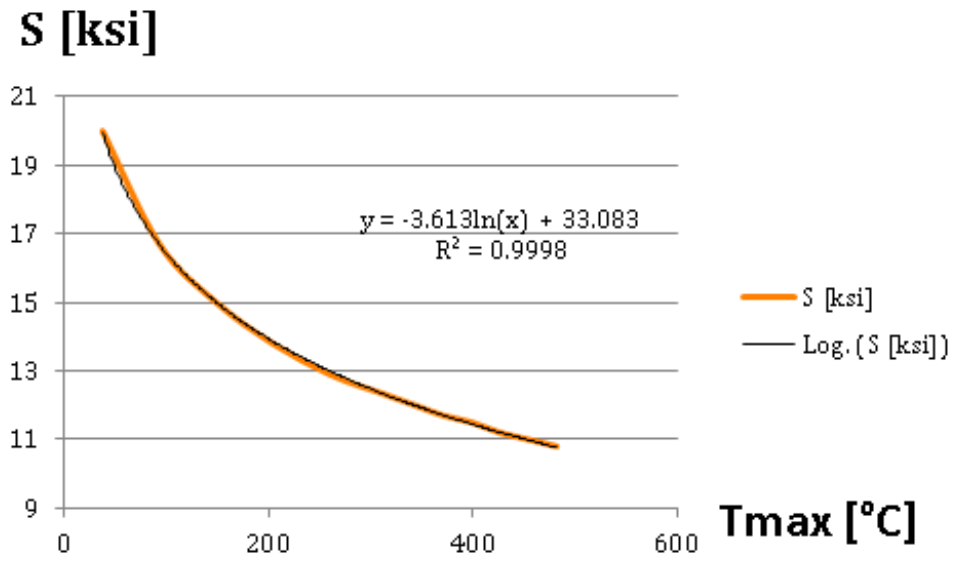

Figure 22: The allowable stress, S, for the material 304 stainless steel, plotted against the corresponding maximum temperature with a logarithmic trend line.

The equation for the logarithmic trend line presented in figure 15 is used for calculating the allowable stress, S, for corresponding to the operating temperature of the respective equipment.

Solar reactor, heliostats, secondary concentrators and tower

The solar reactors are costed as stainless steel vertical pressure vessels using the cost correlations found in Sinnot & Towler [41].

The volume of the solar reactors are derived from the simulated flowrate of the catalyst, the catalyst density, catalyst molar mass and the pressure swing hercynite cycle's cycle time.

In order to withstand the high temperatures, the solar reactors are made of a ceramic material similar to that of the ceramic high temperature heat exchanger described in

chapter 6 which is recommended to be estimated to 20 times the cost of a conventional heat exchanger [39]. Therefore, the solar reactors are estimated to cost 20 times more than a conventional stainless steel vertical pressure vessel.

In order to account for towers, secondary concentrators, catalyst and that water is heated to such a high temperature inside the reactors, as well as accounting for that this is new technology, a complexity factor of 2 is used and is directly multiplied with the 2015-purchase cost of the equipment [43].

The investment cost of the heliostats is derived by using the cost correlation found in Kolb et al.[17] and Stine & Geyer [19]. This yields a cost correlation directly proportional with the solar thermal energy required, of which is achieved from simulations in Aspen Energy Analyzer and Aspen HYSYS.

Heat exchanger network

The heat exchangers are costed as U-tube shell and tube heat exchanger using the cost correlations found in Sinnot & Towler [41]. The heat exchanger area from the best case optimized AEA HEN simulation is used for the investment cost calculation and the heat exchangers are costed using the stainless steel material cost factor.

Fischer Tropsch reactor

The FT reactor is costed as a stainless steel vertical pressure vessel using the cost correlations found in Sinnot & Towler [41].

The volume of the FT reactor is given from the best case Aspen HYSYS simulation and the height to diameter ratio of 4.29, which is found to be optimal for the FT slurry bubble column in Sehabiague et al. [15] is used to find the mass of the pressure vessel.

The average price of 99.3% pure cobalt in year 2015 of US$ 29.74/kg is used to account for the purchase cost of the initial catalyst in the FT reactor [50]. The cost of catalyst is multiplied by a factor of 3 to account for catalyst support.

Separators

The two-phase separators are costed as stainless steel vertical pressure vessels and the three-phase separator is costed as a stainless steel horizontal pressure vessel using the cost correlations found in Sinnot & Towler [41].

The mass of these pressure vessels are calculated using by determining the superficial fluid velocity required for separation as described in Sinnot & Towler [41].

Amine plant

The amine plant is costed as an MDEA-amine plant, using the cost correlations found from personal communication with Sogge [44], which is listed below.

- CO_2 captured in the amine plant (basis): 80 Metric Ton/h
- Fixed capital cost (basis) MM US$ 300 (2008-value)
- Low pressure steam required: 1.8MJ/kg CO_2 captured
- Power required: 30kWh/Metric Ton CO_2 captured
- Cooling required: 1.7MJ/kg CO_2 captured

The fixed capital cost is multiplied by a factor 0.5 in order to account for the low capture of CO_2 in the amine plant proposed in this thesis.

Pre reformer and autothermal reformer

The investment cost of an ATR is derived by scale parameters of base volumetric flow capacity and a base cost using the cost correlations found in Kreutz et al. [36].

Compressors and vacuum pump

The compressors and vacuum pump are costed as centrifugal compressors using the cost correlations found in Sinnot & Towler [41]. The compressor duty from the best case Aspen HYSYS simulation is used for the cost calculations, whereas Carnot efficiency is accounted for in Aspen HYSYS. The compressors are costed using the stainless steel material cost factor.

Operating costs and net present value basis

The method used for estimating the operating costs and net present value analysis is described in detail in Turton et al. [42].

- The total operating cost including insurance and all other miscellaneous costs for the solar plant including heliostats is found in International Renewable Energy Agency [22]. Therefore the investment cost of the solar plant and heliostats is subtracted when calculating the investment cost correlated direct and fixed manufacturing costs

- The direct manufacturing cost is estimated as the sum of the raw material costs, utility costs, 1.33 times the operating labor cost and 0.069 times the fixed capital investment, of which is accounting for raw materials, utilities, operating labor, direct supervisory and clerical labor, maintenance, repairs and laboratory charges as described in Turton et al. [42].
- The fixed manufacturing cost is estimated as the sum of 0.708 times the operating labor cost, 0.068 times the fixed capital investment and depreciation of 10%, of which is accounting for depreciation, taxes, insurance and plant overhead cost as described in Turton et al. [42].
- The number of workers is approximated to 40 by a correlation related to the number of equipment with 2 workers handling solid material and the average number of operator is found to be 17.89 from correlations in Turton et al. [42].
- The average salary of operating labor is set to US$ 20,000/year.
- The final FT product distribution has a mass fraction of 0.945 of hydrocarbons with average carbon number 60 and is approximated to be sold as pure FT wax, for comparing to market prices, due to the high concentration of heavy hydrocarbons [2, 3].
- Approximation is made that the average sale price in 2012 for FT wax of US$ 1300/Metric Ton can be used for the entire FT product for comparison, due to its high average carbon number [48]. High melting point and low viscosity FT wax sale price can be as high as US$ 2500/Metric Ton, and is used for comparison during calculation of net present value, due to the FT products' high average carbon number [48].
- The average commercial charge for water use during 2015-2016 is US$ 0.00336/L [45].
- The average industrial price of electricity in South Africa during 2014-2015 is 51.79 South African cent/kWh = US$ 0.035/kWh. [46].
- The default values from Aspen Energy Analyzer simulation is used for calculating the electricity generated in the steam turbines. The average efficiency from hot stream to steam generation to electrical energy is calculated to be 0.26 for high pressure steam generation, 0.23 for medium pressure generation and 0.19 for low pressure generation [37].
- Average price for natural gas the past 5 years, is about US$ 3/GJ = US$ $3*10^{-6}$/kJ [47].